


# GEOLOGI FOR SAMFUNNET

*GEOLOGY FOR SOCIETY*





Report no.: 2013.017		ISSN 0800-3416	Grading: Open
Title: Detection and characterisation of fracture zones in bedrock in a marine environment - possibilities and limitations.			
Authors: Georgios Tassis, Panagiotis Tsourlos, Jan S. Rønning and Torleif Dahlin		Client: Statens vegvesen, Vegdirektoratet / NGU	
County:		Commune:	
Map-sheet name (M=1:250.000)		Map-sheet no. and -name (M=1:50.000)	
Deposit name and grid-reference:		Number of pages: 74	Price (NOK): 300,-
Fieldwork carried out:		Date of report: 12.03.2014	Map enclosures:
		Project no.: 329500	Person responsible: 

## Summary:

In a continuation of the work conducted by F. Reiser et al. (2009) testing the efficiency of Electrical Resistivity Traversing (ERT) land surveys over fracture zones, we have performed a similar study for marine environments and have investigated the possibility of detecting sea-bottom fracture zones. This report summarizes our efforts to establish basic rules to be applied when considering whether or not sea water ERT can satisfactorily detect weak zones inside resistive bedrock which is overlain by sedimentary formations.

Forward modelling and inversion was conducted with two separate programs: RES2MOD/RES2DINV by M.H. Loke (2002, 2010) and DC2DPRO by J.H. Kim (2012). Using array settings of 81 electrodes and 5.0 m spacing, we have determined that in an idealised noise free 2D environment a dipole-dipole configuration is the preferable array for marine ERT. In a real case the small signal-to-noise level of the dipole-dipole array can be a limiting factor leading to choice of e.g. multiple gradient array instead. We have tested both floating and sea-bottom electrode measurement modes for all cases. We also investigated the effect of highly important related factors such as the sea water resistivity and the knowledge of the bathymetry (morphology of the sea bed).

Our results indicate that ERT surveys for fracture zone detection in marine environments, is promising under certain conditions, but at the same time can suffer from reduced resolution and major artefacts. In detecting weak zones the success of the method relies on a combination of factors such as the sea water depth and resistivity, the width of the fracture zone, the resistivity contrast with the hosting bedrock, and the resistivity and thickness of the overlying soft sediment layer.

The most important controlling factor is the sea water itself. Whether we perform floating or sea-bottom surveys, the resistivity and morphology of the sea water layer must be known in detail in order to be used in the inversion process. Not fixing the water layer is an option, but the resulting models lack accuracy. Modelling results suggest that ERT surveys can be successful in up to 10 m of sea water. At larger depths most of the current is drained away, ruling out ERT as a useful technique in the detection of weak zones in such scenarios.

Based on the modeling results, we were able to improve interpretations of ERT measurements made across the straits at Kvitsøy.

Keywords: Geophysics (Geofysikk)	Bedrock (Bergrunn)	Fracture zones (Sprekkesoner)
Resistivity (Resistivitet)	Marine ERT (Marin ERT)	Synthetic models (Syntetiske modeller)
Modeling (Modellering)		Scientific report (Fagrapport)





## CONTENTS

1. INTRODUCTION .....	9
2. WATER ERT MEASUREMENTS .....	10
3. ELECTRODE CONFIGURATIONS .....	12
4. RESULTS .....	14
4.1 Testing the response of several arrays to a simple model .....	14
4.2 The effect of fixing the water layer resistivity and depth.....	17
4.3 Effect of variations in sea-water resistivity .....	21
4.4 The effect of variations in sea-water depth .....	24
4.5 The effect of fracture zone thickness.....	30
4.6 The effect of overburden thickness .....	33
4.7 The effect of bedrock/fracture resistivity contrast.....	36
4.8 The effect of overburden resistivity.....	38
4.9 The effect of varying bedrock resistivity.....	41
4.10 Mixed survey - combination of land and floating electrode ERT modeling .....	44
5. CROSS VALIDATION PROCESS.....	50
5.1 The effect of fixing the water layer .....	50
5.2 The effect of seawater resistivity.....	50
5.3 The effect of seawater depth.....	55
5.4 Mixed survey – combination of land and seawater electrode location.....	55
6. FIELD MEASUREMENTS CROSSING SALINE WATER STRAITS .....	59
6.1 Data acquisition and inversion .....	59
6.2 Influence of seawater and metallic fence .....	60
6.3 Floating vs. sea-bottom electrodes .....	61
6.4 The effect of fixing the water layer. ....	62
6.5 Validation of the Kvitsøy data inversion.....	65
6.6 Field results from Kvitsøy vs. modeled synthetic data.....	65
7. DISCUSSION .....	67
7.1 Modeling performance .....	67
7.2 Model parameters .....	68
7.3 Possibilities and limitations in marine resistivity .....	69
7.4 Field data vs. modeled data. ....	70
8. CONCLUSIONS.....	71
9. AKNOWLEDGEMENTS.....	72
10. REFERENCES.....	73

## FIGURES

Figure 2.1: Water Resistivity Surveying modes: (a) cable floating on the water surface and (b) cable at the sea-bottom (after Tsourlos et al. 2001). .....	10
Figure 2.2: Diagram illustrating the difference between land and sea-bottom ERT. The electrical current is conducted entirely through the ground with land ERT (a) while it passes through both resistors with sea-bottom ERT (b) (Chiang et al. 2012). .....	12
Figure 3.1: Electrode configurations for dipole-dipole, multiple gradient, pole-dipole and Wenner electrode arrays. ....	13
Figure 4.1.1: Testing several sea-bottom electrode arrays on a simple fracture zone model with standard constrain inversion. The model is shown in the uppermost part of the figure. .	15
Figure 4.1.2: Testing several sea-bottom electrode arrays on a simple fracture zone model with robust inversion. The model is shown in the uppermost part of the figure. ....	16
Figure 4.2.1: Effect of fixing the water layer before robust inversion for dipole-dipole array - sea-bottom and floating electrode modes. The model is shown in the uppermost part of the figure. ....	18
Figure 4.2.2: Effect of fixing the water layer before robust inversion for multiple gradient array - sea-bottom and floating electrode modes. The model is shown in the uppermost part of the figure. ....	19
Figure 4.2.3: Effect of fixing the water layer before robust inversion for pole-dipole array - sea-bottom and floating electrode modes. The model is shown in the uppermost part of the figure. ....	20
Figure 4.3.1: The effect of variations in sea water resistivity (0.25, 0.5, 1.0 Ohm•m) using sea-bottom dipole-dipole electrode array, robust inversion and common color scale. The model is shown in the uppermost part of the figure. ....	22
Figure 4.3.2: The effect of variations in sea water resistivity (0.25, 0.5, 1.0 Ohm•m) using a sea-bottom multiple gradient electrode array, robust inversion and common color scale. The model is shown in the uppermost part of the figure. ....	23
Figure 4.3.3: The effect of variations in sea water resistivity (0.25, 0.5, 1.0 Ohm•m) using a pole-dipole sea-bottom electrode array, robust inversion and common color scale. The model is shown in the uppermost part of the figure. ....	24
Figure 4.4.1: The effect of variations in sea water depth (1.0, 3.0, 5.0, 10.0, 50.0 m) using a sea-bottom dipole-dipole electrode array and robust inversion. The model is shown in the uppermost part of the figure. ....	26
Figure 4.4.2: The effect of variations in sea water depth (1.0, 3.0, 5.0, 10.0, 50.0 m) for floating electrode configuration without any layer fixing, dipole-dipole array and robust inversion. ....	27
Figure 4.4.3: The effect of sea water depth (1.0, 3.0, 5.0, 10.0, 50.0 m) for floating electrode configuration with fixed water layer, dipole-dipole array and robust inversion. ....	28
Figure 4.4.4: The effect of variations in sea water depth (1.0, 3.0, 5.0, 10.0 m) for sea-bottom electrode configuration, pole-dipole array and robust inversion. ....	29

Figure 4.5.1: The effect of variations in fracture width (5.0, 10.0, 15.0, 20.0 m) for sea-bottom dipole-dipole electrode configuration and robust inversion.....	31
Figure 4.5.2: The effect of variation in fracture width (5.0, 10.0, 15.0, 20.0 m).for floating dipole-dipole electrode configuration and robust inversion.....	32
Figure 4.6.1: The effect of variations in overburden thickness (0.0, 5.0, 10.0, 20.0 m) on sea-bottom dipole-dipole configuration and robust inversion. ....	34
Figure 4.6.2: The effect of variations in overburden thickness (0.0, 5.0, 10.0, 20.0 m) on floating dipole-dipole electrode configuration and robust inversion. ....	35
Figure 4.7.1: The effect of variations in bedrock/fracture resistivity contrast (100, 20, 10) on both sea-bottom and floating dipole-dipole configurations and robust inversion.....	37
Figure 4.8.1: The effect of variations in overburden resistivity (5.0, 10.0, 30.0, 50.0 Ohm•m) on sea-bottom dipole-dipole configuration and robust inversion.....	39
Figure 4.8.2: The effect of variations in overburden resistivity (5.0, 10.0, 30.0, 50.0 Ohm•m) on floating dipole-dipole electrode configuration and robust inversion. ....	40
Figure 4.9.1: The effect of variation in bedrock resistivity when resistivity contrast with the fracture zone is kept constant at 20 for increasingly resistive environments (500, 1000, 2000 and 3000 Ohm•m) - sea-bottom dipole-dipole electrodes and robust inversion. ....	42
Figure 4.9.2: The effect of variation in bedrock resistivity when resistivity contrast with fracture zone is kept constant at 20 for increasingly resistive environments (500, 1000, 2000 and 3000 Ohm•m) - floating dipole-dipole electrodes and robust inversion. ....	43
Figure 4.10.1: Mixed survey - single fracture zone outside the influence of the sea water (top) two weak zones with one under the influence of sea water (bottom) - dipole-dipole array. Robust inversion with and without fixing of the water layer.....	46
Figure 4.10.2: Mixed survey - single fracture zone outside the influence of the sea water (top) two weak zones with one under the influence of sea water (bottom) - multiple gradient array. Robust inversion with and without fixing of the water layer.....	47
Figure 4.10.3: Mixed survey - single fracture zone outside the influence of the sea water (top) two weak zones with one under the influence of sea water (bottom) - pole-dipole array Robust inversion, without and with fix of water layer. ....	48
Figure 4.10.4: The influence of inversion parameters in the detection of sea-bottom fracture zones for multiple gradient array, water layer is fixed in all cases, standard and robust inversion, V/H filter 1 and 2, damping factors 0.1/0.005 and 0.25/0.1.....	49
Figure 5.1.1: The effect of fixing the water layer before inversion for dipole-dipole array - floating and sea-bottom electrode modes. The model is shown in the uppermost part of the figure. ....	51
Figure 5.1.2: The effect of fixing the water layer before inversion for Wenner-Schlumberger array - floating and sea-bottom electrode modes. The model is shown in the uppermost part of the figure. ....	52
Figure 5.1.3: The effect of fixing the water layer before inversion for pole-dipole array - floating and sea-bottom electrode modes. The model is shown in the uppermost part of the figure. ....	53
Figure 5.2.1: The effect of sea water resistivity (0.25, 0.5, 1.0 Ohm•m) for floating and sea-bottom dipole-dipole array. The model is shown in the uppermost part of the figure.....	54

Figure 5.3.1: The effect of seawater depth (1.0, 3.0, 5.0, 10.0 m)for floating electrode configuration with fixed and unfixed water layer - dipole-dipole array. The model is shown in the uppermost part of the figure. ....	56
Figure 5.3.2: The effect of variations in sea water depth (1.0, 3.0, 5.0, 10.0 m) for sea-bottom electrode configuration with fixed and unfixed water layer - dipole-dipole array.....	57
Figure 5.4.1: Mixed survey - single fracture zone outside the influence of the sea water (top) and two weak zones with one under the influence of sea water (bottom) - dipole-dipole array. ....	58
Figure 6.1.1: Location of resistivity lines at Kvitsøy.....	59
Figure 6.2.1: Inverted resistivity from multiple gradient array along profile 1 at Kvitsøy using RES2DINV, Standard inversion V/H filter 1.5 (upper) and Robust inversion V/H filter 1 (lower). Interpreted fractures in black dotted lines. ....	60
Figure 6.3.1: Inverted resistivity from multiple gradient array along profile 4 Kvitsøy. Upper: Floating electrodes, standard inversion, V/H = 1.5, interpreted fracture zones as dashed black lines. Middle: Floating electrodes, Robust inversion, V/H = 1. Lower: Sea-bottom electrodes, robust inversion, V/H = 1. ....	61
Figure 6.4.1: Inverted multiple gradient resistivity from profile 5 Kvitsøy without fixing water layer. From top: standard inversion V/H filter 1.0, robust inversion V/H filter 1, standard inversion V/H filter 1.5 and robust inversion V/H filter 1.5. ....	63
Figure 6.4.2: Inverted multiple gradient resistivity from profile 5 Kvitsøy with correct fixing water layer. From top: standard inversion V/H filter 1.0, robust inversion V/H filter 1, standard inversion V/H filter 1.5 and robust inversion V/H filter 1.5. ....	64
Figure 6.5.1: Real data from Kvitsøy measured with a multiple gradient array, (fixed water body: 3.5 m depth with 0.25 Ohm·m, starting at 217 m and ending at 280 m). ....	65
Figure 6.6.1: Profile 5 at Kvitsøy, robust inversion of different data multiple gradient array. From top: Modeled data without fracture zone, modeled data with fracture zone, measured data with no fix of water layer, measured data with fixed water layer and (bottom) measured data with fixed water layer and V/H filter 1.5.....	66

## TABLES

Table 2.1: Sea water resistivity (in Ohm·m) vs. temperature (in °C) and salinity in (g·kg <sup>-1</sup> ). 11	
Table 3.1: Technical specifications and protocol files (grid of points where resistivity measurements are made) for the forward modeling (provided by Thorleif Dahlin). ....	13

## 1. INTRODUCTION

Resistivity surveying is a method widely used in Norway for solving engineering and environmental problems. Since 2000, the Geological Survey of Norway (NGU) has performed various ERT surveys in order to characterize fracture zones in bedrock (Rønning, 2003; Rønning et al., 2003; Rønning et al., 2009; Ganerød et al., 2006; Dalsegg, 2012, Rønning et al. 2013). The theoretical response of such structures to ERT measurements has been studied and tested thoroughly by Reiser et al. (2009) as a part of an internship at NGU. However, this modeling procedure has been limited to dry land conditions. Although the use of resistivity measurements in marine environments is a low resolution technique compared to others (e.g. seismic), and despite difficulties undertaking such surveys, it is increasingly used in marine situations for reasons similar to those concerning dry land surveys. Rucker and Noonan (2013) used marine resistivity to map the Panama Canal, and Satriani et al. (2011) mapped coastal salt water intrusion in Southern Italy with resistivity tomography while Dahlin et al. (2014) incorporated underwater ERT in their investigations of a new line for the Stockholm Metro. The main reasons for this method becoming more and more popular in such settings are that it is robust, it is low-cost, it operates in conductive areas, and most importantly the interpreted images are a realistic representation of the subsurface, easily understood by other geoscientists.

In Norway, resistivity measurements in marine environment have already been tested in seawater in order to detect subsea fracture zones (Lile et al. 1994; Dalsegg, 2012). However, most of these data have been processed without taking into account the effect of sea water. In this report, and in a continuation to Reiser's work, we are trying to ascertain the conditions under which ERT can detect and characterize fracture zones in marine environments. It is common knowledge amongst geophysicists that sea water ERT surveys can be difficult to perform and interpret successfully since the geoelectrical methodology is being pushed to its limits. The method's exact limitations can only be investigated through modeling.

According to Reiser et al. (2009), when investigating fracture zones on land, the optimal arrays for this task are multiple gradient and dipole-dipole arrays. Other standard arrays have also proven to be somewhat successful in revealing vertical fracture zones in dry land conditions however, the presence of an extremely conductive medium (sea water) causes several of them to be inapplicable in marine environments. The implementation of these arrays results in high inversion instability which leads to low quality inversion results. This means that multiple gradient and dipole-dipole are most possibly our only options in marine ERT, between which the better results were obtained with the latter. The multiple gradient array configuration could also produce similarly successful results; however the dipole-dipole array appears to work much better than any of the other standard arrays when sea water is present, at least if we narrow down our expectations to zone detection only. The inherently low signal to noise ratio for this array may make it less suitable for actual marine resistivity surveys.

The forward modeling was done using two different programs. The first software was the specialized modeling program RES2DMOD x64 version 3.01.83 Plus (Loke 2002) for creating synthetic data. The majority of the modeling data was produced using arrays of 81 electrodes and 5.0 m spacing, and they were subsequently inverted without adding any artificial noise in order to have optimal conditions for testing the method's efficiency. The inversion was performed with RES2DINV x64 version 3.59.112 (Loke 2010) utilizing standard and robust inversion. These factors (no noise, and using robust inversion in some



cases) were chosen in order to overcome imaging problems caused by the presence of sea water. The second software used was DC2DPRO version 0.99 (Kim 2012), an independent software compiled and supplied to us by Dr. Jung Ho Kim of the Korean Institute of Geosciences and Mineral Resources (KIGAM). This software offers both modeling and inversion possibilities, in a similar manner to Loke's program. The models produced and inverted with DC2DPRO were performed by Dr. Panagiotis Tsourlos, an Associate Professor of Geophysics from the Aristotle University of Thessaloniki (AUn) who visited NGU from March 11th to 17th, 2013 for this purpose.

Our aim is to clarify the conditions and provide guidelines that need to be followed in order to maximize the chances of successful marine ERT surveys. Although the electrical resistivity method may be successful in dry land applications, this is not the case when sea water has been introduced. Rephrasing the aforementioned goal of this report, we are aiming to form rules which may help define whether ERT is advisable or not when trying to detect fracture zones below the sea-bottom.

## 2. WATER ERT MEASUREMENTS

There are two main modes by which resistivity techniques can be used in water surveys, and they differ simply in the placement of the electrodes. The first and relatively easy way is the floating electrode mode in which the electrodes are placed on the water surface with the help of floaters and are dragged along the measuring line (figure 2.1a). The second and more difficult way is the direct placement of electrodes on the sea-bottom where they are in direct contact with the underlying formation (figure 2.1b).

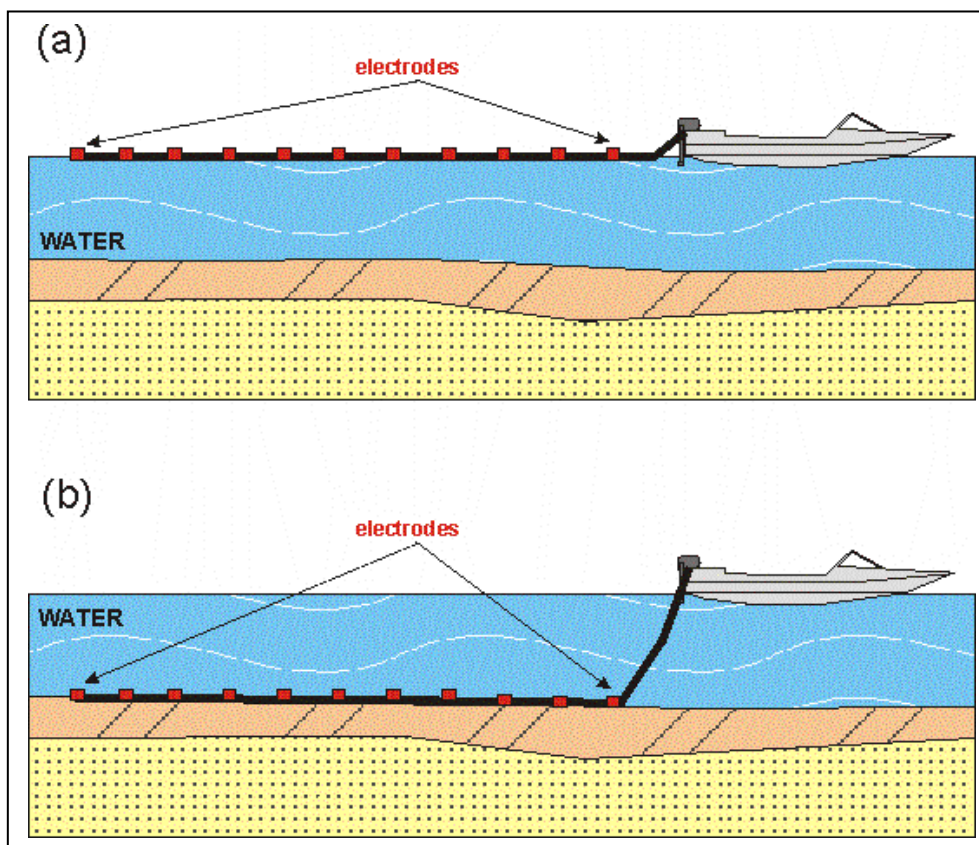


**Figure 2.1: Water Resistivity Surveying modes: (a) cable floating on the water surface and (b) cable at the sea-bottom (after Tsourlos et al. 2001).**

According to Tsourlos et al. (2001), floating electrode configurations have several advantages over sea-bottom electrode placement:

- It is easier to carry out the survey and consequently high data collection speed can be achieved.
- No software modification is required for interpreting the collected data sets: the water layer is treated as another "geological" layer of unknown or fixed resistivity.
- As a result this mode is ideal for mapping resistivity changes in the water-layer (i.e. changes in water conductivity, fresh-salt water interfaces etc.) and giving a relatively low-resolution image of sea-bottom geological formations, when and if this is required.

Yet, in many cases this mode is ineffective for mapping subsurface geological formations:

- In highly conductive water environments (sea water, saline water) this measuring mode cannot achieve adequate current penetration and thus usually fails to provide information about sea-bottom formations.
- Furthermore when the survey aim is to map sea-bottom formations as in our case, it usually fails to provide the required resolution. In such a case its performance is inversely proportional to the water layer thickness and (as mentioned above) it becomes worse in areas with a relatively conductive (sea) water layer.

To overcome the disadvantages described above, a mode using a cable laid at the sea-bottom is used (Fig 2.1b). The obvious advantage of the sea-bottom electrode mode is that the sensors are in direct contact with the target; as a result a better depth of investigation is expected, even in highly conductive areas. Furthermore the sea-bottom formations can be mapped with improved resolution. Therefore, this mode is superior for mapping subsea formations but on the other hand it has increased technical difficulties:

- special cables which can withstand increased stress have to be used;
- cable has to be positioned on the seafloor, and survey speed is reduced;
- to process data successfully, the thickness of the water layer and the resistivity of the water must be known, and so these data have to be monitored during the survey:

Resistivity interpretation software has to be adapted in order to be able to cope with the existing water layer above the survey line, and topography corrections have to be considered in areas of rough bottom terrain. RES2DINV offers this kind of modification for sea-bottom surveys.

<i>Temperature</i>	<i>Salinity / (g · kg<sup>-1</sup>)</i>				
°C	20	25	30	35	40
	<i>R / (Ohm · m)</i>				
0.....	0,5731	0,4679	0,3964	0,3441	0,3044
5.....	0,4963	0,4055	0,3438	0,2989	0,2647
10.....	0,4348	0,3557	0,3018	0,2626	0,2327
15.....	0,3854	0,3155	0,2677	0,2331	0,2067
20.....	0,3447	0,2823	0,2398	0,2089	0,1853
25.....	0,3108	0,2547	0,2164	0,1886	0,1674

**Table 2.1: Sea water resistivity (in Ohm·m) vs. temperature (in °C) and salinity in (g·kg<sup>-1</sup>).**

Table 2.1 presents sea water resistivity for a variety of temperatures and salinities. From this table we can see that sea water resistivity can range between 0.16 and 0.57 Ohm·m. However,

a value close to  $0.25 \text{ Ohm}\cdot\text{m}$  is considered a good mean approximation for modeling purposes in the Norwegian marine environment.

Figure 2.2 presents the inherent problem connected with sea-bottom ERT. In ERT measurements, it is essential to insert as much electrical current into the ground as possible. As we see in figure 2.2a, with land ERT the ground is more conductive than the air. In this case, the electrical current will flow through the ground due to the insulating effect of the air. Figure 2.2b illustrates the situation when performing sea-bottom ERT. In this case, the layer above the ground (sea water) is more conductive than the ground, drawing away a significant part of the electrical current. This represents the main disadvantage of sea-bottom ERT, and should be taken into consideration whenever performing such measurements.

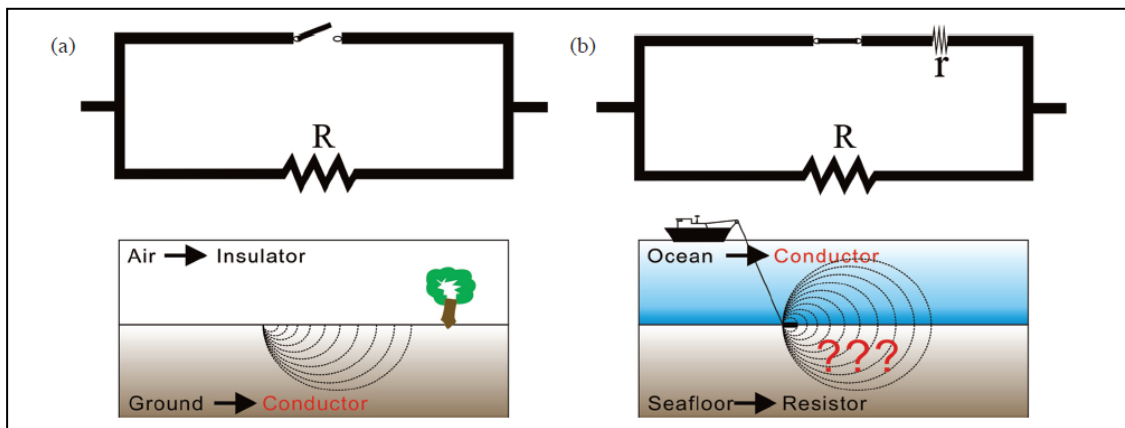


**Figure 2.2: Diagram illustrating the difference between land and sea-bottom ERT. The electrical current is conducted entirely through the ground with land ERT (a) while it passes through both resistors with sea-bottom ERT (b) (Chiang et al. 2012).**

In this report, we test both floating and sea-bottom electrode modes in order to highlight the aforementioned advantages and disadvantages of each configuration.

### 3. ELECTRODE CONFIGURATIONS

Investigating fracture zones embedded in resistive bedrock is a common engineering problem that can be successfully solved with the application of ERT measurements. Reiser et al. (2009) have shown that the most successful arrays for this purpose are dipole-dipole arrays and multiple gradient arrays. Considering that our effort is focused on imaging a vertical or sub-vertical structure such as a weak zone, dipole-dipole and multiple gradient arrays are intuitively our preferred choices.

A dipole-dipole array performs depth sounding by moving the potential dipole to several distances from the current dipole (figure 3.1). This array is not of the nested type, i.e. the potential dipole is outside the current dipole, causing it to have a small signal to noise ratio, and its vertical resolution of horizontal structures is poor. In our case however, a Dipole-dipole array offers two major advantages: we can achieve slightly higher depth penetration than for nested arrays, therefore following a fracture throughout its depth; and it is sensitive to vertical resistivity boundaries such as a fracture zone. The distance "a" is normally kept constant throughout the measurement process but increasing this value helps us to gather data of better quality.

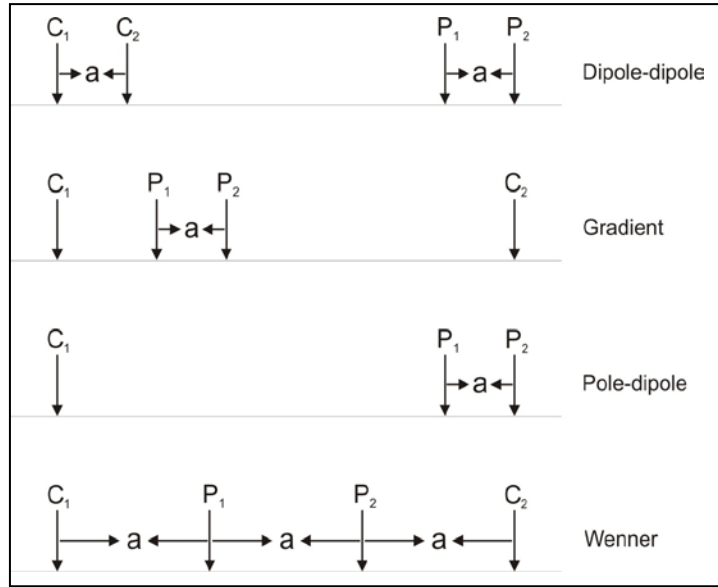


**Figure 3.1: Electrode configurations for dipole-dipole, multiple gradient, pole-dipole and Wenner electrode arrays.**

For the multiple gradient configuration, the potential electrodes have a constant separation and are moved along the line between the current electrodes, i.e. it is a nested array. This setting offers the advantages that both the signal to noise ratio and data density are high. Imaging at greater depths requires an increase of the distance "a".

In this study, we have also tested the pole-dipole and the Wenner configurations (figure 3.1).

In order to create optimal conditions for testing the efficiency of marine ERT measurements, we have used array protocols constructed by Torleif Dahlin of Lund University, Sweden. The array most commonly used by NGU when performing ERT measurements is the Lund setting (a multiple gradient array) developed by Dahlin, which incorporates 81 electrodes with either 5 or 10 meters spacing. Therefore all our model arrays simulate this particular electrode setting and hence imitate real conditions. The main features of the arrays used in this modeling procedure can be seen in table 3.1. All of the arrays contain 81 electrodes with 5 m spacing, with a total length of 400 m. Both standard and robust inversion techniques were used, and other parameters (such as Vertical Horizontal (V/H) filter and damping factors) were also investigated in order to monitor their effect on the inversion process

<i>Electrode Configuration</i>	<i>No. of data points</i>	<i>No. of data levels in pseudosection</i>	<i>Name of protocol files for the modeling</i>
Dipole-dipole.....	1525	15	DipolDipol4LS_5m
Multiple gradient.....	1416	15	Grad4XLS8plus_5m
Pole-dipole.....	3173	21	PolDipol4LSplus_5m
Wenner.....	445	15	WennerXLS_5m

**Table 3.1: Technical specifications and protocol files (grid of points where resistivity measurements are made) for the forward modeling (provided by Torleif Dahlin).**

## 4. RESULTS

In the following section the modeling results obtained while varying important geophysical and inversion parameters are presented. Note that for sea-bottom electrodes, only the subsea resistivity image is shown.

### 4.1 Testing the response of several arrays to a simple model

#### Model description

Before using more complex models, we have tested the performance of several common ERT arrays with a simple sea-bottom model. For this purpose we have computed the response of a 15 m thick vertical fractured zone of 50 Ohm•m which is located in a “healthy” 1000 Ohm•m resistive bedrock. This model is overlain by 1 m of sea water whose resistivity is 0.25 Ohm•m. This model could correspond to a low resistivity fracture zone infiltrating a moderately resistive crystalline bedrock. We have chosen limited sea water thickness (1.0 m depth) and a resistivity contrast between the fractured zone and surrounding environment similar to real conditions (1000/50 i.e. 20). The arrays that have been tested are those using multiple gradient, dipole-dipole, pole-dipole and Wenner configurations.

#### Modeling results

Figure 4.1.1 presents the results of standard constrain (L2 norm) inversion while figure 4.1.2 presents the results of robust inversion (L1 norm, Loke 2010). There is considerable difference in quality between the two inversion method results. This is to be expected since our initial model contains a vertical structure; however it seems that for some array configurations robust inversion produces better modeling results.

When using standard constrain inversion, dipole-dipole and pole-dipole configurations present similarly successful results while multiple gradient and Wenner configurations produce only a slight indication of the weak zone. Of the two less successful arrays, the multiple gradient configuration seems to be somewhat closer to detecting the zone than the Wenner configuration, which displays a very weak response. When using robust inversion, results improve for all arrays, especially with the multiple gradient configuration which produces a very clear indication of the weak zone compared to its results with standard inversion (figure 4.1.1). The Wenner configuration does not give satisfactory results for either of the inversion methods. Bearing in mind that this model uses optimal conditions, we can disqualify this configuration from further testing.

Focusing on the arrays that actually succeed in detecting the fracture zone, it can be clearly seen that using robust inversion, all three arrays manage to detect the fracture zone but with different characteristics. Multiple gradient and pole-dipole arrays produce resistivities closer to those of the model (1000-1800 Ohm•m for the bedrock, 50-100 Ohm•m for the zone) but fail to reproduce the true dimensions of the zone. The dipole-dipole array on the other hand fails to produce resistivity values similar to the model but does manage to approximate the initial model geometry.

#### Summary

As in the case of dry land measurements (Reiser et al. 2009), dipole-dipole and multiple gradient configurations show the best results for mapping sea-bottom fracture zones when compared with other sensor configurations. The pole-dipole configuration produces similar results, and so is included in further investigations of this study. Multiple gradient and pole-dipole configurations produce a better estimate of the actual model resistivities but fail to



reproduce the true dimensions of the zone. In assessing the results we should bear in mind that detecting the presence and location of a fracture zone is more important in engineering problems than determining its actual resistivity properties.

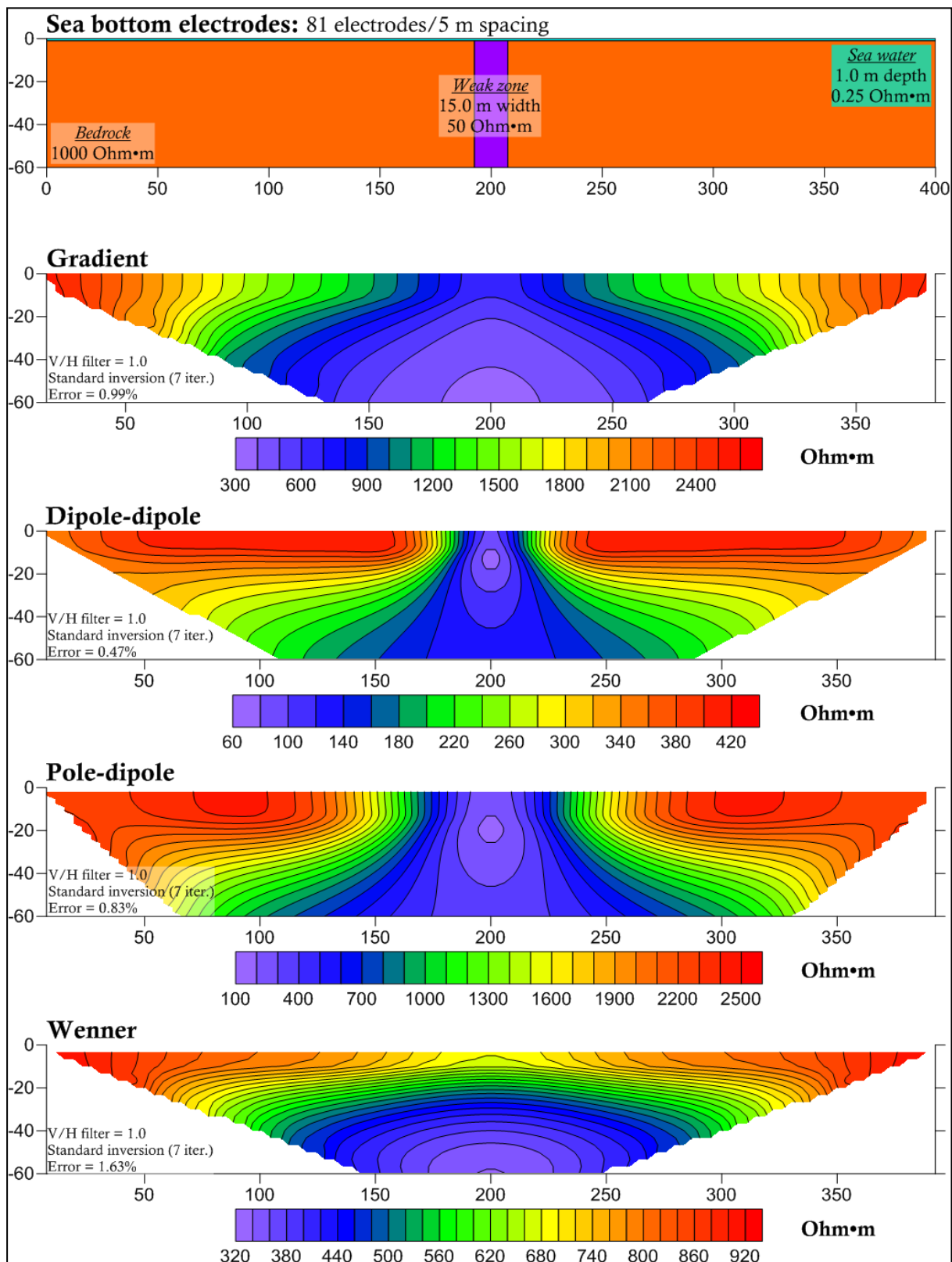


Figure 4.1.1: Testing several sea-bottom electrode arrays on a simple fracture zone model with standard constrain inversion. The model is shown in the uppermost part of the figure.

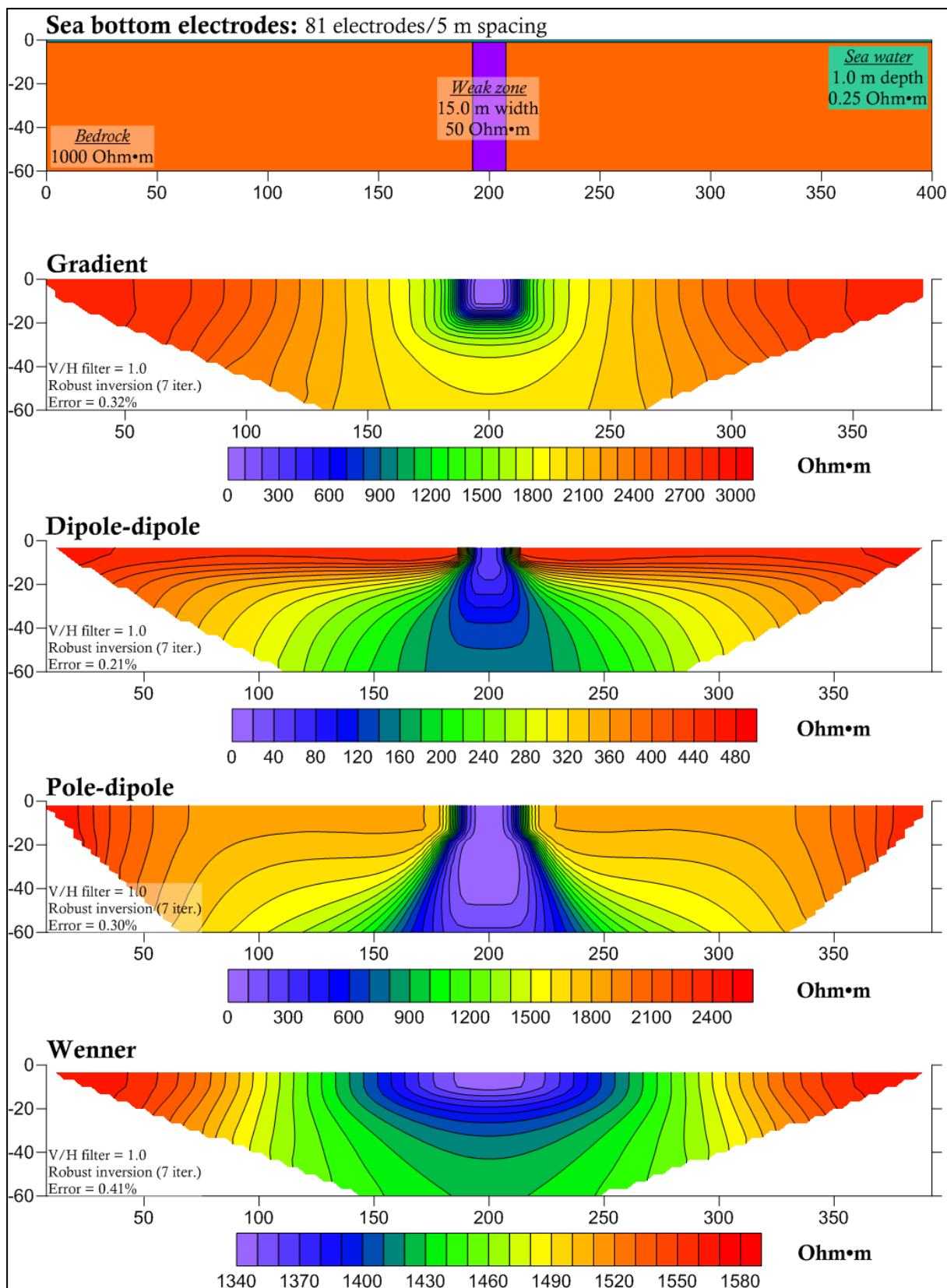


Figure 4.1.2: Testing several sea-bottom electrode arrays on a simple fracture zone model with robust inversion. The model is shown in the uppermost part of the figure.

## 4.2 The effect of fixing the water layer resistivity and depth

### Model Description

In order to show the importance of fixing the water layer before performing robust inversion on floating electrode configuration data, we have slightly modified the model used in the previous section. A 15 m wide fracture zone of 50 Ohm•m resistivity was modeled within a 1000 Ohm•m bedrock, overlain by a sediment layer of 30 Ohm•m resistivity and 2.0 m depth, and a sea water body of 0.25 Ohm•m resistivity and 1.0 m depth, both for sea-bottom and floating electrode modes. For sea-bottom electrodes, it is not possible with RES2DINV software (Loke 2010) to run inversion without fixing the overlying water resistivity and thickness. The floating electrode synthetic data were inverted in four different ways: inversion without any layer fixing; inversion with realistic values of sea water resistivity and depth (0.25 Ohm•m and 1.0 m); inversion with unrealistic sea water resistivity value (0.20 Ohm•m) and finally inversion with unrealistic sea water depth value (2.0 m) but realistic water resistivity (0.25 Ohm•m). This procedure was repeated for dipole-dipole (figure 4.2.1), multiple gradient (figure 4.2.2) and pole-dipole configurations (figure 4.2.3).

### Modeling results

The first observation we can make from figures 4.2.1-4.2.3 is that fixing realistic sea water properties significantly improves the depiction of the detected fracture zone. Fixing the water layer properties with realistic values differentiates the inversion beneath the water layer such that the fracture zone becomes clearer in resistivity value from its surrounding environment and its observed width is closer to the modeled one. If one decides not to fix the water layer, the fracture zone's response becomes wider and the water layer causes the calculated resistivity values to vary less. If we extend this observation to less convenient conditions that may be found in the field, we can say that correctly fixing the water layer can turn a poor assessment into a successful one.

The most important result coming out of figures 4.2.1-4.2.3 however comes from the two lowermost cross sections. These two results indicate the importance of having an accurate knowledge of water layer properties before fixing them in the inversion process. Let us imagine the case where we perform a floating electrode survey somewhere. Let us also assume that our sea-bottom topography monitoring is not as accurate as we would like it to be and that after completing our survey, we sample some sea water in-situ in order to measure its resistivity back at the lab. Sea water of a medium salinity at 5 °C has a resistivity of approximately 0.25 Ohm•m. Measuring the properties of the same sample at the lab in a temperature of 20 °C will result in a lower resistivity of 0.20 Ohm•m (table 2.1). As we can see, such a slight difference in water properties can have considerable consequences when fixing the water layer resistivity. A similar effect also arises from using an incorrect sea water depth but to a lesser extent, as can be seen in the lowermost cross sections of figures 4.2.1-4.2.3.

### Summary

Accurate monitoring of sea water resistivity and sea-bottom topography is essential when performing floating electrode mode measurements. Slight differences in measurements of these values may lead to severely misleading inversion results. Small differences result in inconsistent models and a general instability of the inversion process. This effect is even more severe with sea-bottom electrode measurements. RES2DINV does not offer the possibility of inverting marine data without any fixing. In either case (with or without fixing), if ERT measurements are to be applied in a marine environment, special care should be taken with the sampling of sea water and with monitoring the bathymetry of the sea-bottom. When

performing floating electrode surveys, it is better to invert without any fixing at all rather than using uncertain fixing values. Unfortunately, this is not an option for sea-bottom electrode surveys with the RES2DINV software (Loke 2010).

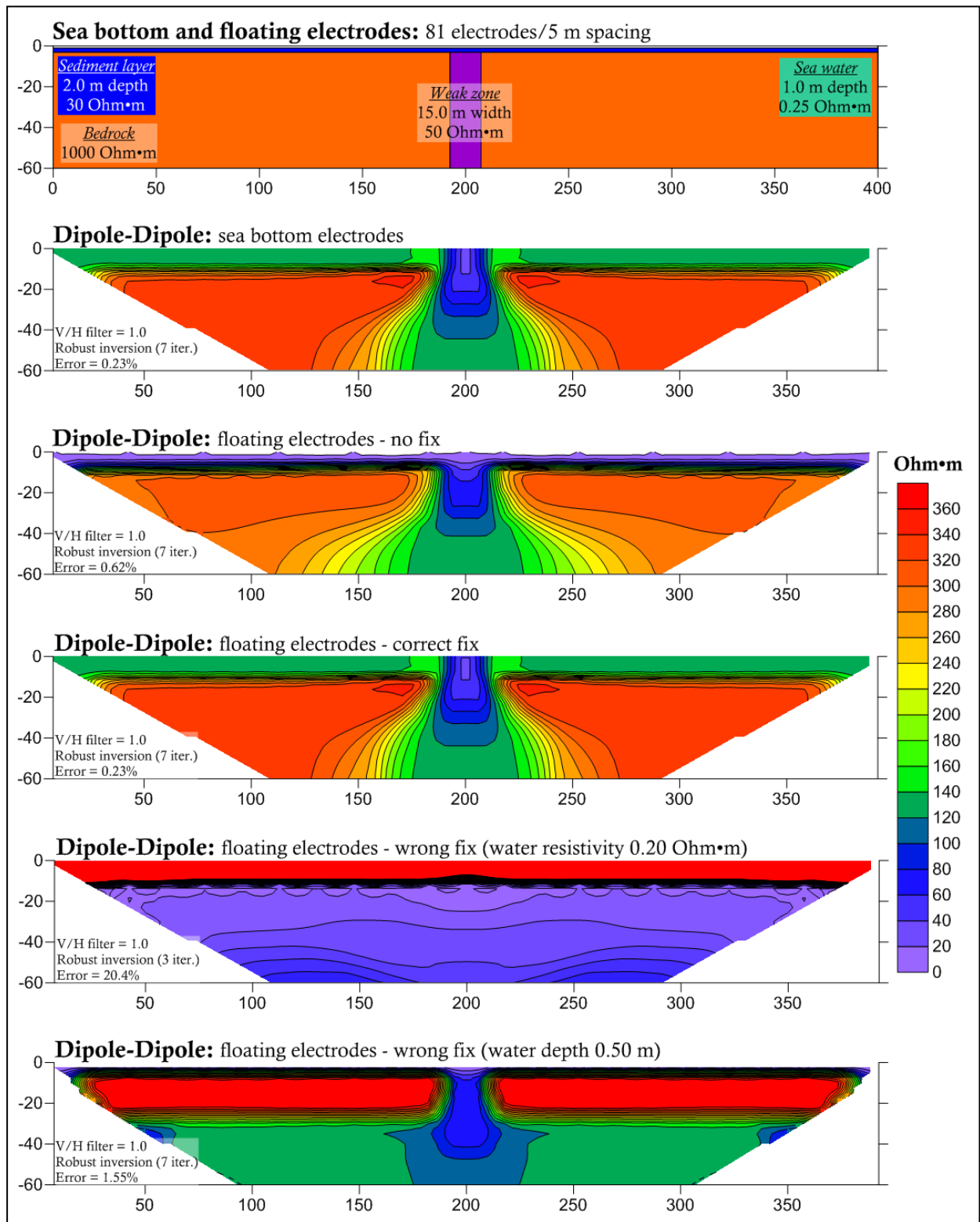


Figure 4.2.1: Effect of fixing the water layer before robust inversion for dipole-dipole array - sea-bottom and floating electrode modes. The model is shown in the uppermost part of the figure.

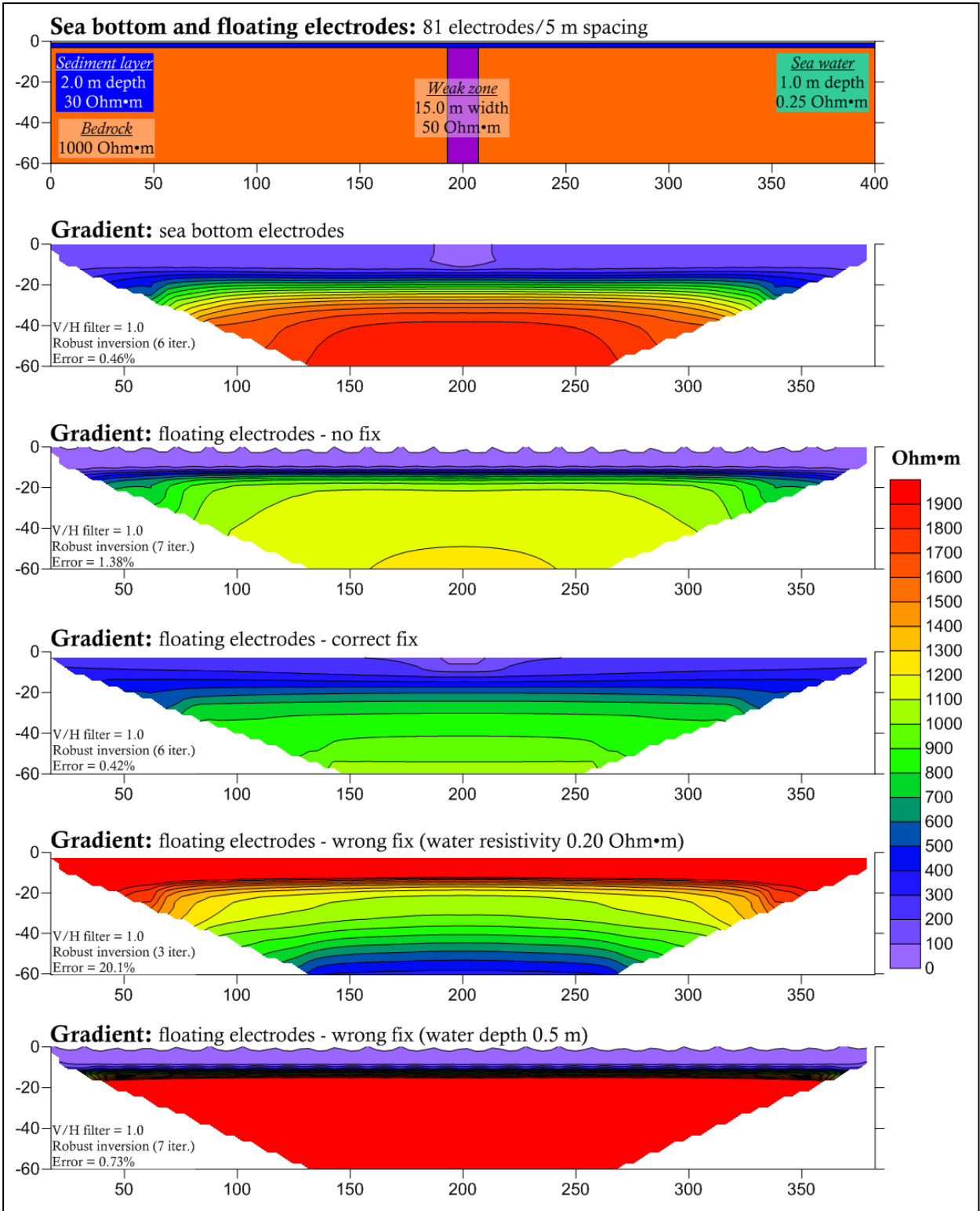


Figure 4.2.2: Effect of fixing the water layer before robust inversion for multiple gradient array - sea-bottom and floating electrode modes. The model is shown in the uppermost part of the figure.



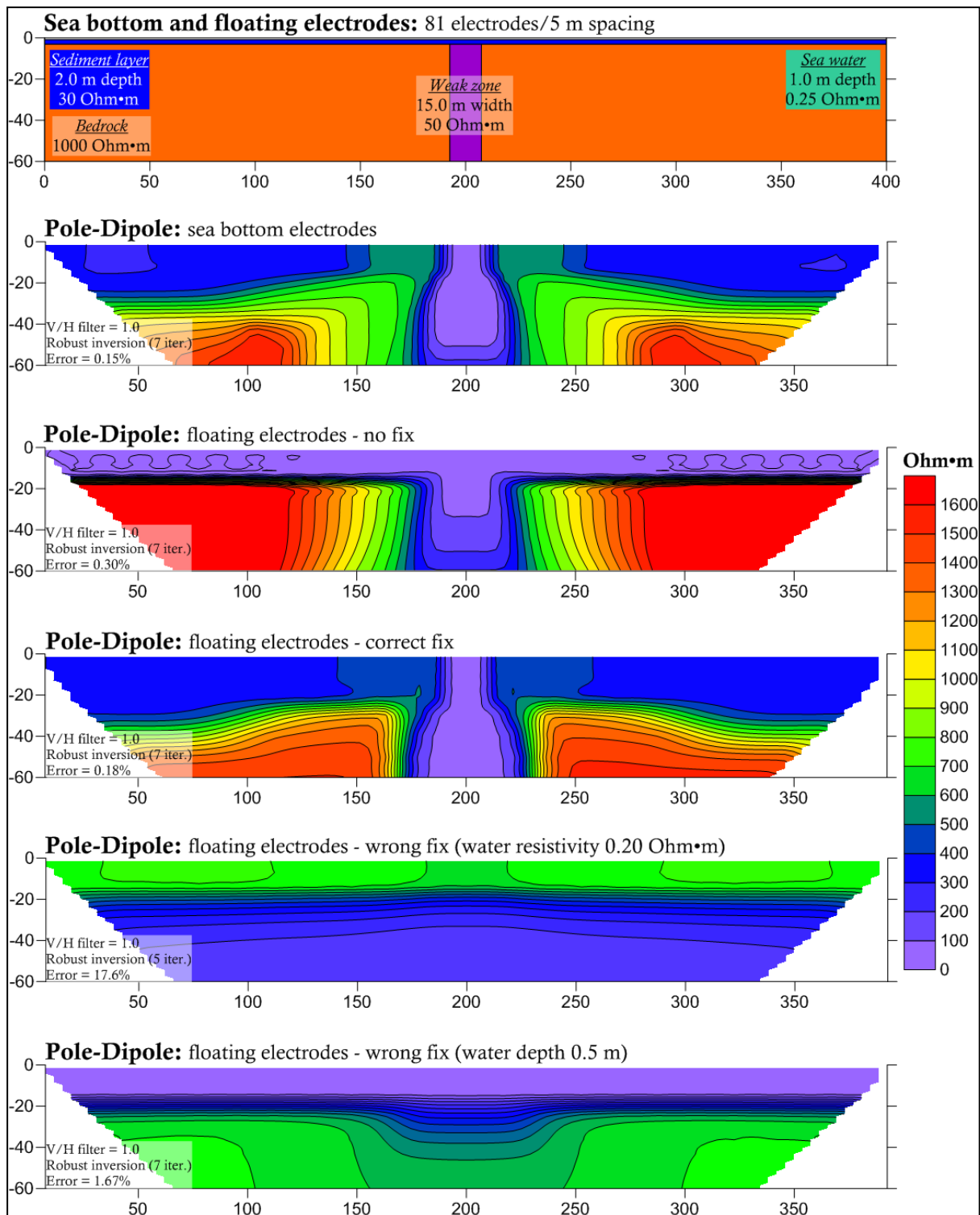


Figure 4.2.3: Effect of fixing the water layer before robust inversion for pole-dipole array - sea-bottom and floating electrode modes. The model is shown in the uppermost part of the figure.

### 4.3 Effect of variations in sea-water resistivity

#### Model description

In order to document the effect of the sea water resistivity on sea-bottom electrode surveys, a 15 m thick fracture zone of 50 Ohm•m has been modeled inside a 1000 Ohm•m bedrock. The sea water depth overlying this setting is 1.0 m, while its resistivity takes values of 0.25, 0.5 and 1.0 Ohm•m. The resistivity of the sea water depends on a series of independent factors such as salinity and temperature. In this case, we have chosen to use a resistivity of 50 Ohm•m for the weak zone in order to imitate a fracture inside crystalline bedrock.

#### Modeling results

Figures 4.3.1, 4.3.2 and 4.3.3 present the results of this modeling procedure for dipole-dipole, multiple gradient and pole-dipole arrays respectively. It is evident that by increasing the resistivity of the overlying sea water layer, the resolution is also increased. More current is able to flow through the subsea area, therefore all the inversion results gradually approach the modeled values. Dipole-dipole (figure 4.3.1) and pole-dipole (figure 4.3.3) arrays show similar behavior in their inversion results. As the sea water resistivity increases, the calculated bedrock resistivity values increase to approach the 1000 Ohm•m modeled value. Those for the multiple gradient array on the other hand (figure 4.3.2) move in the opposite direction, starting from excessive resistivity values and decreasing to approach the modeled bedrock resistivity as the sea water resistivity increases. From our models we can say that with 1 Ohm•m of water resistivity and 1 m of sea depth our calculated values begin to converge with our modeled ones. However, despite the good convergence of resistivity values, the multiple gradient array fails to reproduce the depth of the weak zone. Therefore, we will not continue with multiple gradient modeling from this point on.

#### Summary

Generally we can say that warmer and more saline waters reduce the method's resolution capability, while colder and less saline conditions increase the resolution and hence improve our chances of detecting subsea fracture zones in their true extent and dimensions. For example, an area of known fresh water intrusion which decreases the salinity of the sea water might point towards choosing sea-bottom ERT as the prospection method. Dahlin et al. (2014) have verified this by performing marine ERT in an area where a new line for the Stockholm metro will be constructed. For this survey they have used the pole-dipole array and have monitored the water properties in detail. In most cases they had to deal with water resistivities ranging between 1.0 and 2.0 Ohm•m while the depth was relatively small, which posed problems during the inversion procedure and eventually led to the detection of several weak zones. To improve the resistivity inversion quality, they measured seawater resistivity and depth and fixed these values during inversion. If we decide that ERT could yield successful results in a marine environment, the best time to carry out measurements would be during the winter.

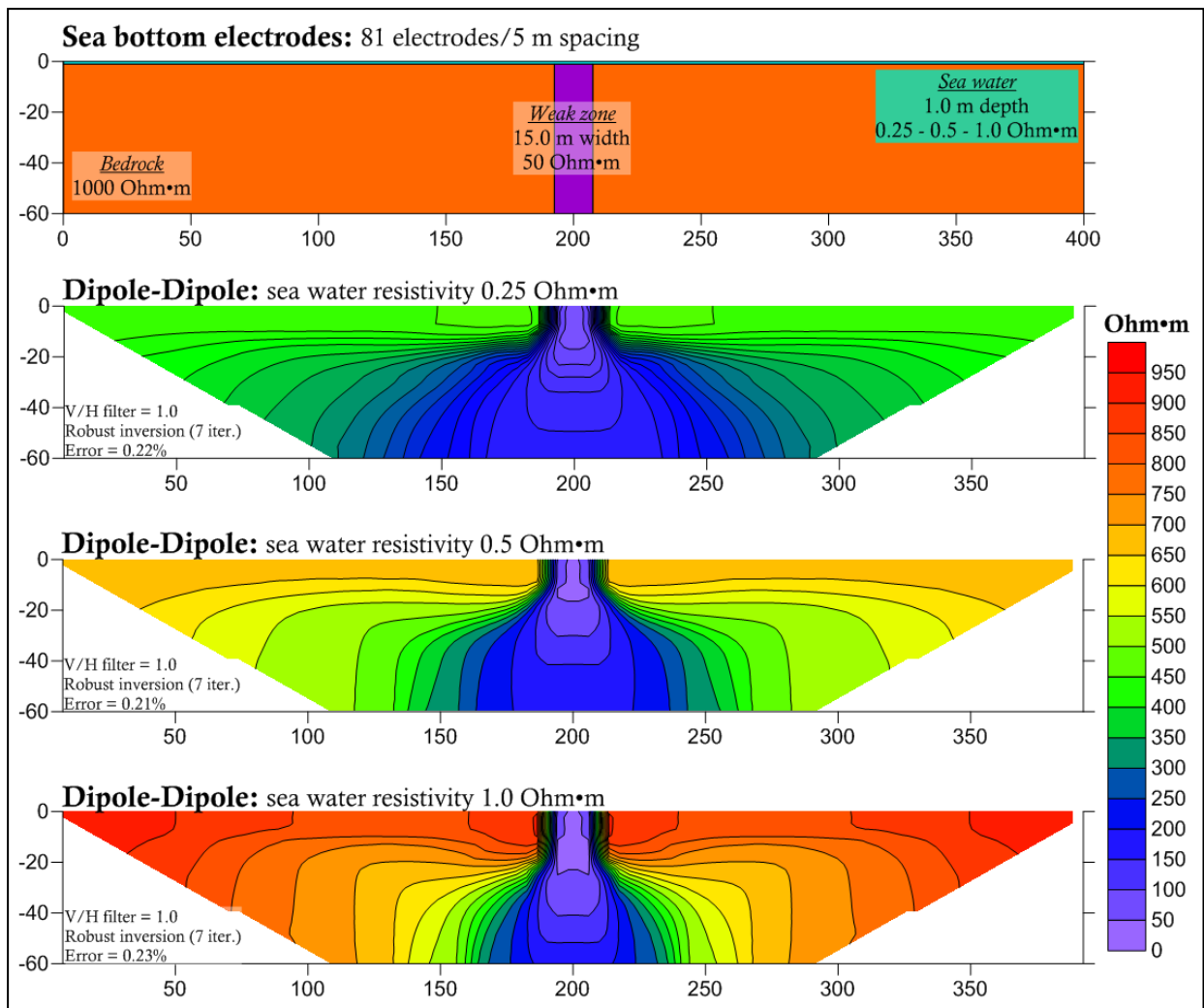


**Figure 4.3.1:** The effect of variations in sea water resistivity (0.25, 0.5, 1.0 Ohm·m) using sea-bottom dipole-dipole electrode array, robust inversion and common color scale. The model is shown in the uppermost part of the figure.

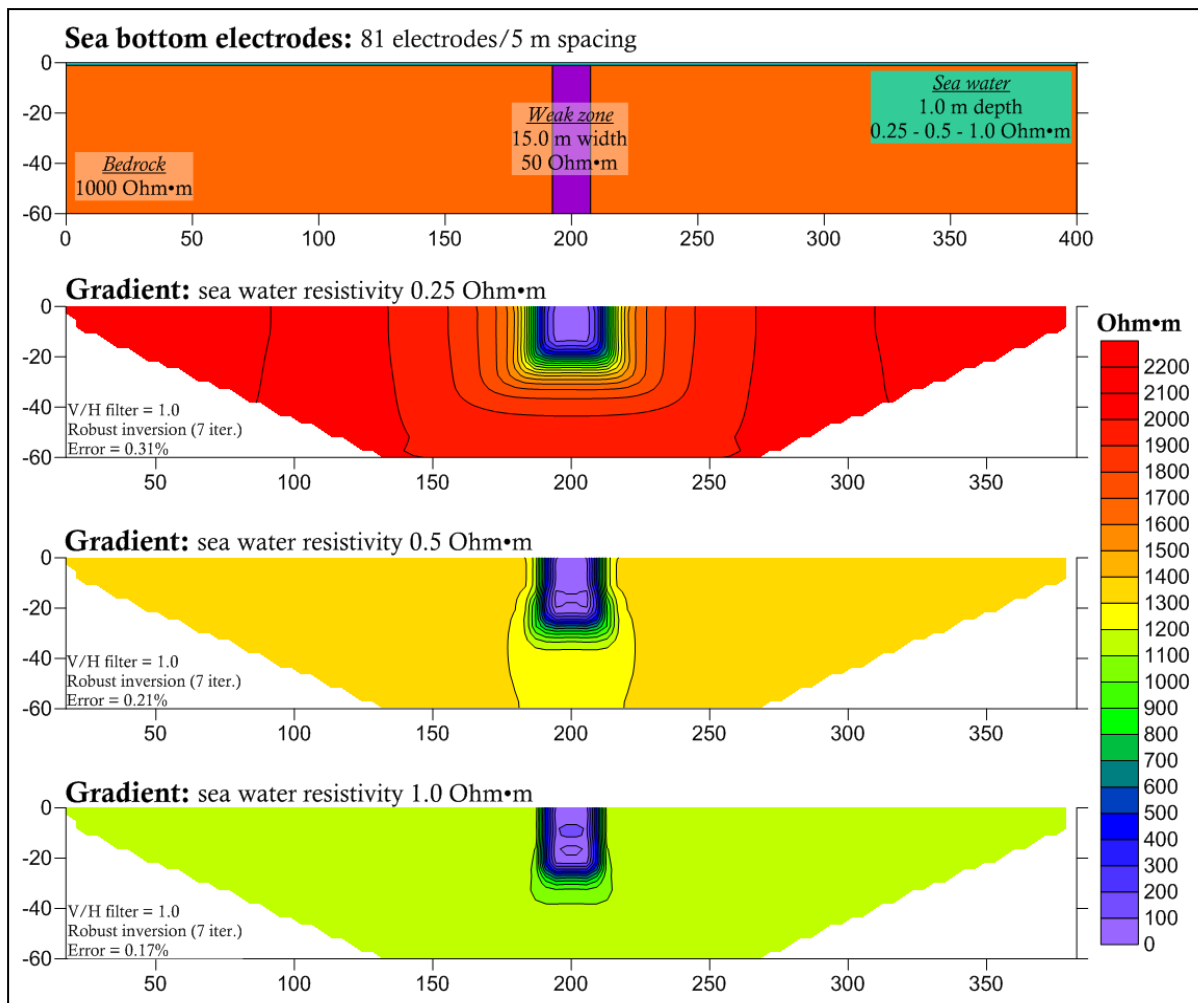


**Figure 4.3.2: The effect of variations in sea water resistivity (0.25, 0.5, 1.0 Ohm·m) using a sea-bottom multiple gradient electrode array, robust inversion and common color scale. The model is shown in the uppermost part of the figure.**

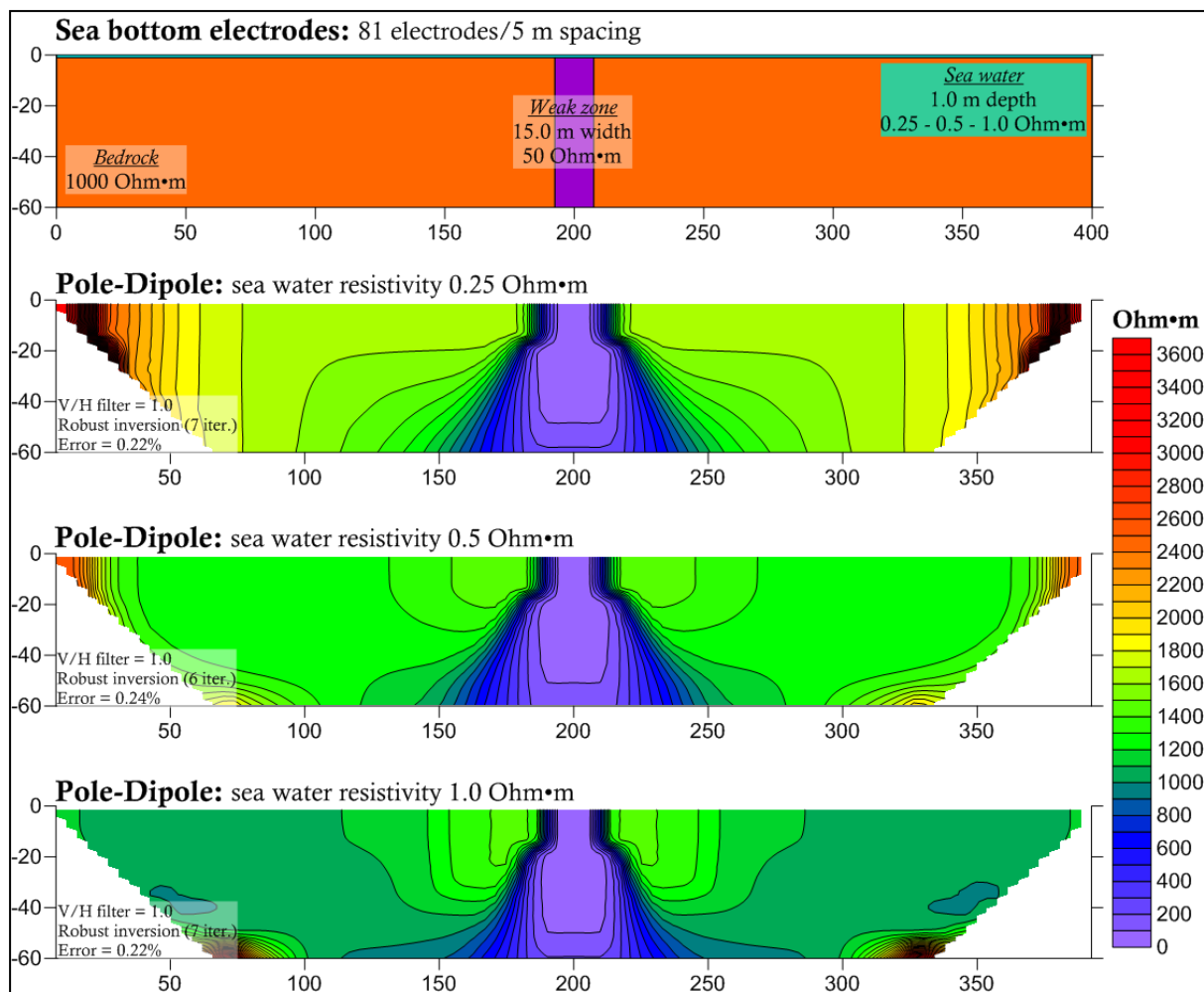


**Figure 4.3.3: The effect of variations in sea water resistivity (0.25, 0.5, 1.0 Ohm·m) using a pole-dipole sea-bottom electrode array, robust inversion and common color scale. The model is shown in the uppermost part of the figure.**

#### 4.4 The effect of variations in sea-water depth

##### Model description

With this model, we investigate the effect of sea water depth on both sea-bottom and floating electrode configurations, and for both dipole-dipole and pole-dipole array configurations. The model underneath the sea-bottom consists of a 15.0 m wide fracture zone of 50 Ohm·m resistivity within a 1000 Ohm·m bedrock. The sea depths tested for both sea-bottom ERT and floating electrode ERT are 1.0, 3.0, 5.0, 10.0 and 50.0 m. In all cases the water resistivity is set to 0.25 Ohm·m. Figure 4.4.1 presents the dipole-dipole results for sea-bottom ERT, 4.4.2 the results for unfixed water layer floating electrode configuration and 4.4.3 the same results for a fixed water layer. Figure 4.4.4 presents the same model configuration for pole-dipole measurements with electrodes at sea-bottom and with a fixed water layer.

##### Modeling results

If we examine the results for the dipole-dipole array and robust inversion, the first general observation to be made is that the sea-bottom electrode mode produces better results than



floating electrode mode, especially as the depth increases. This is of course due to the operational advantage of sea-bottom ERT which has its electrodes in immediate contact with the underlying formations.

Further comparison between the two configurations reveals a series of similarities which demonstrates how sea water affects our resolving ability. First and most important is the sea depth at which both modes fail to detect the fracture zone. Figure 4.4.1 indicates that even at 10.0 m sea water depth there is still some indication of the weak zone, although with a resistivity contrast of only 2.5 (100 Ohm•m in bedrock/40 Ohm•m in zone). In the case of 1.0 m sea water depth, this contrast is about 7.5 (300 Ohm•m in bedrock/40 Ohm•m in zone), dropping to 3 (120 Ohm•m bedrock/40 Ohm•m zone) with an addition of only 2.0 m of water. This also demonstrates the loss of current penetrating the ground when the water layer above is increased in depth, indicated by the lower resistivity values calculated by the inversion. For this particular configuration, beneath a depth of 10.0 m, the fracture zone cannot be detected.

Similar results may also be noted in figures 4.4.2 and 4.4.3 where the zone's response is lost somewhere below 5.0 m of sea depth. It is also very important to note the significant improvement of results when fixing the water layer prior to inversion. This leads to results which are very similar to the sea-bottom electrode configuration. At 5.0 m depth, the fracture zone may be already detectable but the calculated resistivity contrast between fracture zone and bedrock is small (less than 1/2). After fixing the layer, the zone becomes more visible while the calculated resistivity contrast is more pronounced and reaches a value of 1/3. A significant decrease of calculated resistivities with depth may also be noted for the floating electrode mode, as with the sea-bottom mode.

Another feature common to both cases is the loss of resolution with depth. The limit for sea-bottom ERT drops from ~40 m to ~15 m, while for floating electrodes the limit is somewhat smaller (~35 m to 10 m). Beneath 25 m depth for sea-bottom ERT, the anomaly assigned to the weak zone widens and the inversion fails to contain the lower resistivities within the modeled dimensions. In the case of floating electrodes this limit lies at about 15 m.

Figure 4.4.4 shows that similar responses are to be expected for small water depths for sea-bottom electrode ERT using pole-dipole array. However, as the depth increases the inversion becomes unstable and the calculated resistivities take on unreasonably high values. It can be noted that with increasing water depth, the pole-dipole array becomes rapidly inapplicable. At 5 m depth, calculated resistivities are already 10 to 20 times greater than those of the model, while at 10 m depth the result is completely unrealistic. Therefore, we can discard this array as well and we continue our modeling using only dipole-dipole arrays.

### **Summary**

Setting a general depth down to which ERT is reliable is not a simple task. Factors such as resistivity contrast between the weak zone and bedrock, sea water resistivity, and the presence and thickness of an overburden layer strongly affect the results. However we believe that sea-bottom bathymetry that exceeds 10.0 m of depth should disqualify sea-bottom ERT as a prospection method. The general sea depth beyond which floating electrode mode ERT no longer gives satisfying results should be set to 5.0 m.

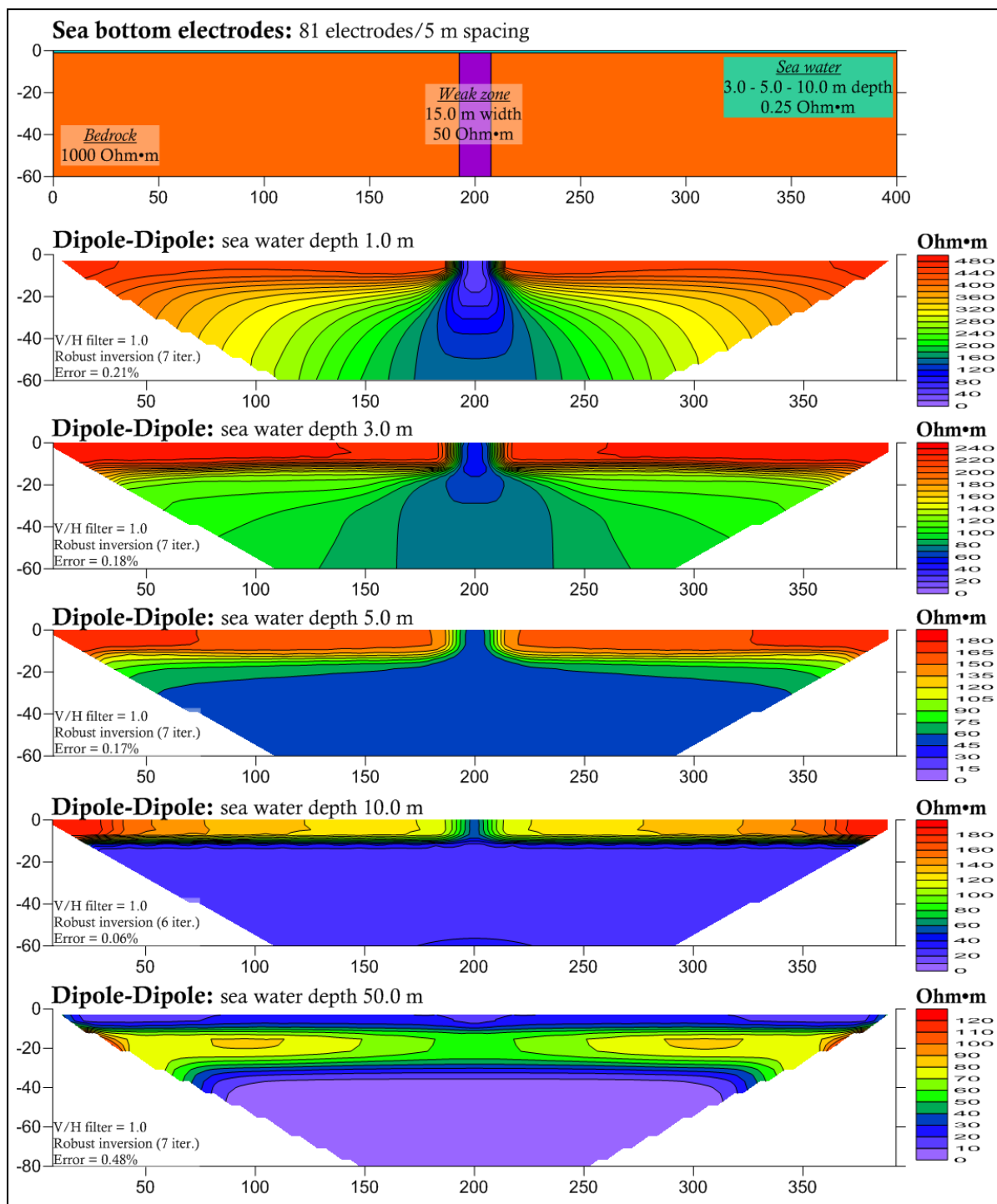


Figure 4.4.1: The effect of variations in sea water depth (1.0, 3.0, 5.0, 10.0, 50.0 m) using a sea-bottom dipole-dipole electrode array and robust inversion. The model is shown in the uppermost part of the figure.

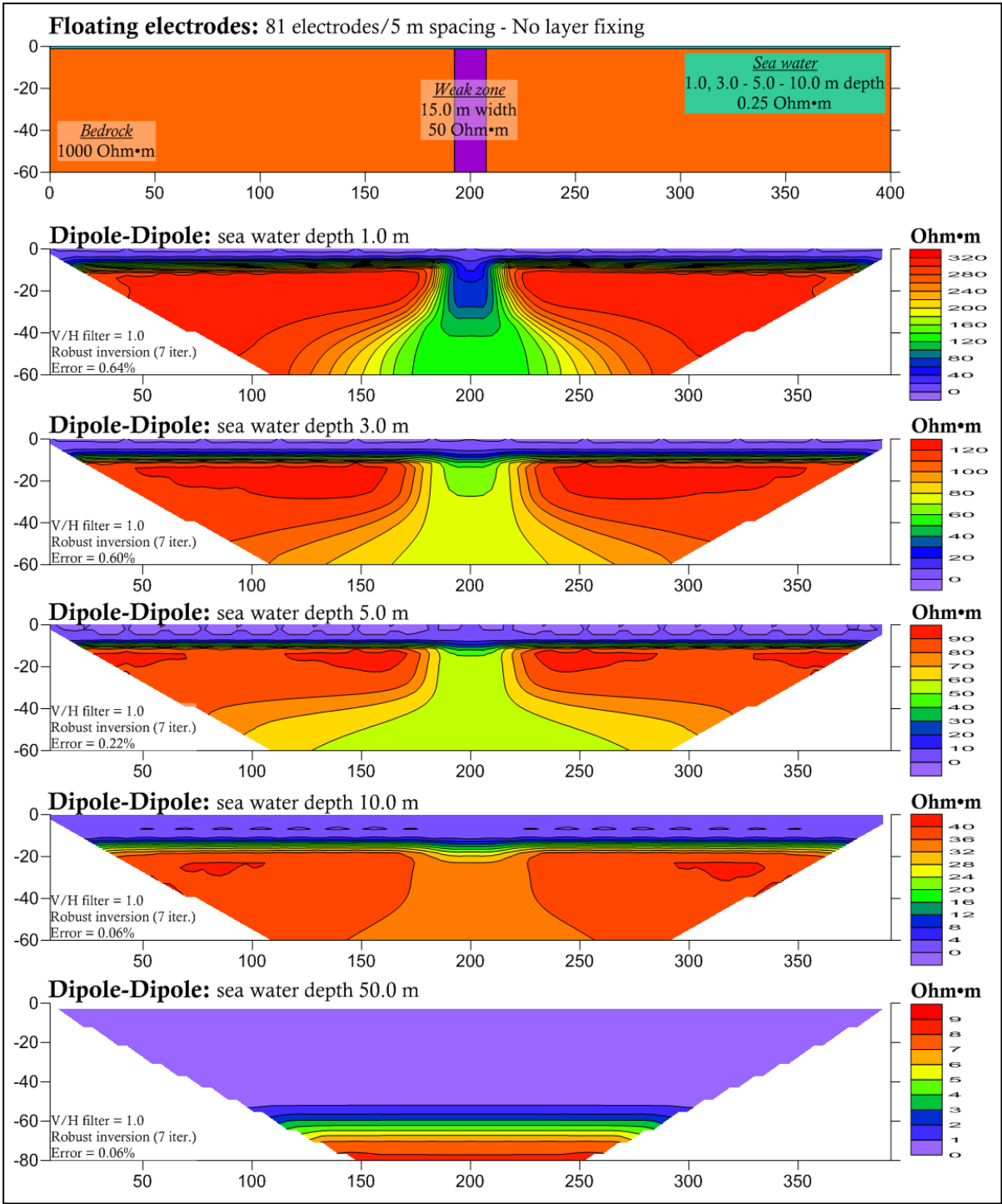


Figure 4.4.2: The effect of variations in sea water depth (1.0, 3.0, 5.0, 10.0, 50.0 m) for floating electrode configuration without any layer fixing, dipole-dipole array and robust inversion.

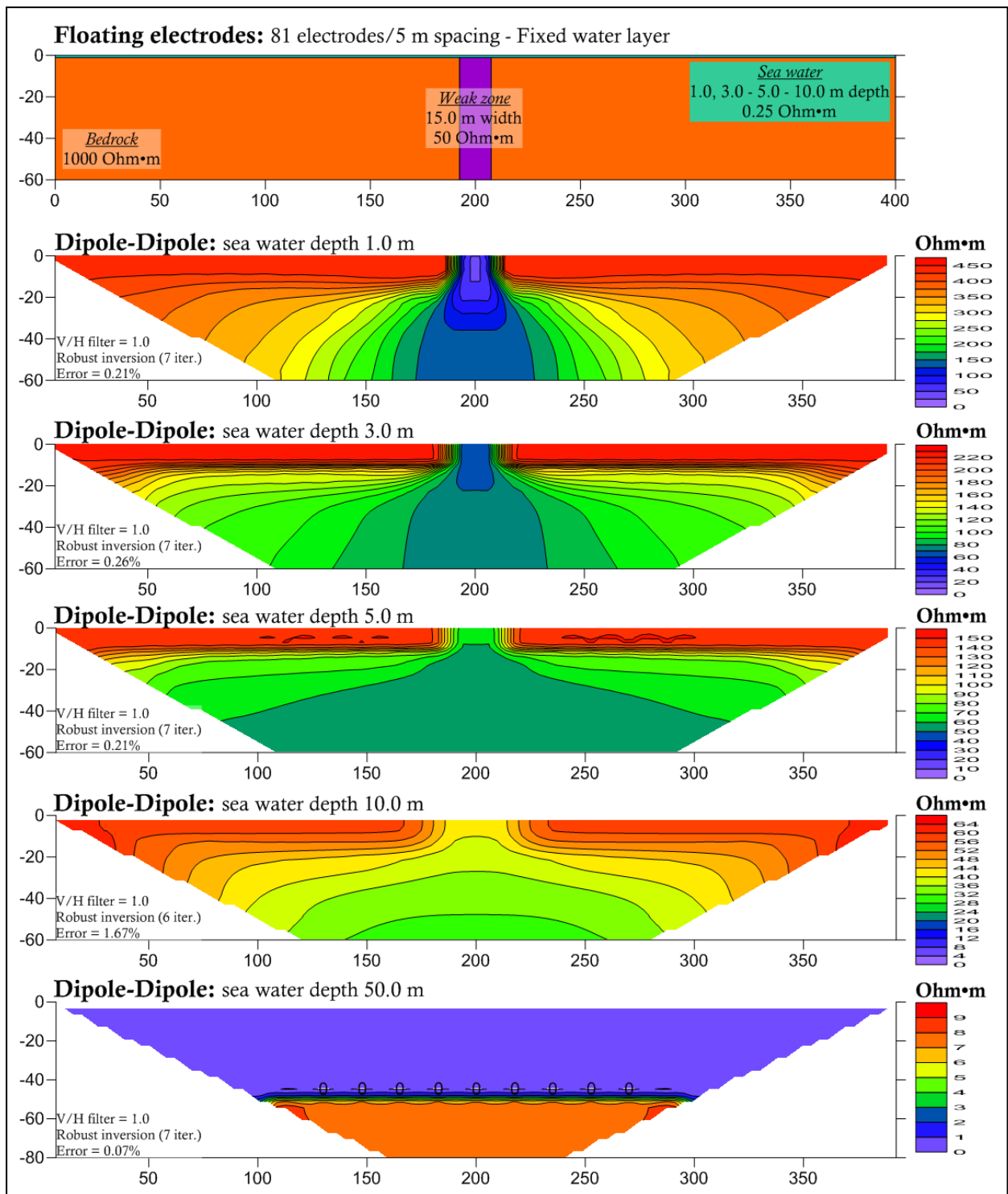


Figure 4.4.3: The effect of sea water depth (1.0, 3.0, 5.0, 10.0, 50.0 m) for floating electrode configuration with fixed water layer, dipole-dipole array and robust inversion.

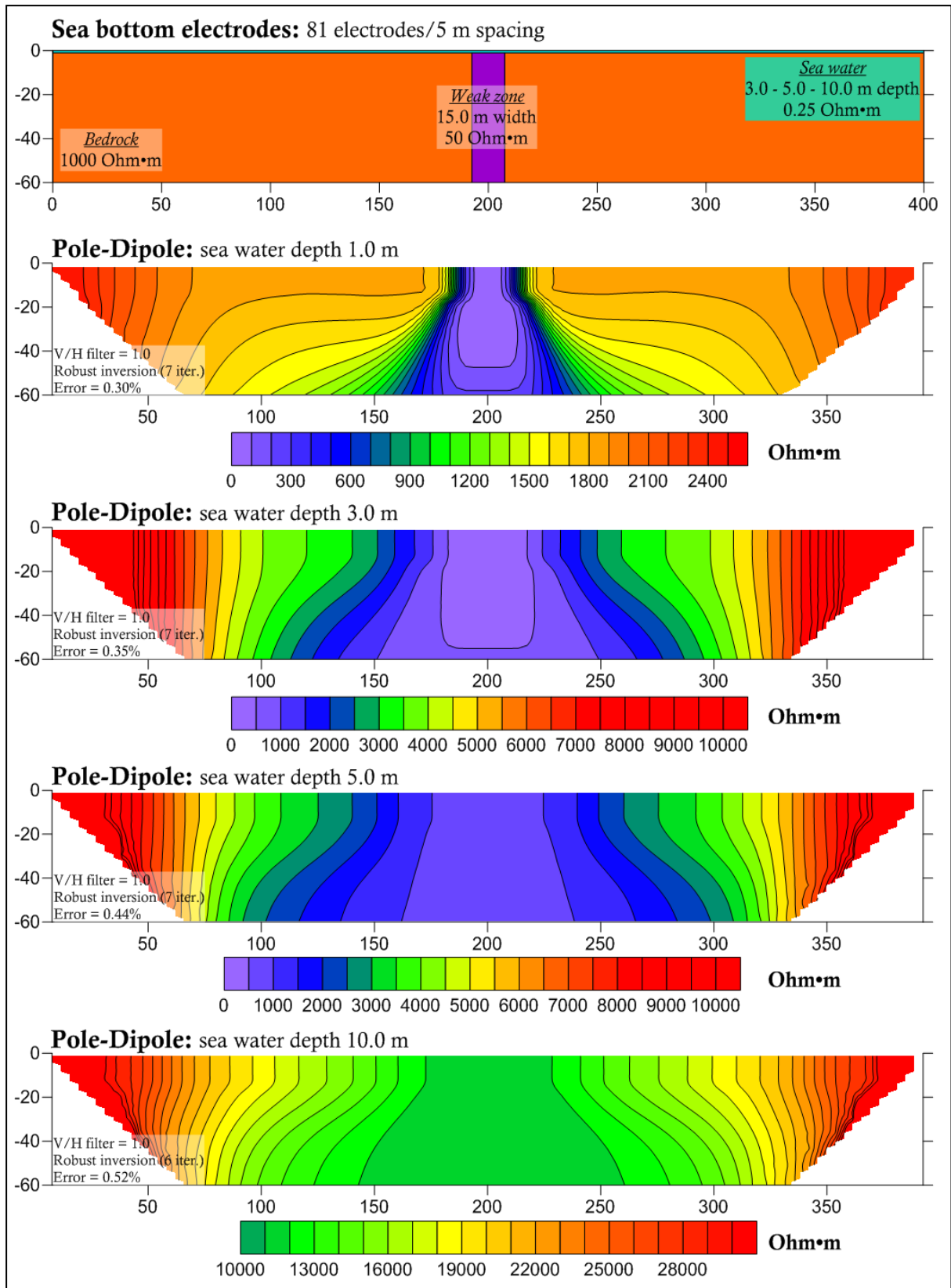


Figure 4.4.4: The effect of variations in sea water depth (1.0, 3.0, 5.0, 10.0 m) for sea-bottom electrode configuration, pole-dipole array and robust inversion.

## 4.5 The effect of fracture zone thickness

### Model description

Theoretically, the array spacing should equal the width of the fracture zone which is to be detected. However, it is interesting to see if this general rule is valid when a sea water layer is present. The modeling configuration for this case is similar to that which we have used previously. Inside a highly resistive bedrock of 1000 Ohm•m we have placed a fracture zone of 50 Ohm•m resistivity. Sea water properties are kept constant throughout the process at 1.0 m depth and 0.25 Ohm•m resistivity. We have investigated four different fracture zone widths for sea-bottom and floating electrode ERT surveys. The zone widths tested are 5, 10, 15 and 20 m. Figure 4.5.1 and 4.5.2 illustrates the results of this modeling procedure with sea-bottom and floating electrode modes.

### Modeling results

As can be seen, both modes are able to qualitatively detect the fracture zone almost identically. It has already been noted that in general a sea-bottom electrode configuration is preferable; however, in these almost ideal conditions both settings seem to be equally successful. The only exception is when the fracture zone's width is equal to the electrode spacing used. In that case, the floating electrode mode has difficulty detecting the fracture zone at all, while the sea-bottom configuration is clearly more successful. In a more quantitative sense, results are slightly better with sea-bottom ERT, which can be seen by comparing sea-bottom and floating electrode results at a zone width of 10.0 m (2 x electrode spacing). Both modes detect the fracture zone, but the sea-bottom configuration leads to an inversion with the correct width and resistivity, at least until a depth of 20 m below seabottom where resolution is lost, as noted in the previous section. The fracture zone begins to form nicely with both modes for a width between 10.0 and 15.0 m. This justifies the use of 15 m as a safe fracture zone width in almost all models

Another important observation is that a constant sea depth of 1.0 m does not guarantee an accurate calculated resistivity contrast after the inversion; as the fracture zone widens its resistivity value is calculated correctly at ~50 Ohm•m, but the host rock's calculated resistivity decreases in value.

### Summary

A general rule derived from this modeling stage is that in order to resolve a fracture zone, we should use an electrode spacing which is at least half the expected width of the zone. In other words, the smaller the electrode spacing of our array compared to the fracture zone, the better our chances of detecting it. For our optimal conditions, a 10 m wide fracture zone is imaged satisfactorily. However, a smaller electrode separation can introduce limitations due to a lower signal to noise ratio. Therefore some kind of compromise should be made between these two demands in order to have the best possible results.

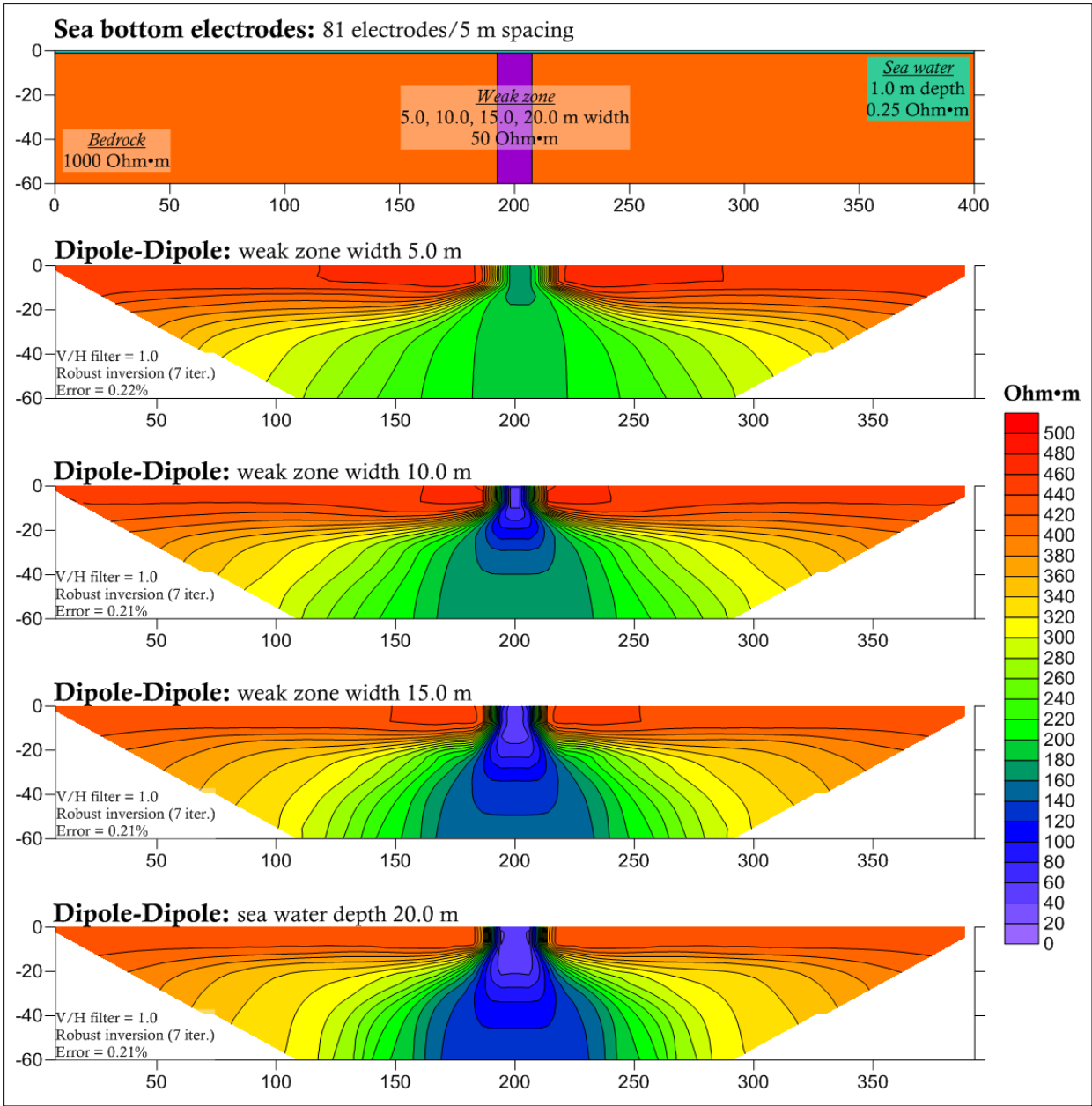


**Figure 4.5.1: The effect of variations in fracture width (5.0, 10.0, 15.0, 20.0 m) for sea-bottom dipole-dipole electrode configuration and robust inversion.**

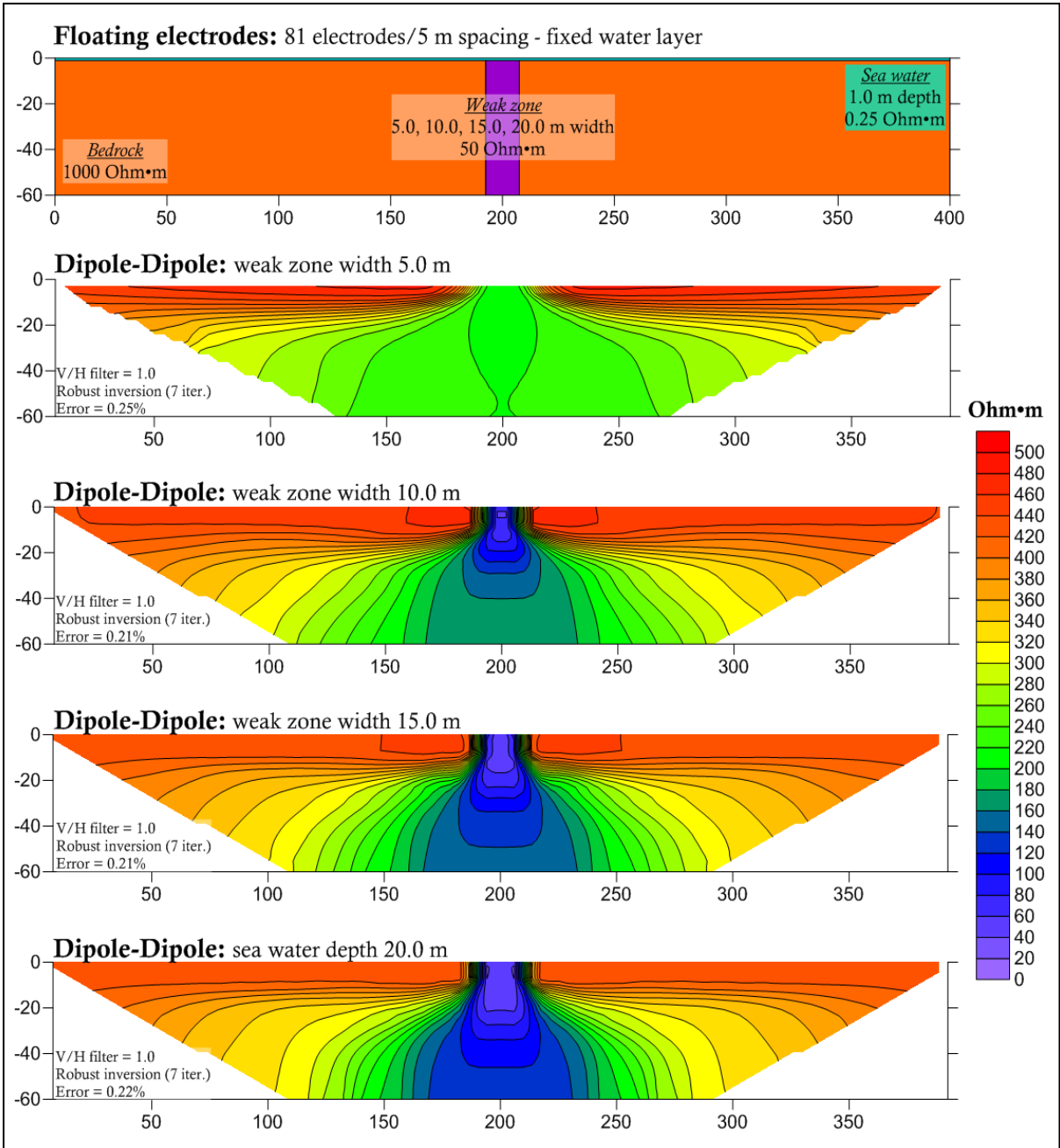


**Figure 4.5.2: The effect of variation in fracture width (5.0, 10.0, 15.0, 20.0 m).for floating dipole-dipole electrode configuration and robust inversion.**



## 4.6 The effect of overburden thickness

### Model description

These models were created in order to investigate the effect of a conductive soil layer on top of bedrock containing a fractured zone. The model is once again the same as in previous cases: a 15 m wide fracture zone of 50 Ohm•m resistivity is found within a 1000 Ohm•m bedrock. The sea water layer is 1.0 m deep and has a resistivity of 0.25 Ohm•m. The overburden layer is absent in the first model, 5.0 m thick in the second, 10.0 m thick in the third and 20.0 m thick in the fourth. As in previous sections, the inversion results are displayed both for sea-bottom and floating electrode ERT modes. Figure 4.6.1 presents the inversion results for the sea-bottom electrode mode and figure 4.6.2 for the floating electrode mode.

### Modeling results

As anticipated, the depth of an overlying sediment formation of low resistivity is crucial to whether the fracture zone will be detected or not. Both sea-bottom and floating electrode modes clearly detect the zone with 5.0 m of overburden, although the zone is widened compared to its modeled dimensions. Both configurations give a suggestion of the fracture zone even with 10.0 and 20.0 m of sediments, but the response can be interpreted as a much wider zone than the one modeled. Another common characteristic is the truncation of the zone with increasing overburden thickness. In floating electrode mode this effect starts with as little as 5 m of top soil, while at the same depth the sea-bottom mode reproduces the zone depth better, although with reduced resolution. From 10 m overburden thickness and upwards, the zone truncation is almost identical for both configurations. There is a notable loss of resolving ability with depth, and the calculated fracture zone resistivities are in better agreement with the model towards the surface, with higher resistivities found at lower depths.

The overlying layer is depicted quite accurately in both sea-bottom and floating electrode configurations only for the thickest overburden layers, and as long as the water layer is fixed. It is interesting to note that for 5.0 m of overburden, the sea-bottom electrode configuration overestimates the overburden thickness, but this is not observed in floating electrode mode. In all other cases the inversion calculates more or less the correct thickness. The overburden resistivity on the other hand is always calculated quite accurately (between 20 and 40 Ohm•m).

### Summary

The conclusion from this modeling exercise can be summarized as follows: 20.0 m of sediments with resistivity 30 Ohm•m overlying a fracture zone of 50 Ohm•m resistivity does not shield the response of the fracture zone. The inversion result could be interpreted as a fracture zone, although the form of the observed zone may differ from that of the model: it may be wider than the model zone, and may appear to be confined to the surface.

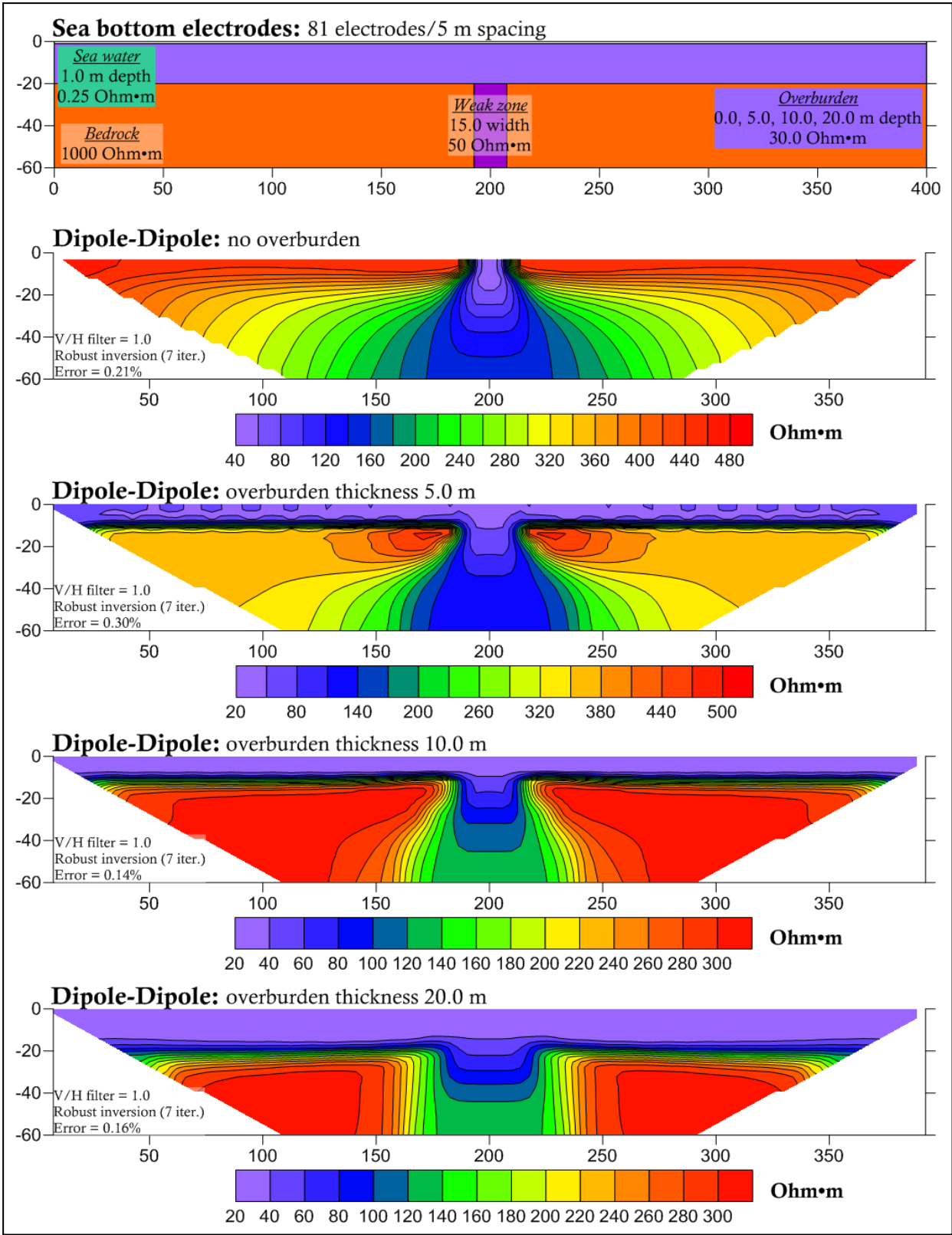


Figure 4.6.1: The effect of variations in overburden thickness (0.0, 5.0, 10.0, 20.0 m) on sea-bottom dipole-dipole configuration and robust inversion.

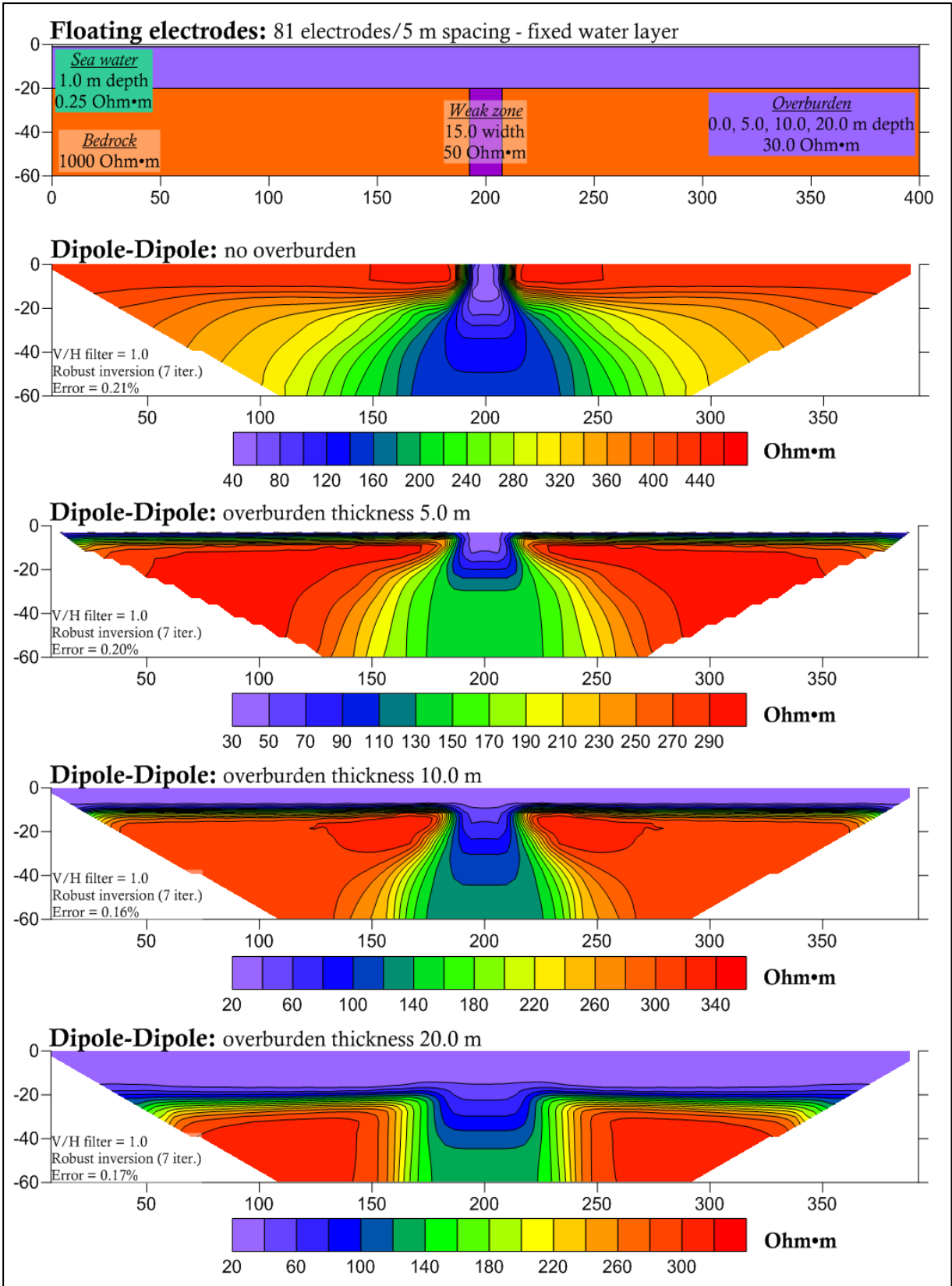


Figure 4.6.2: The effect of variations in overburden thickness (0.0, 5.0, 10.0, 20.0 m) on floating dipole-dipole electrode configuration and robust inversion.

## 4.7 The effect of bedrock/fracture resistivity contrast

### Model description

Having concluded that 5.0 m of overburden is not enough to shield a 50 Ohm•m fracture, we have investigated if this is also valid for less conductive zones. Here our model consists of a 15 m wide fracture zone inside a 1000 Ohm•m bedrock, underlain by 5.0 m of 30 Ohm•m sediment and 1.0 m of 0.25 Ohm•m sea water. The investigated resistivity contrasts come from values of 10, 50 and 100 Ohm•m used for our fracture zone. Yet again, both sea-bottom and floating electrode dipole-dipole configurations are tested. Figure 4.7.1 presents the modeling results.

### Modeling results

Starting from the clearly detected zone for a resistivity contrast of 100 (1000 Ohm•m bedrock/10 Ohm•m zone), our results gradually degrade as the contrast decreases, but not significantly. The zone is still detectable both in sea-bottom and floating electrode ERT modes for lower resistivity contrasts such as 10 (1000 Ohm•m bedrock/100 Ohm•m zone) or 20 (1000 Ohm•m bedrock/50 Ohm•m zone). It should be noted however that with a higher resistivity contrast, the sea-bottom electrode mode produces much better results than the floating configuration, and as the contrast decreases the results become more and more similar.

We note that even when the zone is most clearly detected, its dimensions are wider than those of the model, while its resistivity is somewhat overestimated (~140 Ohm•m instead of 100 Ohm•m). The sediment layer on the other hand is well depicted in all resistivity contrast cases.

### Summary

If we were to put forward a general rule derived from the aforementioned models, it would be that in the presence of conductive overburden, a high resistivity contrast between bedrock and fracture is necessary for the zone to be detected using sea-bottom ERT.

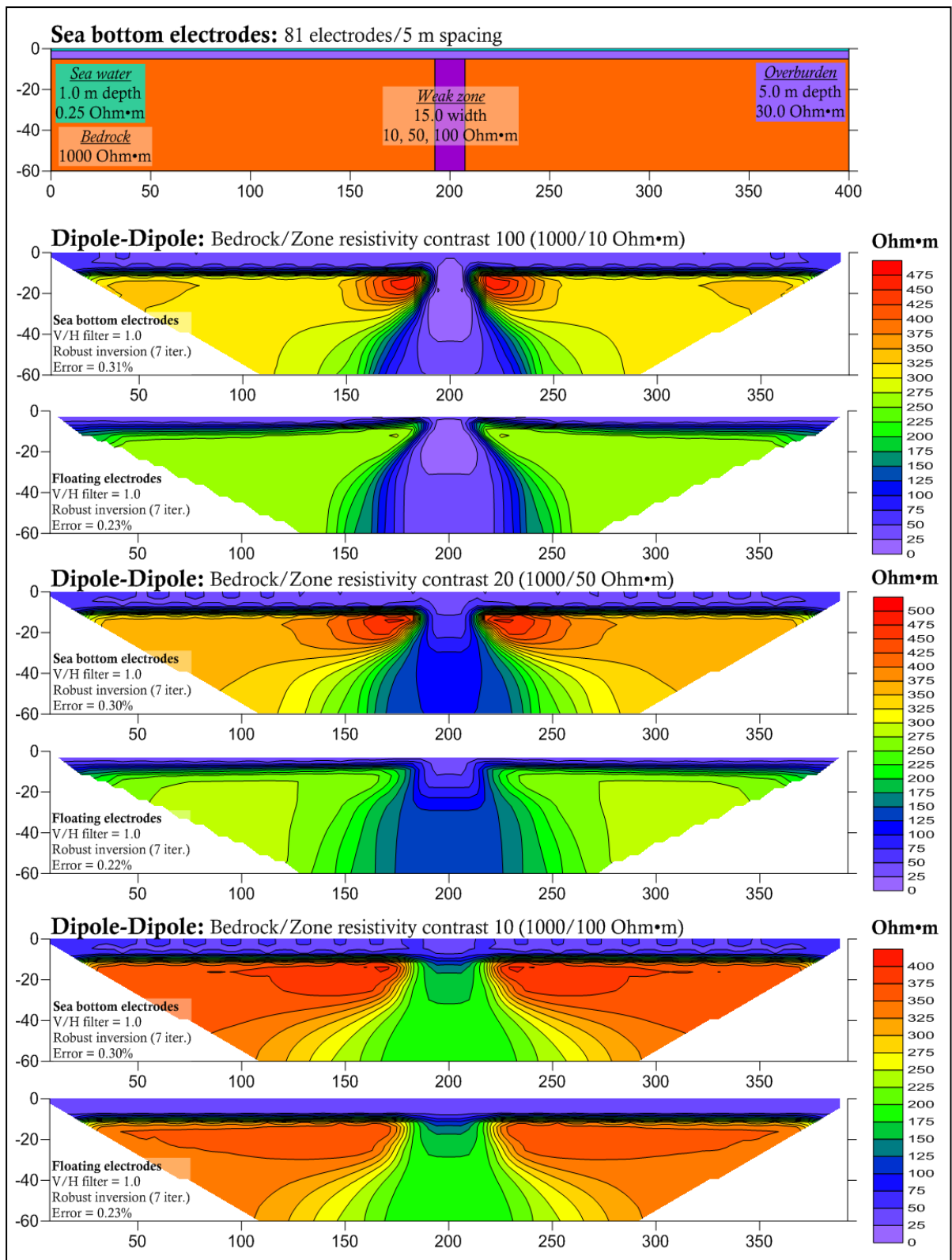


**Figure 4.7.1: The effect of variations in bedrock/fracture resistivity contrast (100, 20, 10) on both sea-bottom and floating dipole-dipole configurations and robust inversion.**

## 4.8 The effect of overburden resistivity

### Model description

We have created a series of models of less favorable conditions in order to test how the resistivity of the overburden layer affects sea-bottom ERT resolving ability. For these models, we have kept the width and resistivity of the fracture zone (15 m and 50 Ohm•m) and the resistivity of the bedrock (1000 Ohm•m) equal to those used in previous modeling. On the other hand, we have increased the thickness of the overburden layer and the sea water to 5.0 m. The resistivity of the sea water was kept at 0.25 Ohm•m as before. The resistivities we assigned to the overburden are: 5.0, 10.0, 30.0 and 50.0 Ohm•m. Figure 4.8.1 presents the results for sea-bottom ERT mode measurements and figure 4.8.2 the results for floating electrode mode.

### Modeling results

Figures 4.8.1 and 4.8.2 show similar behavior as the resistivity of the overburden increases. The higher the resistivity of the overburden layer, the better the detection of the fracture zone. As the top layer becomes less resistive, the detected fracture zone becomes wider and less pronounced. The calculated resistivity contrast between fracture and bedrock starts off as 2 (100 Ohm•m bedrock/50 Ohm•m fracture) for 5.0 m soil with 5 Ohm•m resistivity and decreases as the top layer becomes less conductive.

An interesting observation is that the calculated bedrock resistivity range decreases as the resistivity of the overburden increases. The overburden thickness is overestimated in all cases, except when its resistivity is equal to 50 Ohm•m. In that case, the inversion process fails to detect the layer in both the sea-bottom and floating electrode configurations.

### Summary

The general conclusion resulting from the aforementioned modeling procedure is that a top layer does not hinder the use of ERT as a prospection method in either sea bottom electrode or floating electrode modes. However, this is the only case where the floating electrode configuration seems to be on a par with sea-bottom ERT, and therefore we still propose the latter as the preferred mode.

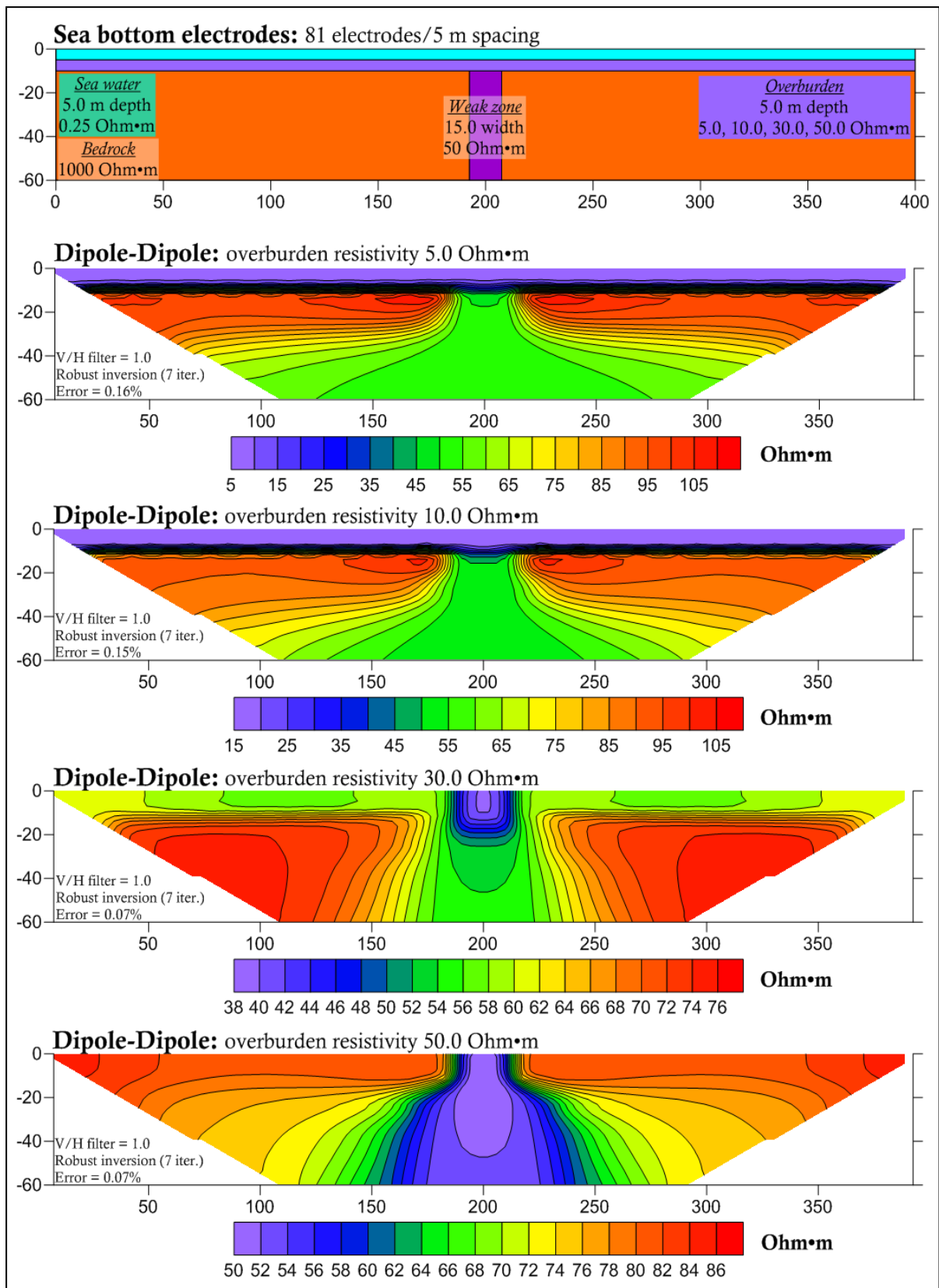


**Figure 4.8.1: The effect of variations in overburden resistivity (5.0, 10.0, 30.0, 50.0 Ohm·m) on sea-bottom dipole-dipole configuration and robust inversion.**



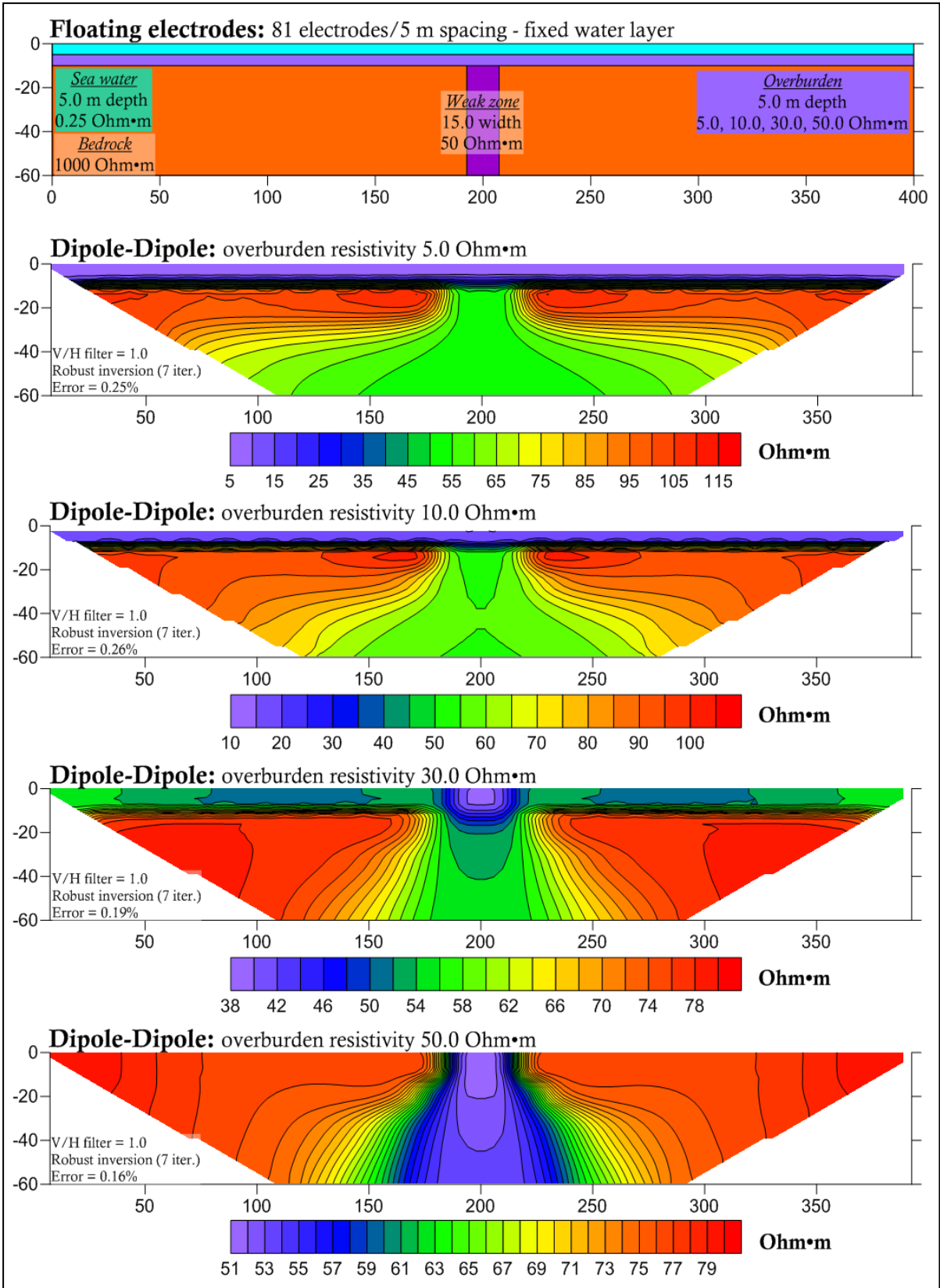


Figure 4.8.2: The effect of variations in overburden resistivity (5.0, 10.0, 30.0, 50.0 Ohm·m) on floating dipole-dipole electrode configuration and robust inversion.

## 4.9 The effect of varying bedrock resistivity

### Model description

Up until now, we have incorporated a compact crystalline bedrock in our models whose resistivity has been set at 1000 Ohm•m. In this subsection we investigate cases where the conductivity of the bedrock varies. According to borehole logging performed by NGU (Elvebakk & Saintot 2011, Dalsegg & Elvebakk 2012), the crystalline bedrock resistivity in Norwegian marine areas can range between 700 and 2000 Ohm•m. Therefore we have decided to modify some of the previous models in order to test the effect of more conductive bedrock in the detection of a sea-bottom fracture zone.

Our initial model consists of a 15 m wide fracture zone inside bedrock and under 1 m of sea water (0.25 Ohm•m). For this modeling procedure, we have used a constant resistivity contrast of 20 between bedrock and fracture zone. Figures 4.9.1 and 4.9.2 show inversion results for four different resistivity models with the same bedrock/zone contrast: 500/25 Ohm•m, 1000/50 Ohm•m, 2000/100 Ohm•m and 3000/150 Ohm•m. Figure 4.9.1 shows the results for sea-bottom electrode mode and 4.9.2 for floating electrode mode.

### Modeling results

Figures 4.9.1 and 4.9.2 show similar results for the role of resistivity contrast between bedrock and fracture zone, in a decreasingly conductive environment. In both sea-bottom and floating electrode mode, we can observe that the fracture zone becomes wider and less pronounced as the environment becomes more and more resistive, even with a standard favorable resistivity contrast such as 20. Starting off at 500/25 Ohm•m we can see that the detected fracture zone is best shaped compared to the other contrast values used in this modeling session. Once again we can observe the zone widening at 25 m depth, an effect becoming worse as the environment becomes less conductive. At 3000/150 Ohm•m, the zone is detectable but unreasonably wide. This widening is more severe in floating electrode configuration. Lastly, it is interesting to note that the contrast best matching that of the model is observed in the first case where the calculated value is 10 (300 Ohm•m bedrock/30 Ohm•m zone). This contrast underestimation is solely connected to underestimation of the bedrock resistivity and not that of the fracture zone itself.

### Summary

From this modeling procedure we conclude that a favorable resistivity contrast is not enough to detect and correctly delineate a subsea fracture zone. The success of marine ERT heavily depends on the conductivity of the whole environment. A more conductive environment aids the detection of the zone while a more resistive setting makes the zone harder to detect. This can be explained by higher conductivity environments allowing a greater portion of the current to flow through the subsea bedrock. However, a generally conductive environment does not significantly improve marine ERT resolution.

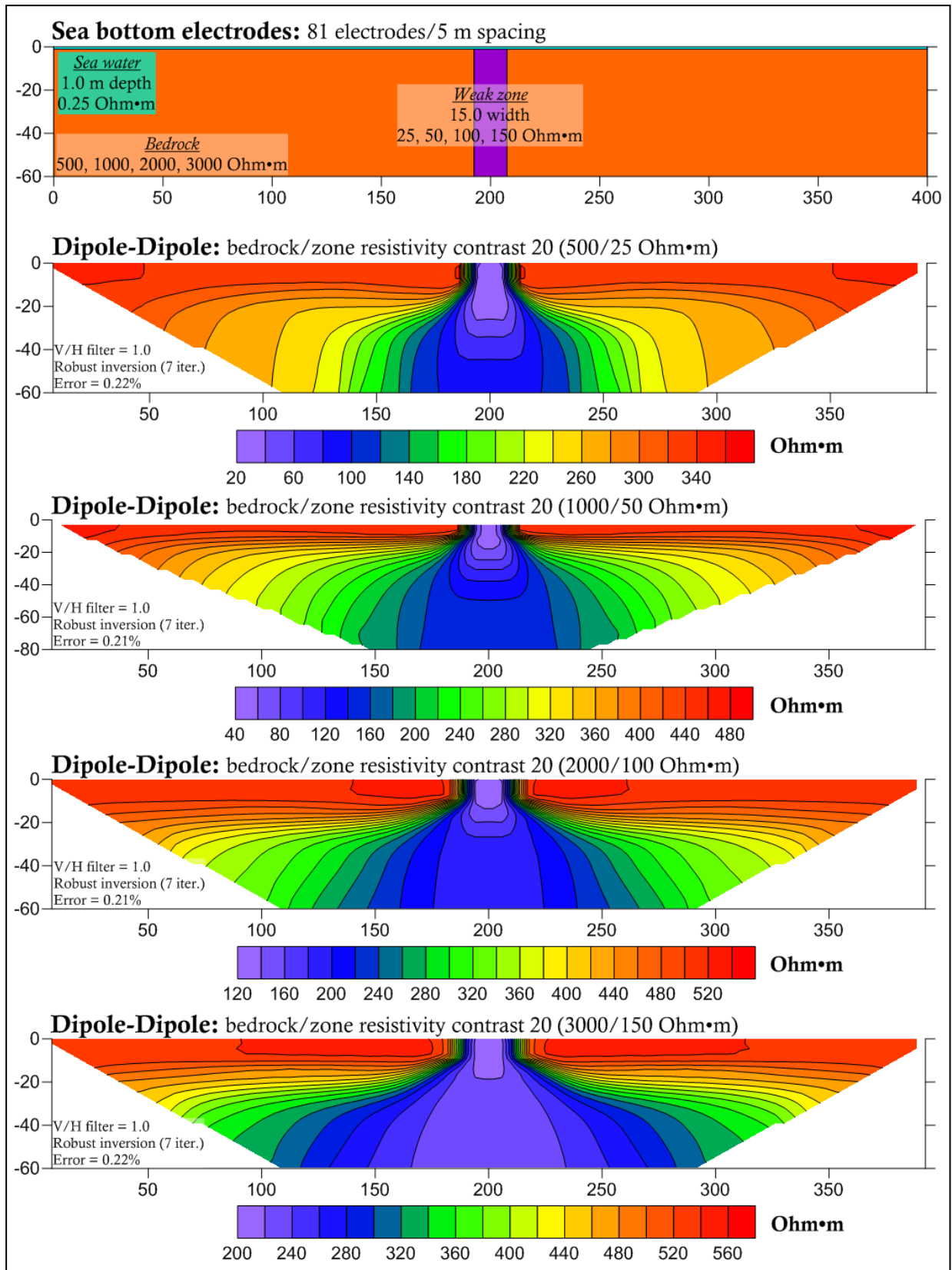


Figure 4.9.1: The effect of variation in bedrock resistivity when resistivity contrast with the fracture zone is kept constant at 20 for increasingly resistive environments (500, 1000, 2000 and 3000 Ohm•m) - sea-bottom dipole-dipole electrodes and robust inversion.

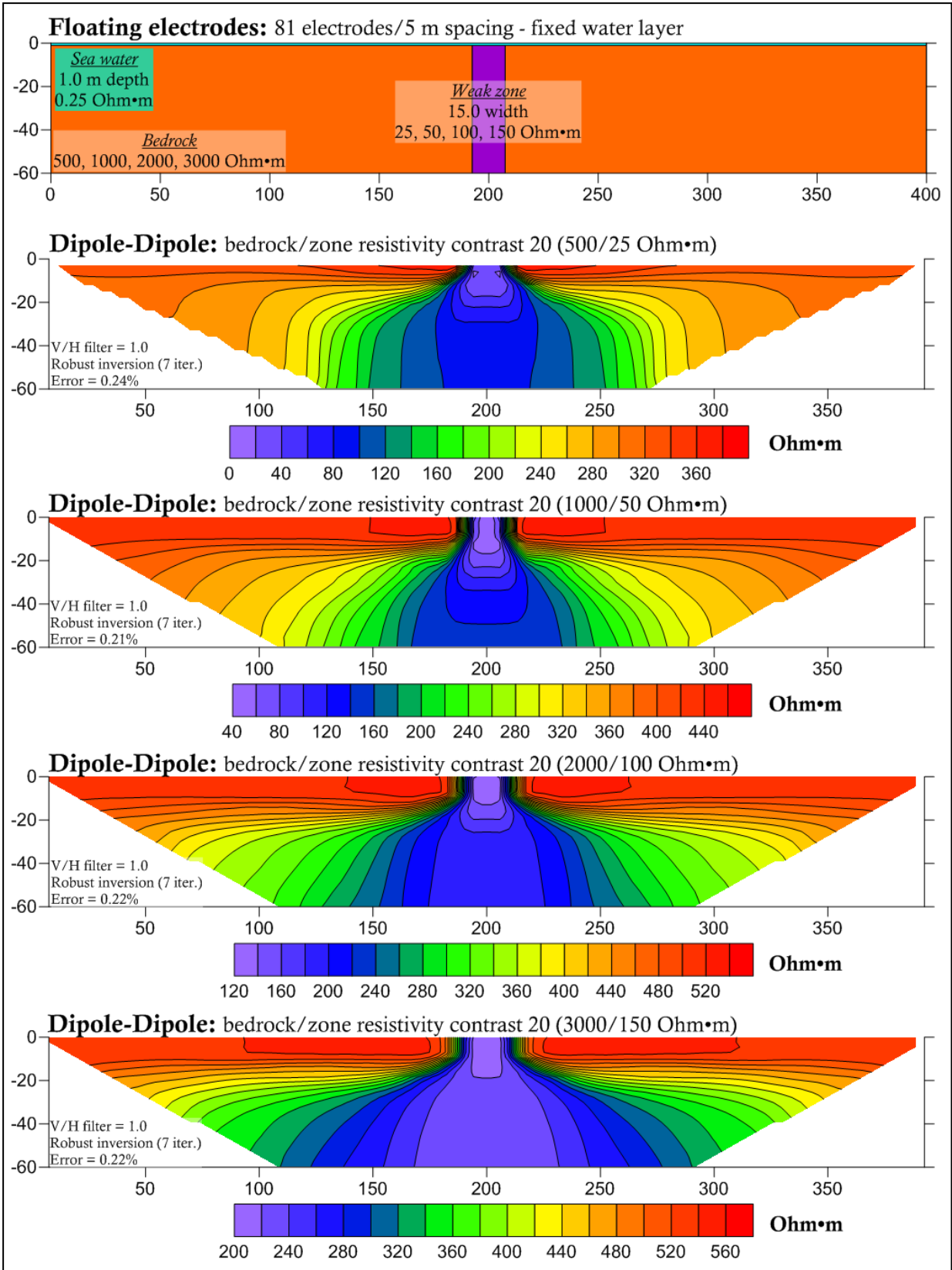


Figure 4.9.2: The effect of variation in bedrock resistivity when resistivity contrast with fracture zone is kept constant at 20 for increasingly resistive environments (500, 1000, 2000 and 3000 Ohm·m) - floating dipole-dipole electrodes and robust inversion.

## 4.10 Mixed survey - combination of land and floating electrode ERT modeling

### Model description

In ERT surveys in Norway, the proposed line occasionally has to cross a strait of sea water. This means that there is an area within the cross section where floating electrodes are used and are in direct contact with highly conductive seawater. The questions remain the same.: Can ERT detect a hidden fracture zone beneath the water? Does the water body shield the underlying zone? Could we be misguided in interpreting an artificial effect as a fracture? To investigate these questions we decided to model such a case with two different settings. The first setting includes a 15 m wide 50 Ohm•m fracture zone outside the influence of water. The second setting places a second fracture zone underneath the strait, completely inside the zone of influence of the overlying water layer which is 5.0 m deep and has 0.25 Ohm•m resistivity. The response of both these models was tested for three different array configurations. Figure 4.10.1 presents the results for dipole-dipole arrays, 4.10.2 for multiple gradient arrays and 4.10.3 for pole-dipole arrays. The inversion process was performed for all cases first without any fixing of the water layer and then with correct fixing. Figure 4.10.4 presents the inversion results when using several different approaches such as standard or robust inversion, larger vertical/horizontal filter values and larger damping factors.

### Modeling results

Figures 4.10.1, 4.10.2 and 4.10.3 present interesting results. We once again note the favorable effect of fixing the water layer before we perform inversion. However it is useful to study the effect of water layer fixing for each array separately. In the case where there is no weak zone underneath the seawater, using a dipole-dipole array and with no fixing of water parameters (figure 4.10.1), an artificial low resistivity value appears underneath the water body, caused by the water's high conductivity. The same effect can also be noticed for the multiple gradient configuration in the upper images of figure 4.10.2. However, in the case of the pole-dipole array the low resistivity values underneath the water have been replaced with high ones. In this case, inversion without layer fixing produces a horizontal high resistivity area underlain by low values instead of low resistivity values directly underneath the water. Fixing the water layer results in losing the lower low value resistivities, but the high value area remains almost intact especially for the multiple gradient and pole-dipole configurations.

The inversion results for the case of two weak zones measured with dipole-dipole, multiple gradient and pole-dipole arrays are shown in the lower parts of figures 4.10.1, 4.10.2 and 4.10.3 respectively. For dipole-dipole array, water layer fixing leads to a general decrease of artificial high values at the limits of the marine area, and an elongation of the low resistivity values at depth. In the case of the multiple gradient array the results are even more dramatic. Fixing the water layer helps the inversion procedure to form the low resistivity area into something closer to the modeled fracture zone. However, as we have seen in previous sections, the entire length of the weak zone is not determined. Finally, in the case of the pole-dipole array, layer fixing improves the results only slightly. As for the calculated resistivities, we can note that in all cases the fracture zone value lies somewhere between 0 and 100 Ohm•m, regardless of whether it is under the influence of the water body or not. The bedrock environment resistivity is somewhat overestimated in several areas (~1500 Ohm•m or more) but is still close to the model value of 1000 Ohm•m.

However, these figures indicate some discouraging aspects of performing such measurements. Let us look at the single weak zone results in the upper images of figures 4.10.1, 4.10.2 and 4.10.3, and assume that we have inverted our measurements without any layer fixing. Focusing on the area underneath the water, we notice that without any prior resistivity fixing,

the calculated values of the resistivity at the edges of the body tend to resemble, and can easily be misinterpreted as, fracture zones. If we go a step further, a geologist could also interpret these two fracture zones as the reason for the formation of the strait. This of course is not the case. Now, let us focus on the same area after fixing the water layer. As already noted, the fixing has removed most of the artificial effects, but at the edges of the water layer we observe - as before - vertical structures, especially with the multiple gradient array (upper images of figure 4.10.2). In all cases, there is a high resistivity area underneath the water which may lead to misinterpretations.

Similarly misleading results can be seen in the lower images of figures 4.10.1, 4.10.2 and 4.10.3 which depict the inversion results for two weak zones. The marine area edges still depict some artificial structures that may be interpreted as fracture zones. However, after fixing the water layer, the structure of the hidden sea-bottom fracture zone becomes much more visible, especially when using the multiple gradient array (figure 4.10.2). In all cases, the resultant structures are not far from those of the model.

Figure 4.10.4 displays the effect of varying several inversion parameters that may influence the detection of a sea-bottom fracture zone using a multiple gradient array (the type most commonly used by NGU). The factors are: standard or robust inversion; V/H filter value; and damping factors. It should be noted that the water layer is fixed in all the cases depicted in figure 4.10.4. As can be seen, a robust inversion with higher V/H filter and higher damping factors leads to the image most closely resembling the model. But again, these factors force the inversion process towards forming sharp edged vertical structures, which of course favors the case of trying to detect fracture zones (i.e. structures of rectangular characteristics in our modeling).

### **Summary**

We can say that mixed surveys can yield satisfactory results. However, we have to be extremely cautious with both choice of inversion parameters and interpretation of the results.

The main rule that comes out of this investigation is no different from that which we have already concluded. Fixing the water layer is imperative, especially when using a multiple gradient array. Whether an ERT survey can be deemed successful or not can only be decided after fixing the water layer. After fixing the water layer, there should be extra care taken regarding which inversion parameters are used. This is of course arbitrary, and the decision depends solely on the data processing scientist.

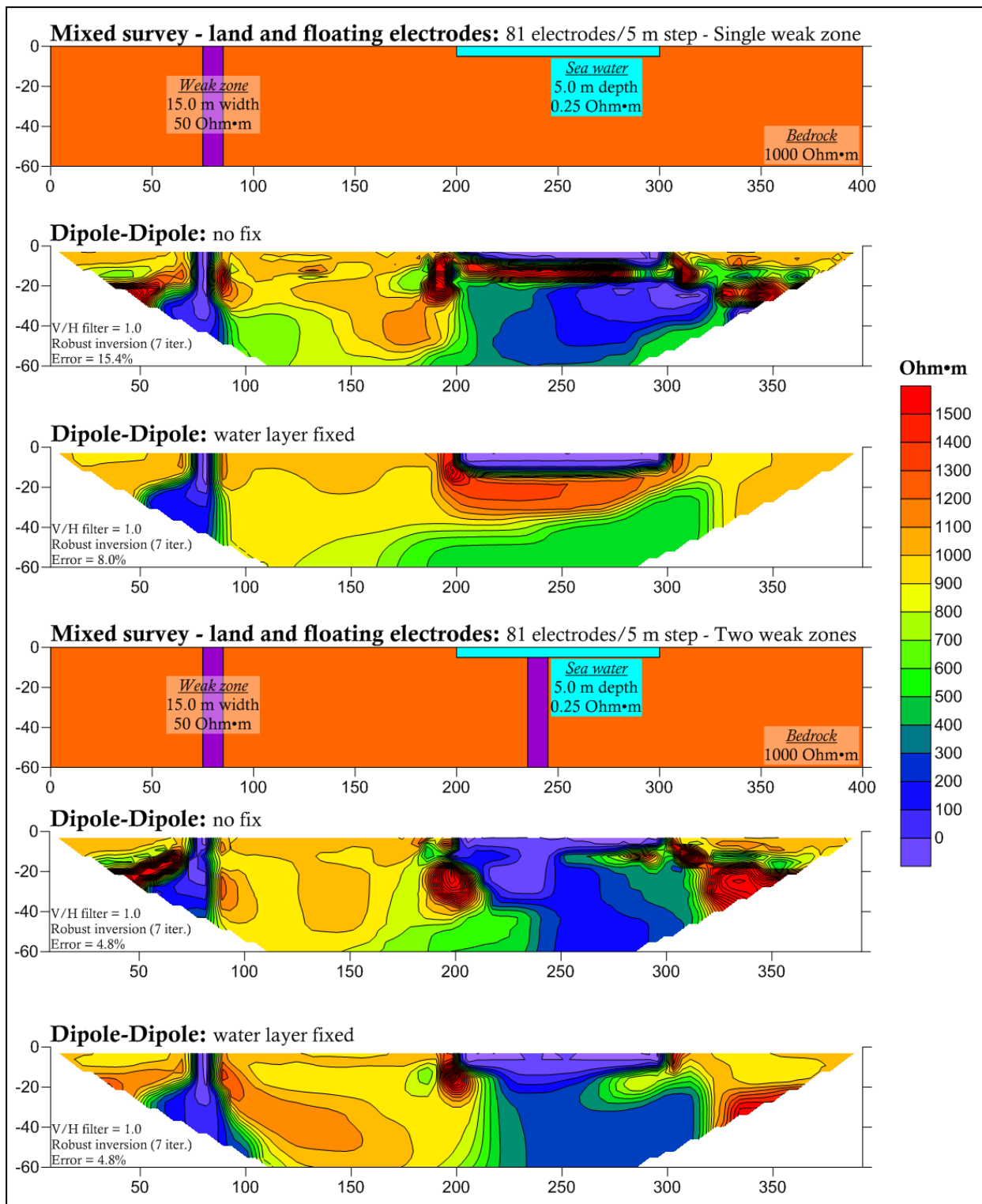


Figure 4.10.1: Mixed survey - single fracture zone outside the influence of the sea water (top) two weak zones with one under the influence of sea water (bottom) - dipole-dipole array. Robust inversion with and without fixing of the water layer.



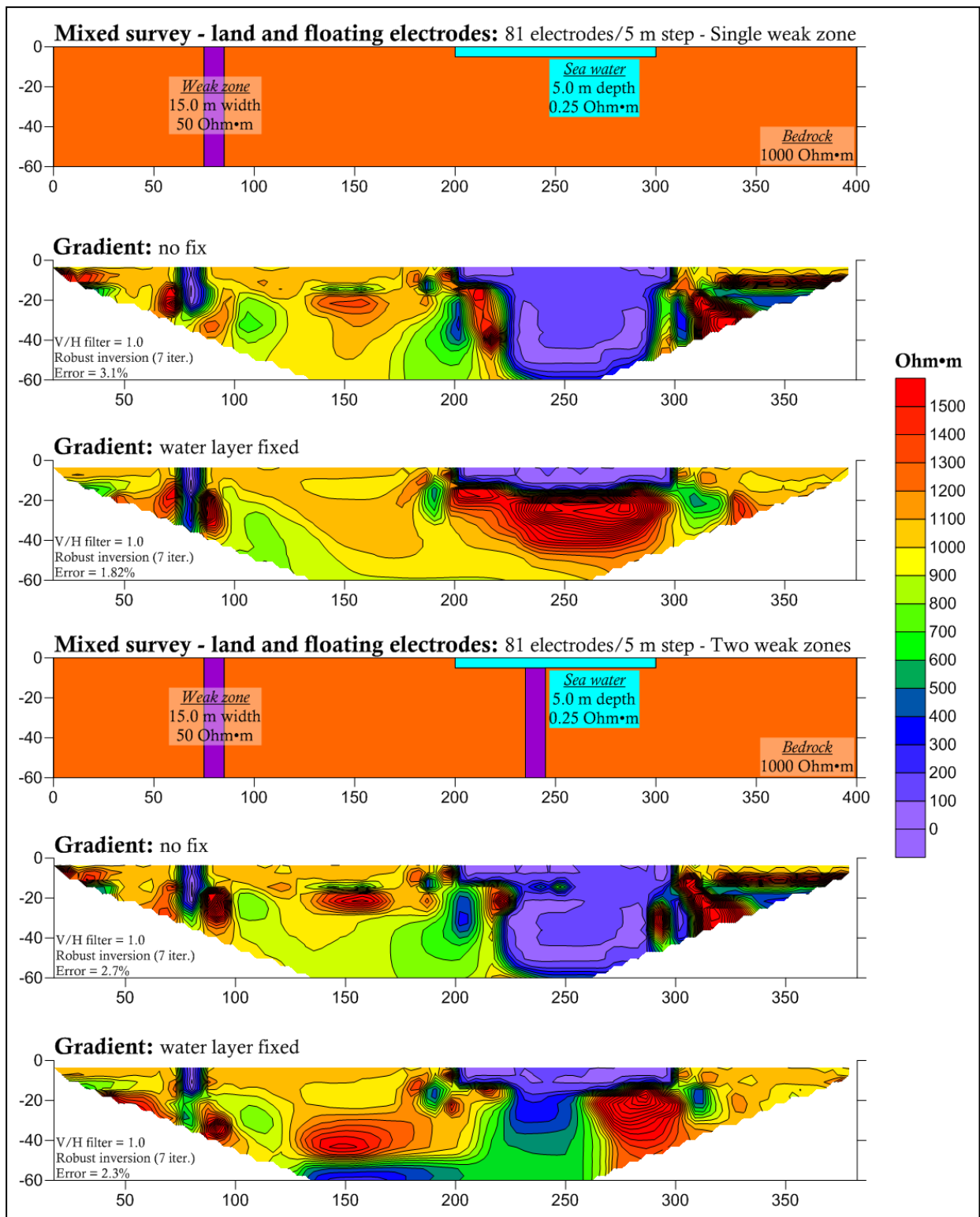


Figure 4.10.2: Mixed survey - single fracture zone outside the influence of the sea water (top) two weak zones with one under the influence of sea water (bottom) - multiple gradient array. Robust inversion with and without fixing of the water layer.

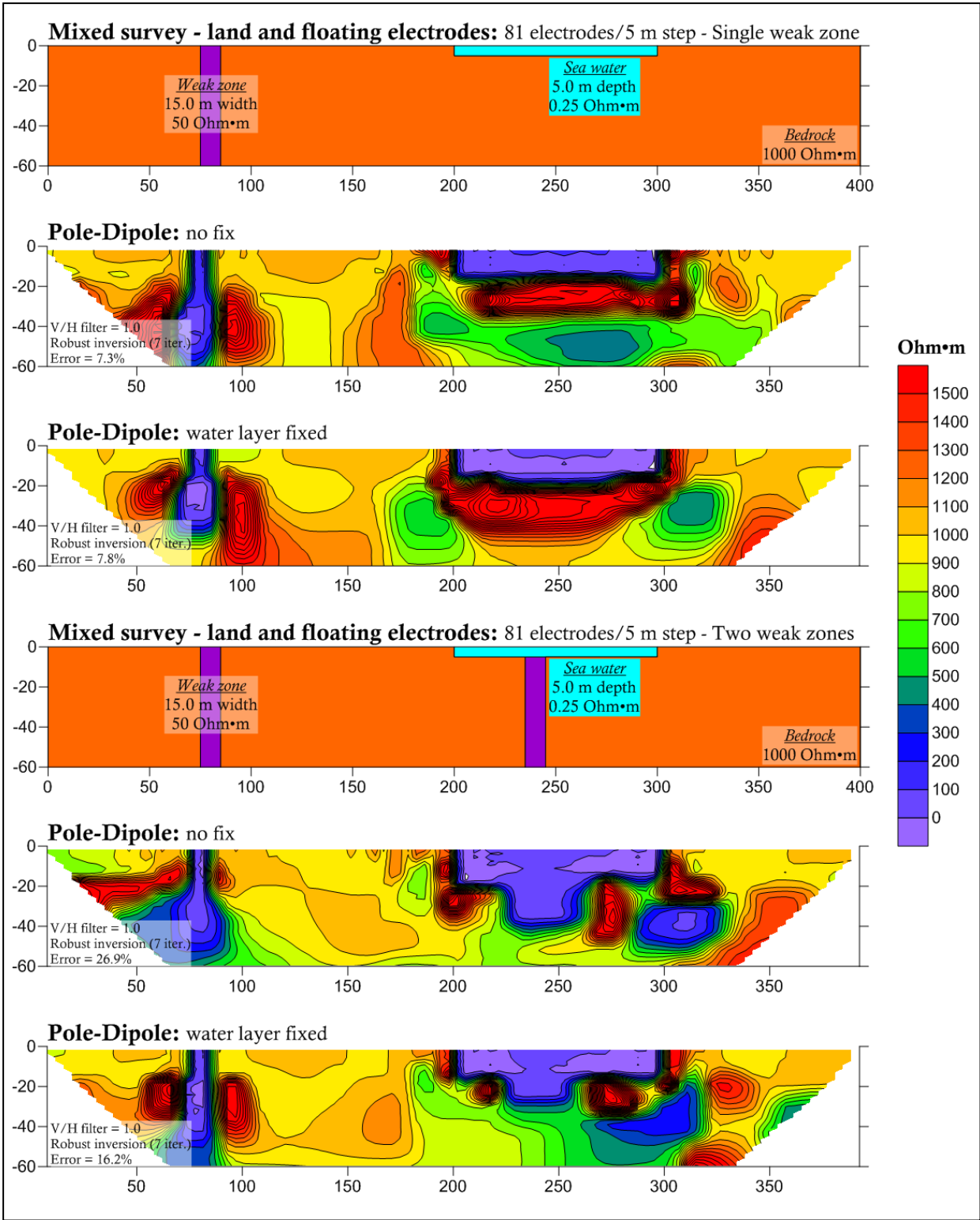


Figure 4.10.3: Mixed survey - single fracture zone outside the influence of the sea water (top) two weak zones with one under the influence of sea water (bottom) - pole-dipole array Robust inversion, without and with fix of water layer.

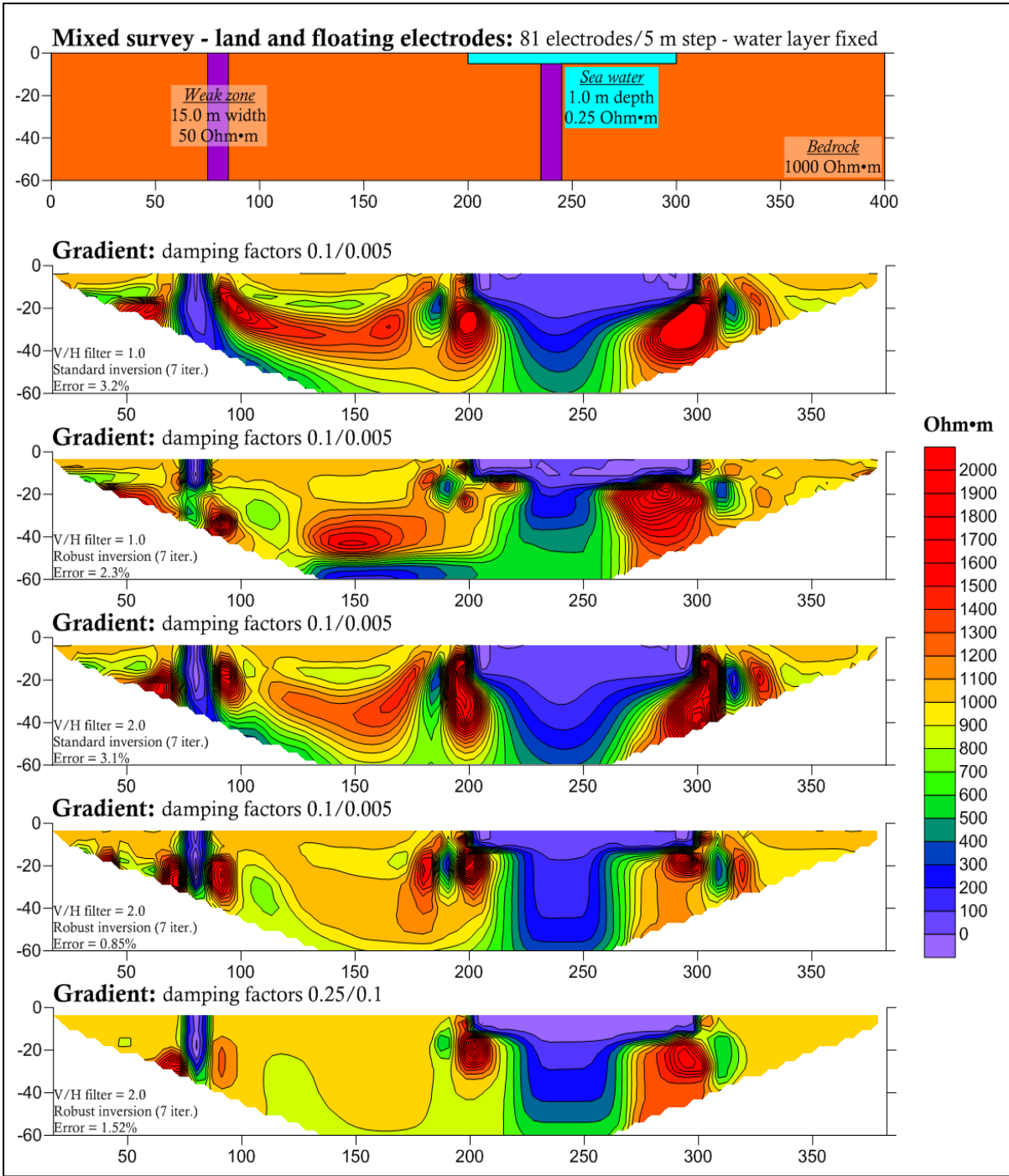


Figure 4.10.4: The influence of inversion parameters in the detection of sea-bottom fracture zones for multiple gradient array, water layer is fixed in all cases, standard and robust inversion, V/H filter 1 and 2, damping factors 0.1/0.005 and 0.25/0.1.

## 5. CROSS VALIDATION PROCESS

In order to validate the results which we have derived with RES2DMOD and RES2DINV, an independent modeling and inversion code has been used for the same or similar cases presented in section 4. This modeling procedure was performed by Dr. P. Tsourlos during his 4 day visit at the NGU in March 2013. The software used in this process was DC2DPRO, developed by Dr. J.H. Kim of the Korean Institute of Geosciences and Mineral Resources (KIGAM). This software uses the same inversion algorithm as M.H. Loke's program, except for some computational differences regarding Lagrangian multipliers, which is a very important feature of any inversion process. This gives us the opportunity to cross validate the results from the previous section and strengthen our conclusions.

As in the case of modeling with M.H. Loke's software, a relatively large number of different structure and value combinations have been used in modeling, before narrowing down our results to those which are more interesting. In this section, selected results from the DC2DPRO modeling and inversion procedure will be presented in order to highlight the most important conclusions.

### 5.1 The effect of fixing the water layer

Since H.M. Loke's software does not offer the possibility of leaving the water layer unfixed for the sea-bottom electrode configuration, figures 5.1.1, 5.1.2 and 5.1.3 present the effect of sea layer fixing before inversion for the case of dipole-dipole, Wenner-Schlumberger (equivalent to multiple gradient array) and pole-dipole arrays respectively. The initial model comprises a 10 m wide and 50 Ohm•m fracture zone, inside a 1000 Ohm•m bedrock, and overlain by sea water 1m deep with 0.25 Ohm•m of resistivity. As observed in figures 4.2.1, 4.2.2 and 4.3.3, fixing the water layer before inversion both for sea-bottom and floating electrode modes significantly assists the inversion procedure in separating fracture zone from bedrock. Not fixing the layer at all leads to ambiguous results and unclear zone formations.

Figures 5.1.1, 5.1.2 and 5.1.3 also confirm that the dipole-dipole configuration gives better results than the Schlumberger-Wenner and pole-dipole configurations.

### 5.2 The effect of seawater resistivity

Testing the response of dipole-dipole array on various sea water resistivities (0.25, 0.5 and 1.0 Ohm•m) we have earlier concluded that increasing marine resistivity also increases the quality of the inversion result (figure 4.3.1). Figure 5.2.1 represents the confirmation of this effect on a 10 m wide fracture zone with resistivity 50 Ohm•m within a 1000 Ohm•m bedrock and under 1 m of water. As already noted, seawater resistivity is directly connected to the water temperature and salinity, making colder and less saline waters more preferable for marine ERT measurements.

Results shown in figure 5.2.1 also confirm that sea-bottom electrodes give a slightly better result than floating electrodes for the dipole-dipole configuration. The DC2DPRO results also appear to be better than RES2DINV for similar models.

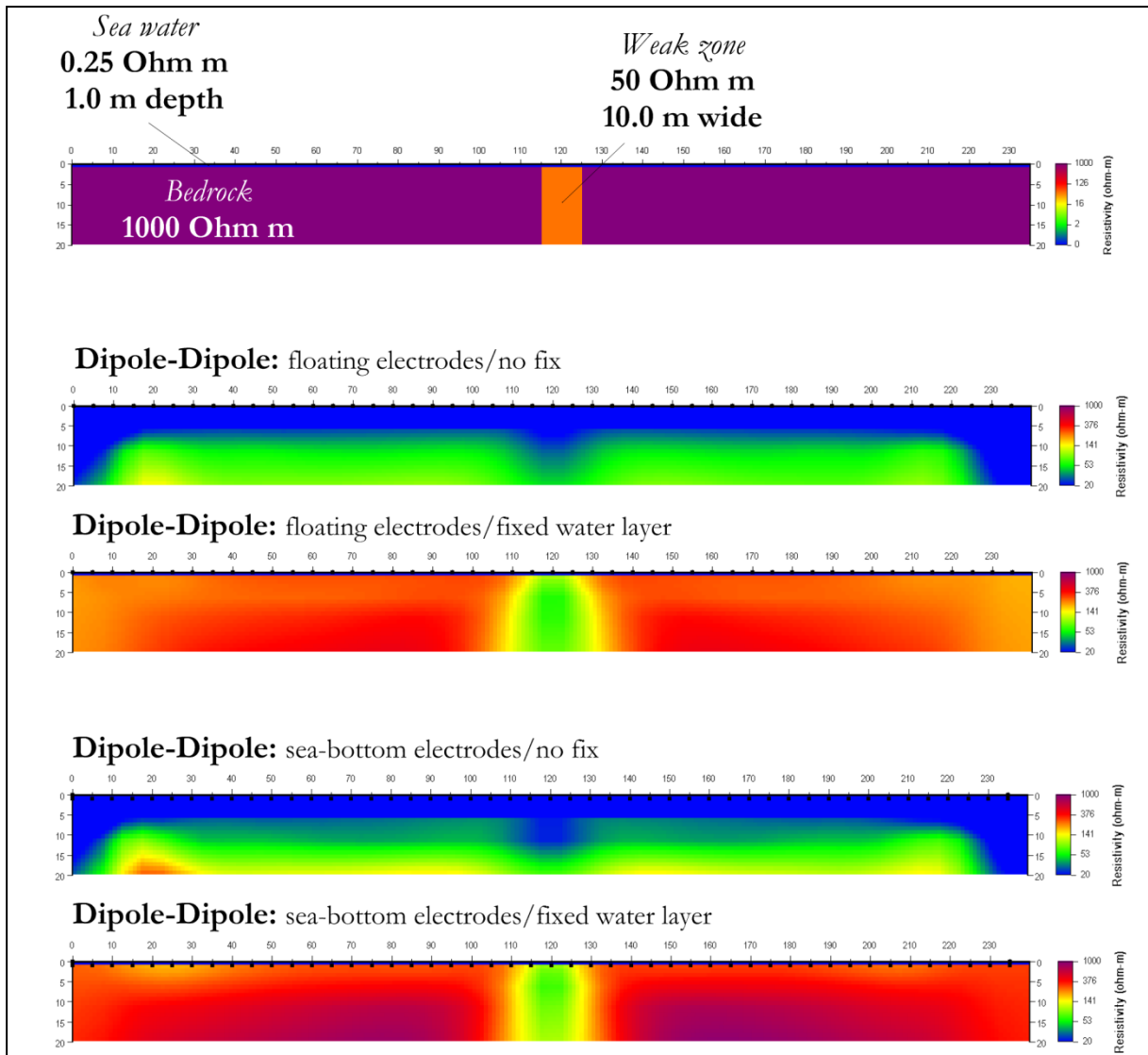


Figure 5.1.1: The effect of fixing the water layer before inversion for dipole-dipole array - floating and sea-bottom electrode modes. The model is shown in the uppermost part of the figure.

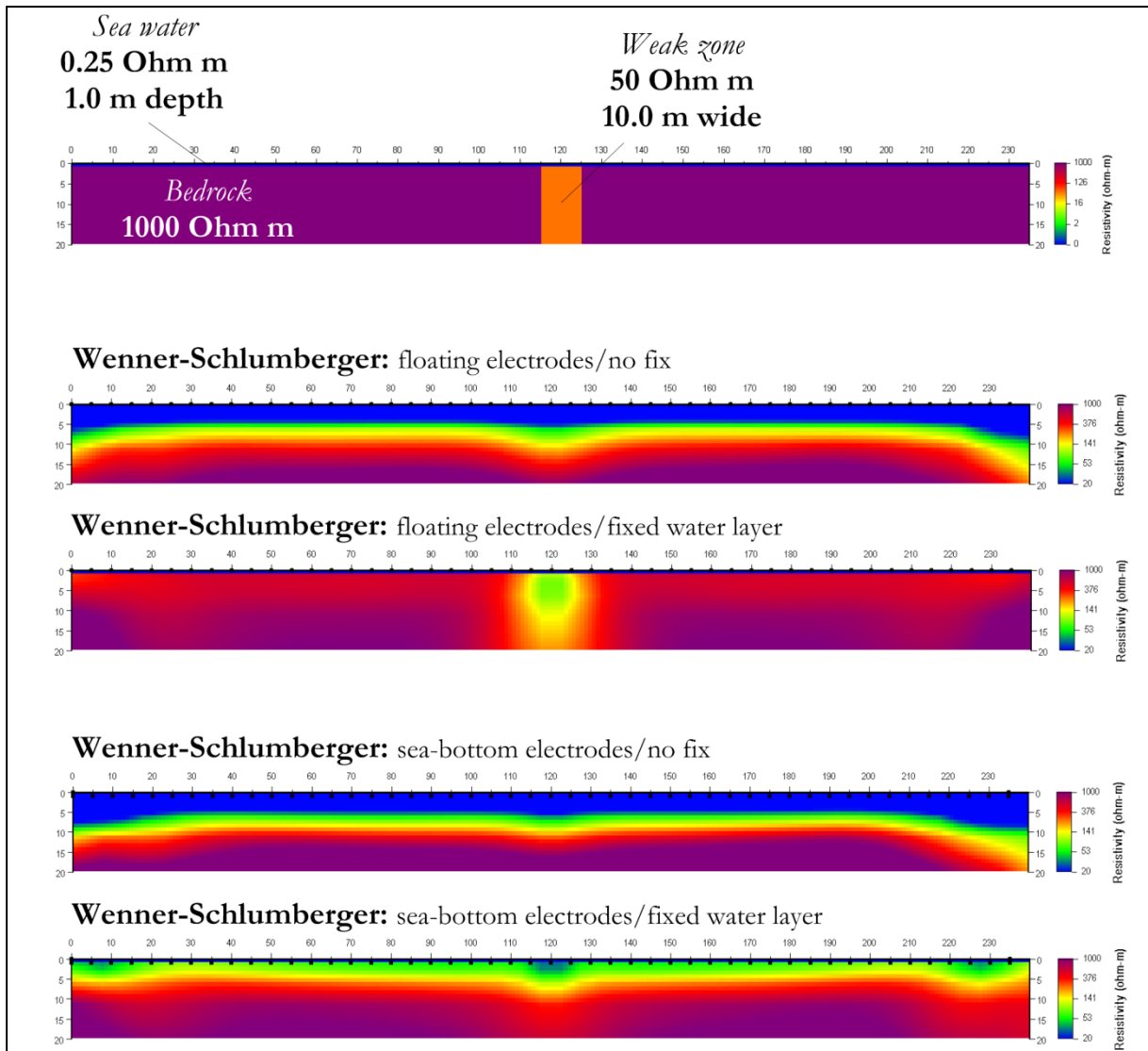


Figure 5.1.2: The effect of fixing the water layer before inversion for Wenner-Schlumberger array - floating and sea-bottom electrode modes. The model is shown in the uppermost part of the figure.

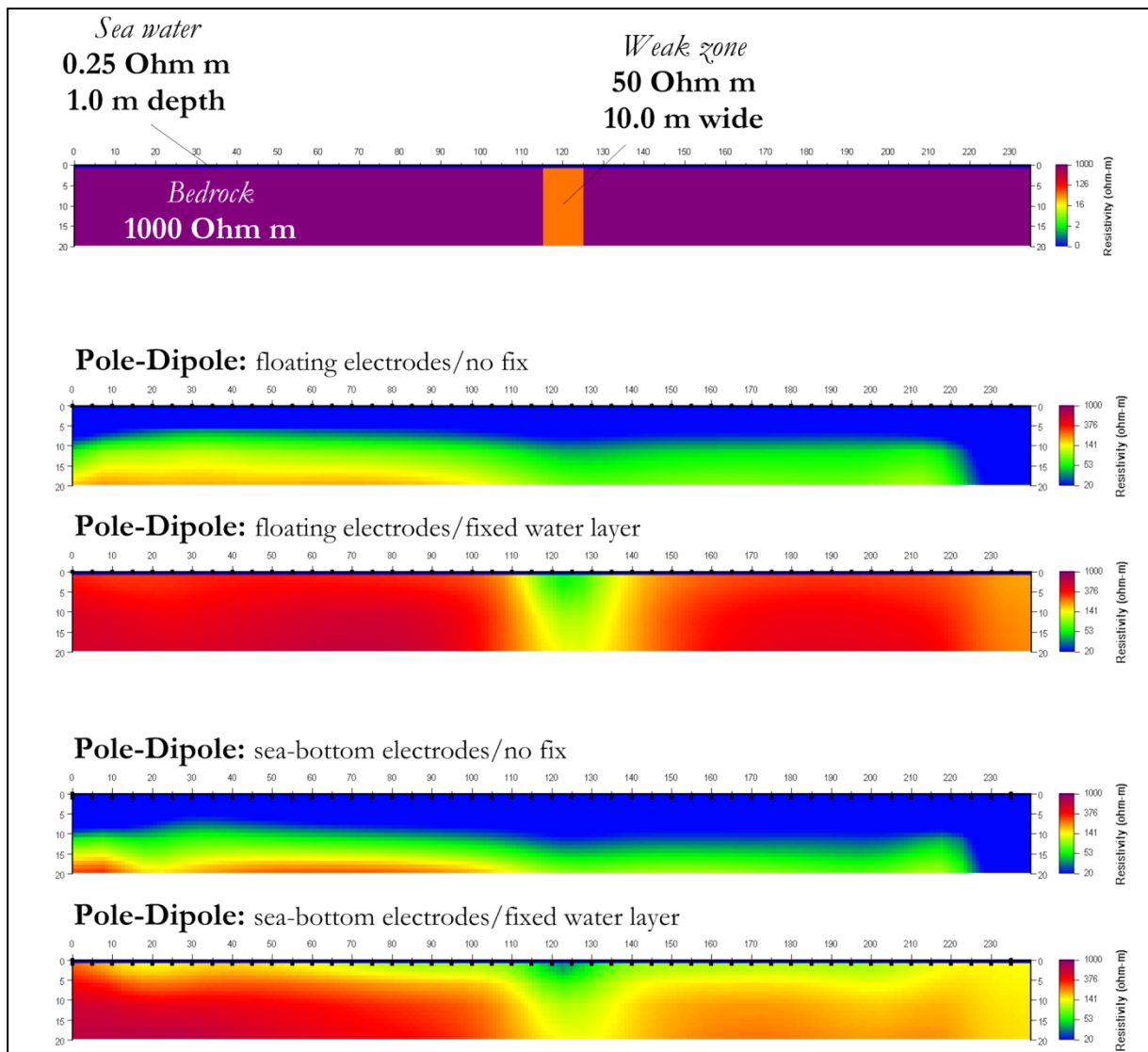


Figure 5.1.3: The effect of fixing the water layer before inversion for pole-dipole array - floating and sea-bottom electrode modes. The model is shown in the uppermost part of the figure.



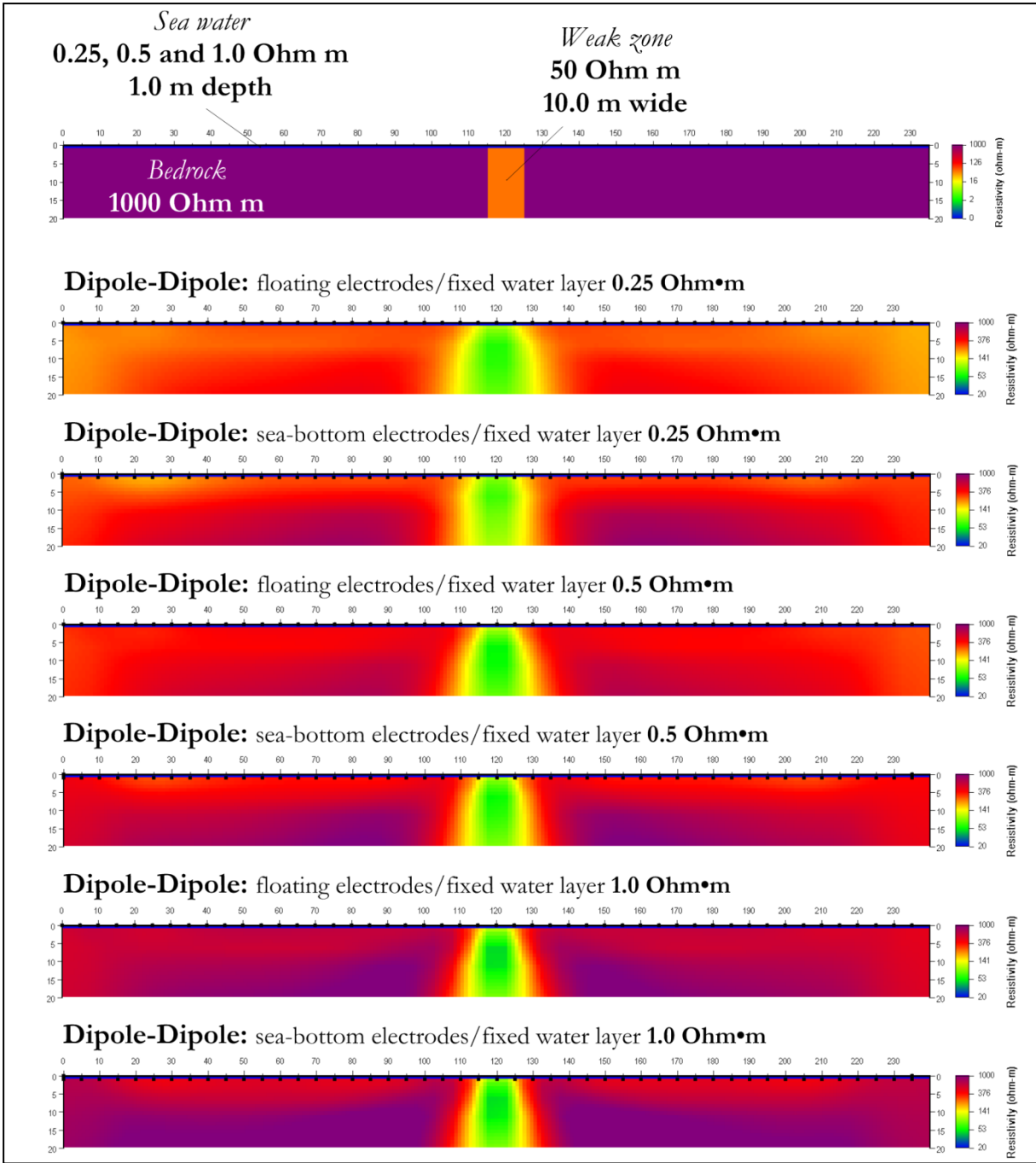


Figure 5.2.1: The effect of sea water resistivity (0.25, 0.5, 1.0 Ohm·m) for floating and sea-bottom dipole-dipole array. The model is shown in the uppermost part of the figure.

### **5.3 The effect of seawater depth**

Figures 5.3.1 and 5.3.2 present the effect of increasing the water depth for both floating and sea-bottom electrode modes. The model used in this case was a 10 m wide and 50 Ohm•m fracture zone, embedded in a 1000 Ohm•m bedrock, under 1.0, 3.0, 5.0 and 10.0 m of sea water (0.25 Ohm•m). In agreement with figures 4.4.1, 4.4.2 and 4.4.3, we can see that the increase of sea depth leads to a shadowing effect on the detection of the modeled fracture zone. As the depth increases, the calculated resistivity range lessens until the zone almost completely disappears at ~10.0 m depth for sea-bottom ERT and ~5.0 m depth for floating mode. We have already stated that sea-bottom electrode ERT mode is preferable to the floating electrode mode, although more difficult to carry out. Figures 5.3.1 and 5.3.2 support and strengthen this claim.

### **5.4 Mixed survey – combination of land and seawater electrode location**

The case of mixed land/marine ERT survey is investigated in figure 5.4.1, in the same manner as that presented in figure 4.10.1. The upper part of figure 5.4.1 presents the results of a fracture zone (50 Ohm•m/10.0 m width) outside the influence of a sea water area (0.25 Ohm•m/5.0 m depth), while the lower part of the figure presents two fracture zones with the same properties, one of which is situated under the sea water. Once again we note the shadowing effect caused by the water layer when performing inversion without fixing the layer's properties. However, when we fix this layer before inversion, the layer is better confined and we obtain a clearer image underneath it. However, the detection of the fracture zone hidden beneath the water becomes problematic. In general interpretation of such surveys requires knowledge of the properties of every water body included in the cross section, and layer fixing can still prove insufficient.

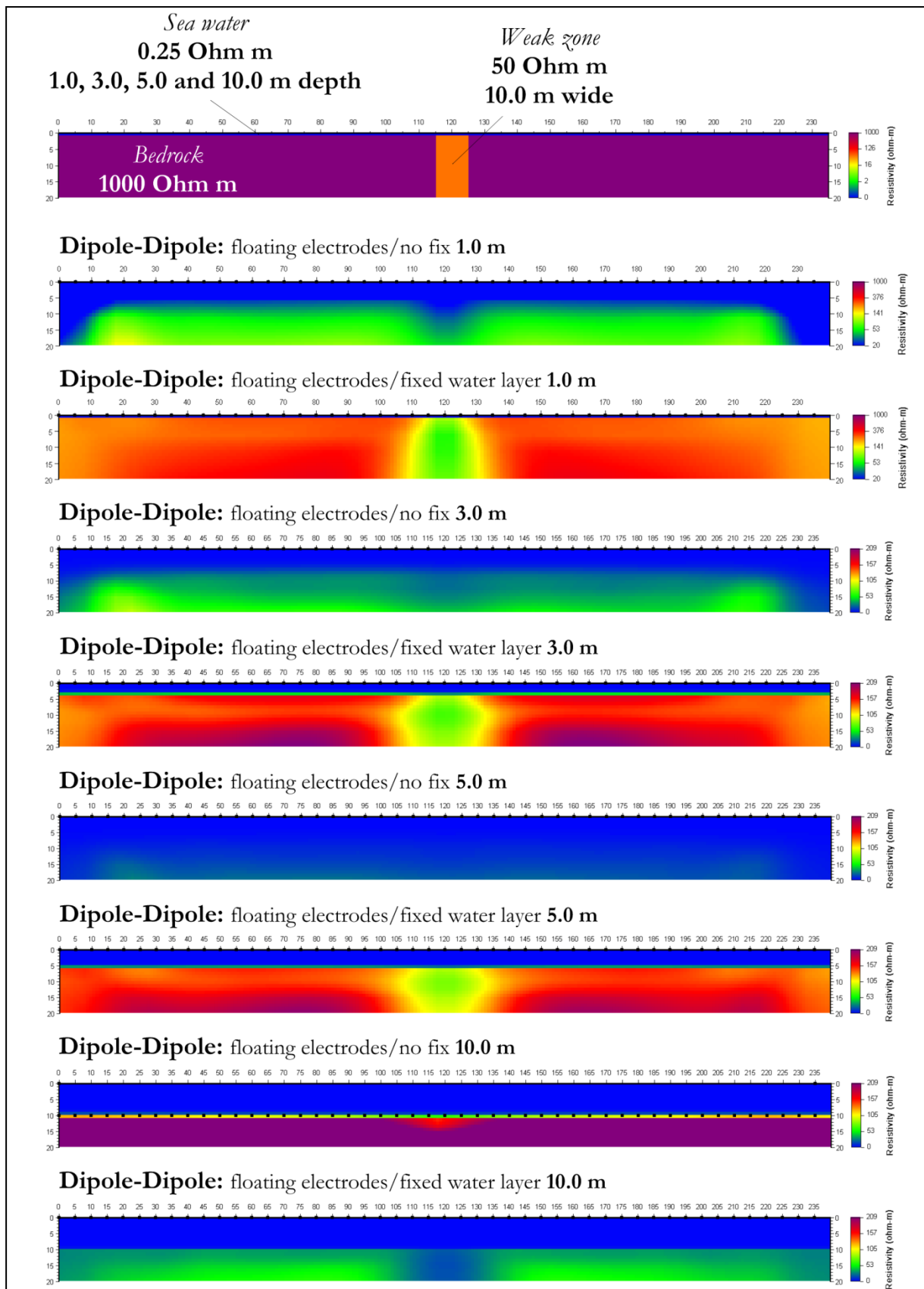


Figure 5.3.1: The effect of seawater depth (1.0, 3.0, 5.0, 10.0 m) for floating electrode configuration with fixed and unfixed water layer - dipole-dipole array. The model is shown in the uppermost part of the figure.

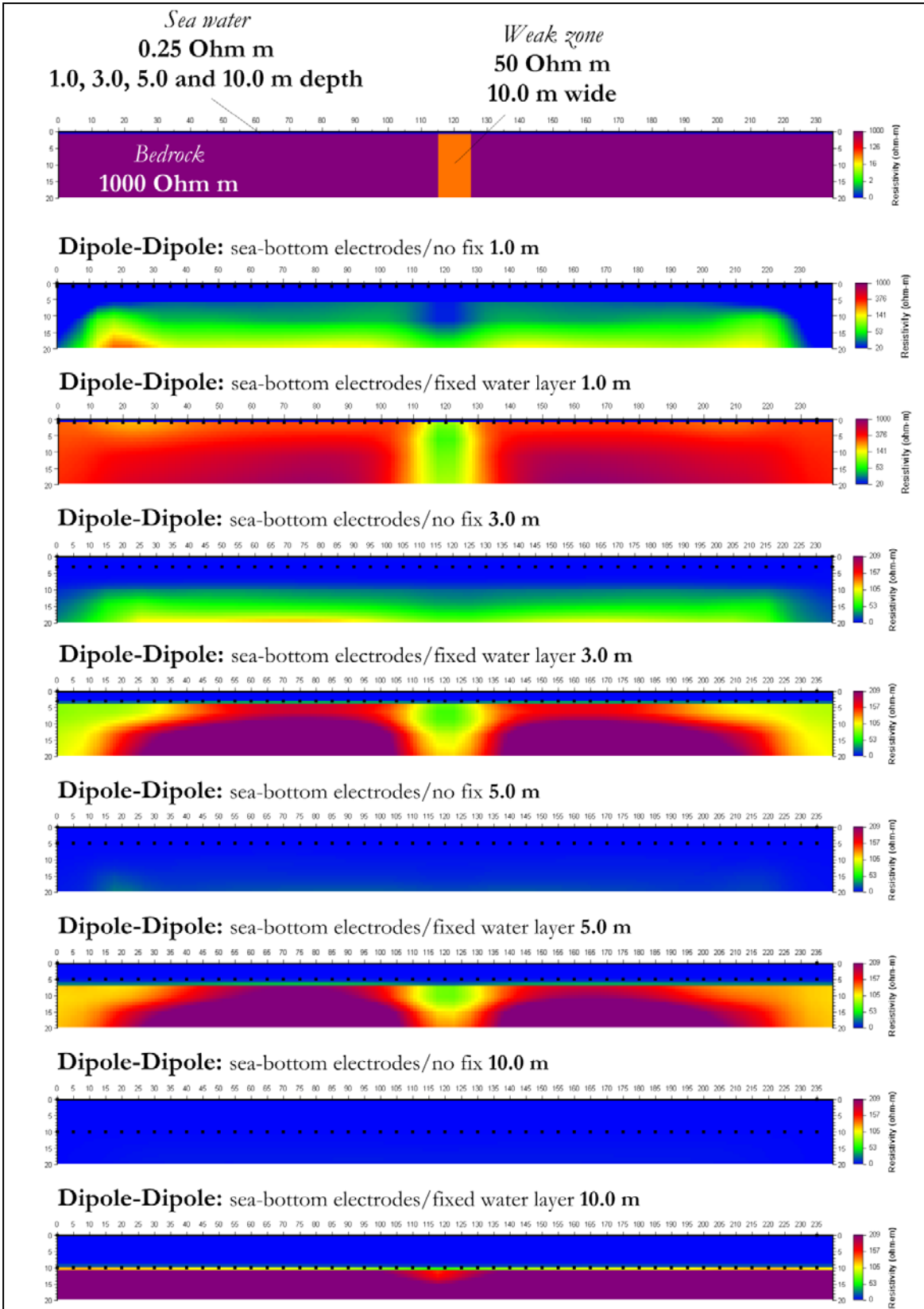


Figure 5.3.2: The effect of variations in sea water depth (1.0, 3.0, 5.0, 10.0 m) for sea-bottom electrode configuration with fixed and unfixed water layer - dipole-dipole array.

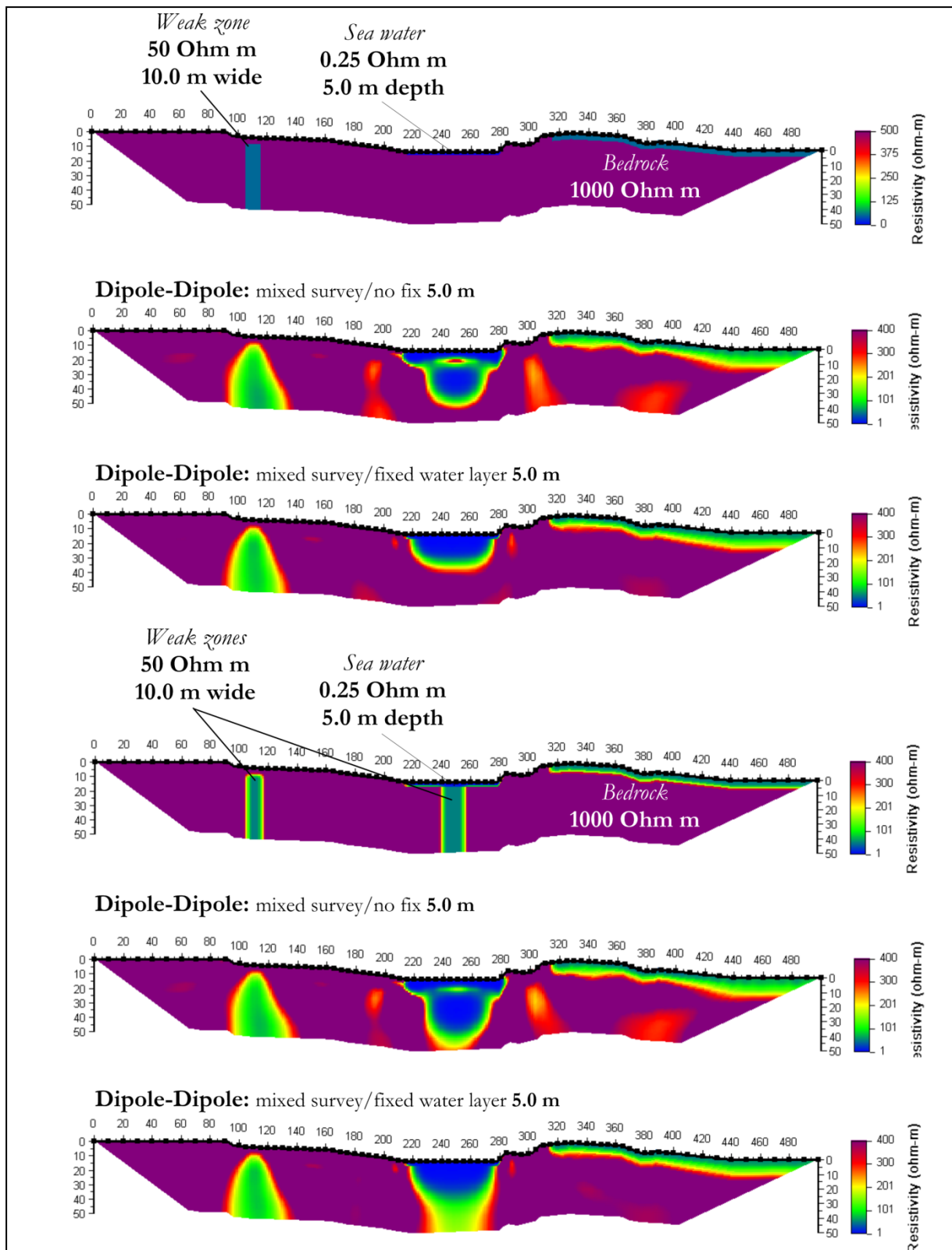


Figure 5.4.1: Mixed survey - single fracture zone outside the influence of the sea water (top) and two weak zones with one under the influence of sea water (bottom) - dipole-dipole array.

## 6. FIELD MEASUREMENTS CROSSING SALINE WATER STRAITS

As part of the ROGFAST project, NGU measured 5 resistivity lines at the island of Kvitsøy north of Stavanger during spring 2012 (Dalsegg 2012). The purpose of this work was partly to map fracture zones that could cause problems during construction of the tunnel to Kvitsøy, and partly to test the effect of seawater in narrow straits as a part of the project reported here. One of the measured lines were far from, and not influenced by, seawater; two lines were located at the end of a strait with seawater on one side, and two lines (Profile 4 and 5, figure 6.1.1) crossed a strait.

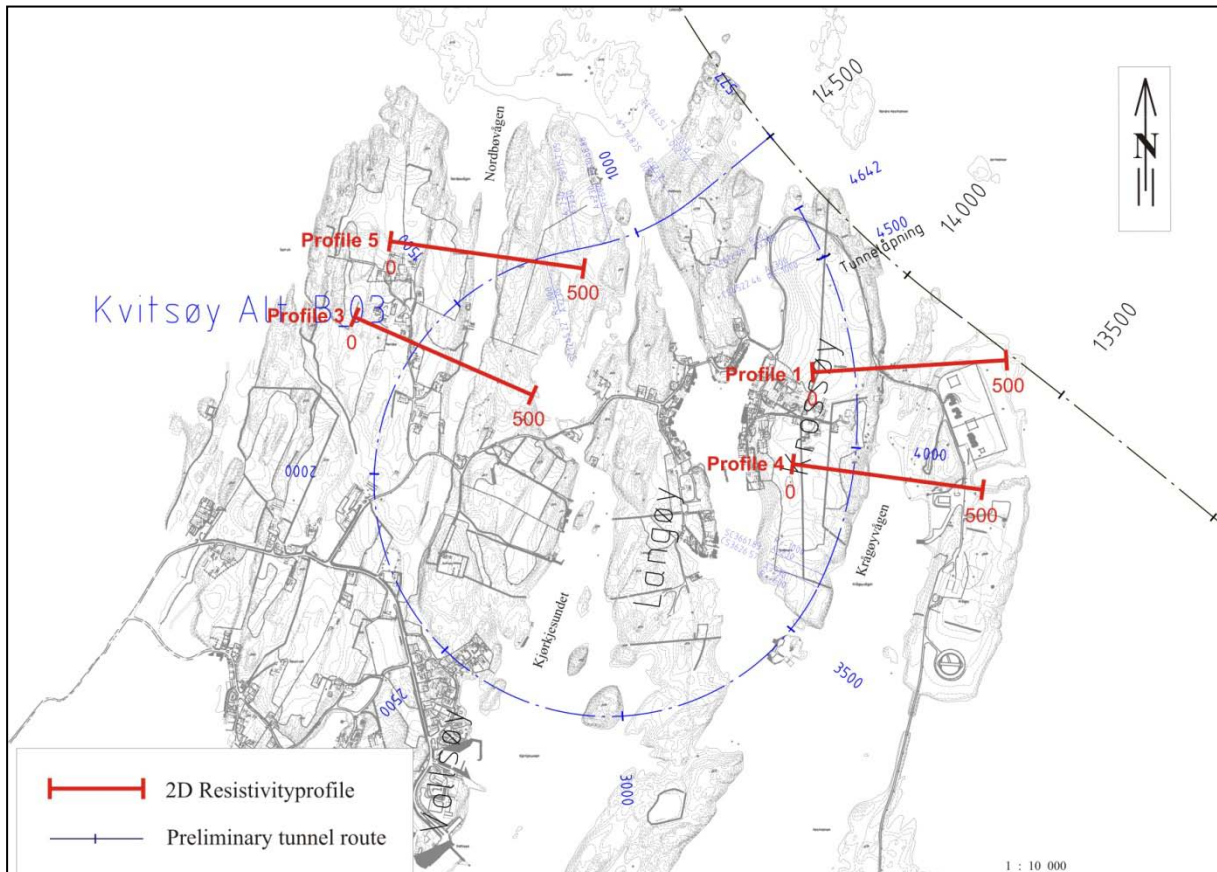


Figure 6.1.1: Location of resistivity lines at Kvitsøy.

### 6.1 Data acquisition and inversion

Data were collected using a cable system developed by the Institute of Technology of Lund University, known as the LUND-system (Dahlin 1993). The system consists of four multi-electrode cables. The ABEM Terrameter LS (ABEM 2012) resistivity and IP instrument were used for the data measurements. In this survey, four cables were used with a multiple gradient electrode configuration and 5 m electrode spacing, giving a maximum penetration depth of about 70 meters. The resolution decreases with depth, and from experience, resistivity data deeper than ca. 50 meters are of low reliability. For more details, see the first report from this work (Dalsegg 2012).



All profiles from field measurements at Kvitsøy are inverted using RES2DINV using both standard and robust inversion. In addition several V/H filters are used.

### 6.2 Influence of seawater and metallic fence

Profile 1, situated at the eastern part of Kvitsøy, lies close to two straits and a metallic fence. In figure 6.2.1, the inverted resistivity using standard and robust inversion is shown. The straits are located at coordinates 200, and from 310 to 335, along the profile.

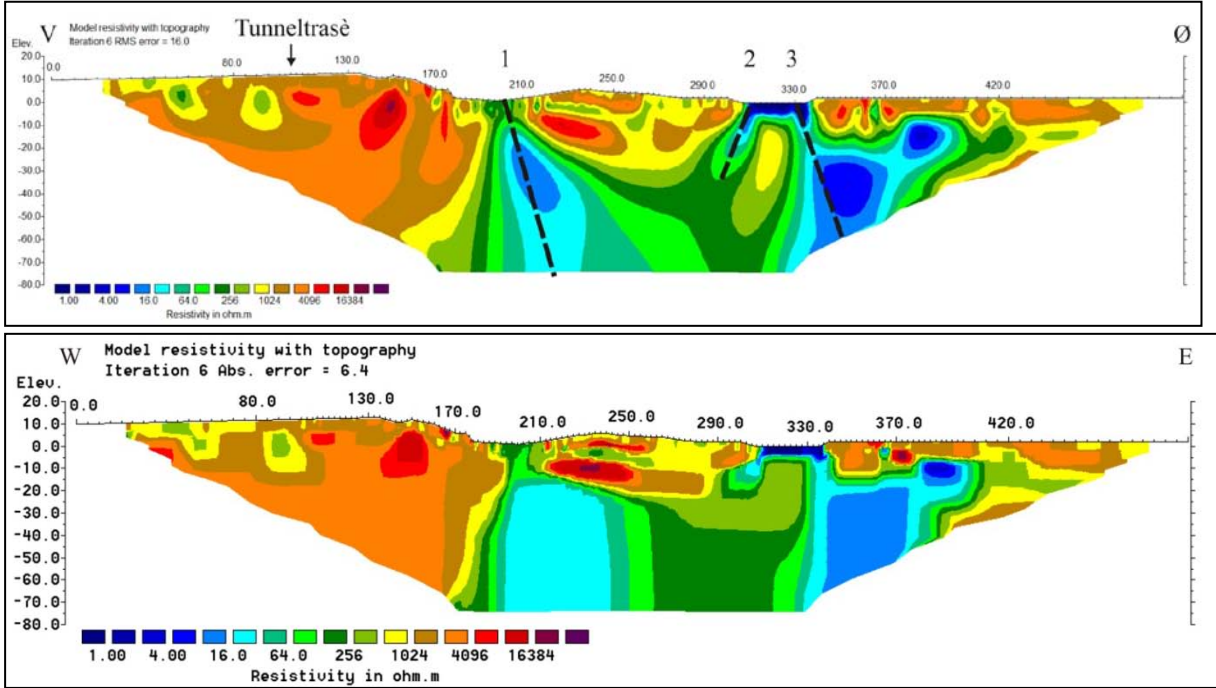


**Figure 6.2.1: Inverted resistivity from multiple gradient array along profile 1 at Kvitsøy using RES2DINV, Standard inversion V/H filter 1.5 (upper) and Robust inversion V/H filter 1 (lower). Interpreted fractures in black dotted lines.**

The main structures and the resistivity levels in the two images shown in figure 6.2.1 are very similar, suggesting that the choice of inversion technique is not critical. Both figures show a number of wide interpreted fractures, with a tendency towards squared structures when using robust inversion.

In this profile the resistivity in bedrock in the western part lies between 1000 and 4000 Ohm•m. To the east the general trend deeper than 20 m below sea level is about 100 to 500 Ohm•m, with some parts less than 16 Ohm•m. This could be explained by variations in geology: sulfides are observed in the north-western part of the island (Dalsegg 2012), and the presence of graphite, known from drilling in the east of the island (Saintot & Solli 2011), can explain the anomalous low resistivity. However, the low resistivity appears when the profile crosses the first strait, and current leakage to the sea on the northern side of the profile may well be the reason for low resistivity. From approximately coordinate 340, the profile is facing a metallic fence surrounding the radio transmitter installation, and this fence is another possible cause for the 16 Ohm•m resistivity level.



We conclude from this that it is not crucial which inversion technique we use, and that conductive material such as seawater and metallic fences may have considerable influence on the resistivity levels.

### 6.3 Floating vs. sea-bottom electrodes

Figure 6.3.1 presents inverted resistivity using RES2DINV along profile 4 using robust inversion and a V/H filter equal to 1, for both floating and sea-bottom electrodes. As a reference, the standard inversion with V/H filter equal to 1 is shown. The sea depth is estimated to be 3 – 4 meters (Dalsegg 2012); however, the inversion is performed without any fixing of water resistivity or depth.

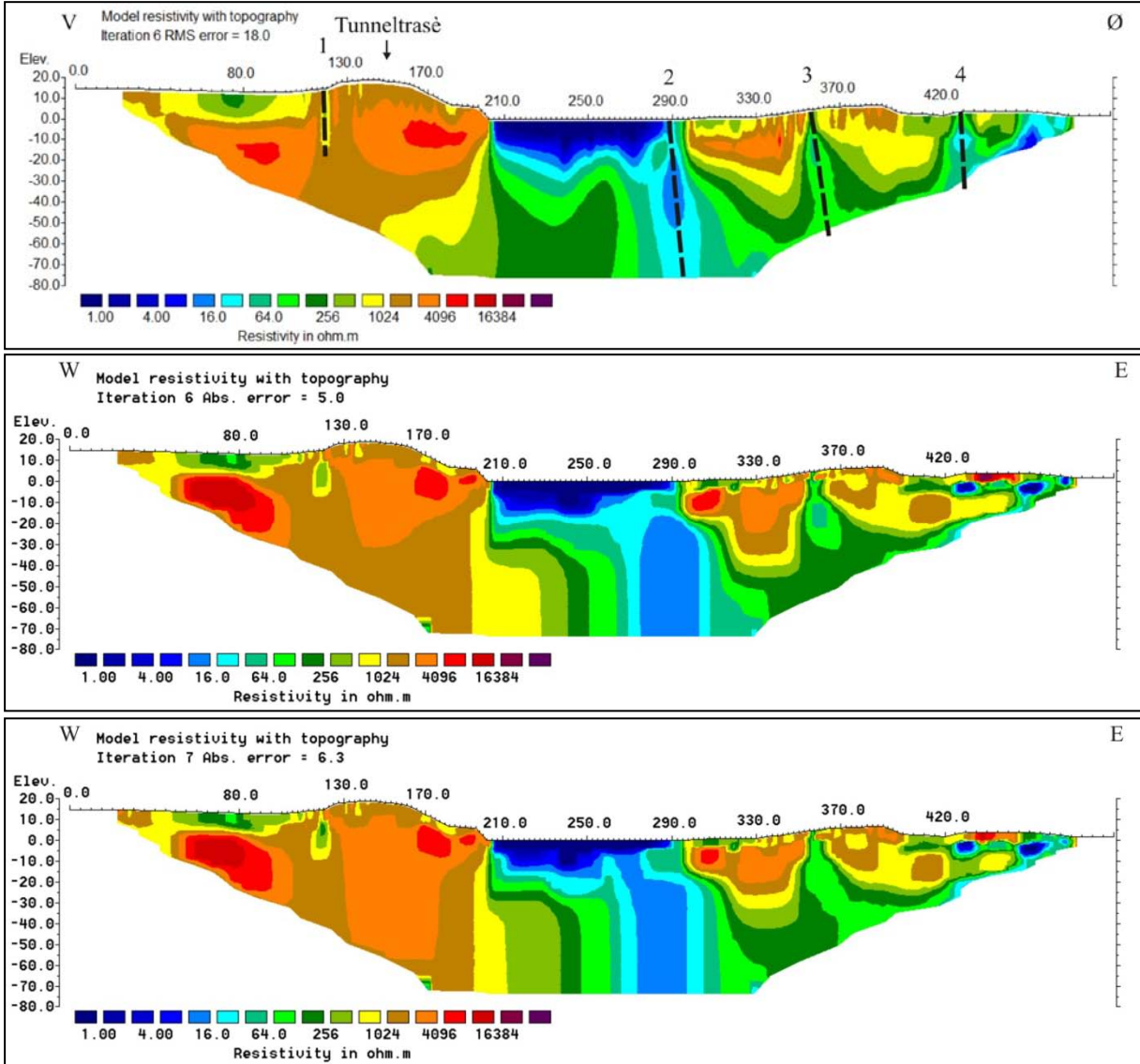


Figure 6.3.1: Inverted resistivity from multiple gradient array along profile 4 Kvitsøy. Upper: Floating electrodes, standard inversion, V/H = 1.5, interpreted fracture zones as dashed black lines. Middle: Floating electrodes, Robust inversion, V/H = 1. Lower: Sea-bottom electrodes, robust inversion, V/H = 1.

If we compare standard and robust inversion, we see here too that structures and resistivity levels are similar, and we see a square pattern with robust inversion. Floating and sea-bottom electrodes show minor deviations in the strait area from ca. coordinate 200 to 295. The most pronounced deviation is at a depth of 5 – 20 m b.s.l. at coordinate 270. This is in agreement with our earlier modeling results (see Figure 4.9.3), and may be confirmation of a fracture zone located here. Along this profile, the interpretation of fracture zones in the upper figure seems realistic; however the one at coordinate 290 could be moved to coordinate 270.

#### **6.4 The effect of fixing the water layer.**

The modeling has shown that it is crucial to know the water depth and resistivity in order to obtain successful inversion of resistivity data in a marine environment (see Figures 4.2.1 and 5.1.1). We will now examine this issue with real data measured at Kvitsøy (Dalsegg 2012). Figures 6.4.1 and 6.4.2 show a real data case with similar conditions to our mixed models. The array crosses sea water in the middle of the cross section, and uses floating electrodes over this part. The data have been inverted both without fixing the sea water layer (figure 6.4.1) and with a fixed water layer (figure 6.4.2). We have also used both standard least-squares and robust inversion techniques along with two different values for V/H filter (1.0 and 1.5). Likewise, the highly conductive sea layer causes a similar shading effect to that which we see in our models, affecting the entire sea-bottom area and spreading the low calculated resistivities throughout its depth. At 240 m distance along the cross section (uppermost image in figure 6.4.1), we can observe a low value lobe extending downwards, a shape that can easily be attributed to a fracture zone. We also note high resistivity values at the edges of the layer, with some extremely high (15.000 Ohm•m) local values. Our modeling has shown that the inversion process, which tries to match a very low resistivity for the unfixed water layer, calculates unrealistically high values in the vicinity of the sea. This miscalculation takes the form of vertical low resistivity artificial effects adjacent to similarly vertical low resistivity areas, which once again can be interpreted as zones of both conductive and resistive characteristics.

Figure 6.4.2 show the same dataset inversion results after fixing the sea water layer. It must be noted that no bathymetry or sea water resistivity information was available except for some approximate observations made during data acquisition. Based on this, we have approximated the marine area with a rectangular body of 3.5 m depth and 0.25 Ohm•m, starting at 217 m and ending at 280 m from the beginning of the cross section. It is evident that the overall picture has changed, especially for the standard inversion. To begin with, the low resistivity area beneath the sea is significantly reduced, and a clear trace of a potential fracture zone is formed. The unrealistically high and low values at the edges of the marine area have been also reduced. Putting our newly acquired experiences from modeling to use, we can conclude that in this case we have an underwater fracture zone of low resistivity (~10 Ohm•m) and around 15 m wide. This weak zone seems to be limited to the surface, but considering that these measurements were carried out with a multiple gradient array, it is not unreasonable to assume that this zone also extends further in depth. In a previous section we have already seen that the superficial limitation of underwater weak zones is an inherent problem for multiple gradient arrays. The anomalies appearing at the limits of the marine area are probably also false.

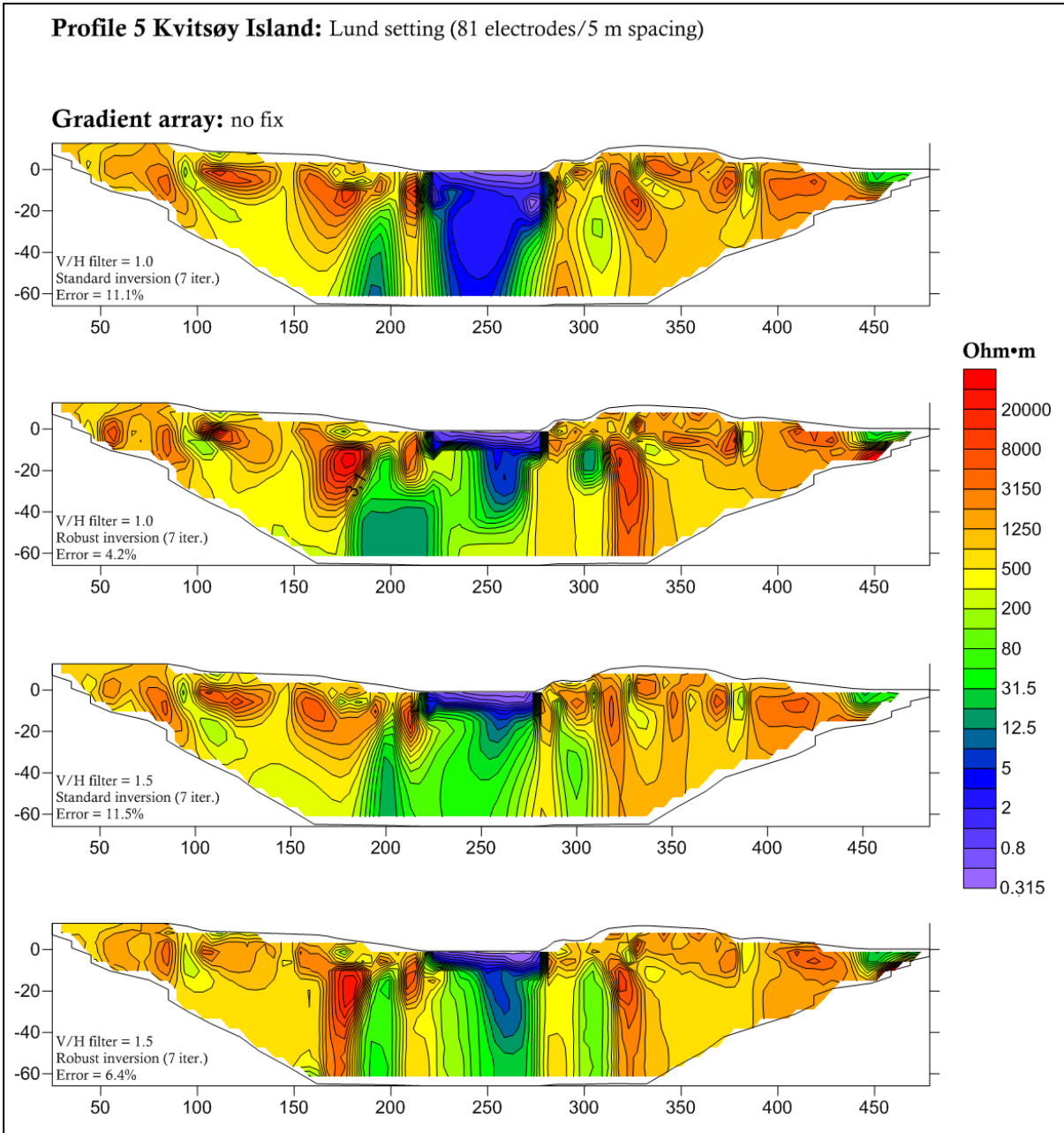


**Figure 6.4.1: Inverted multiple gradient resistivity from profile 5 Kvitsøy without fixing water layer. From top: standard inversion V/H filter 1.0, robust inversion V/H filter 1, standard inversion V/H filter 1.5 and robust inversion V/H filter 1.5.**

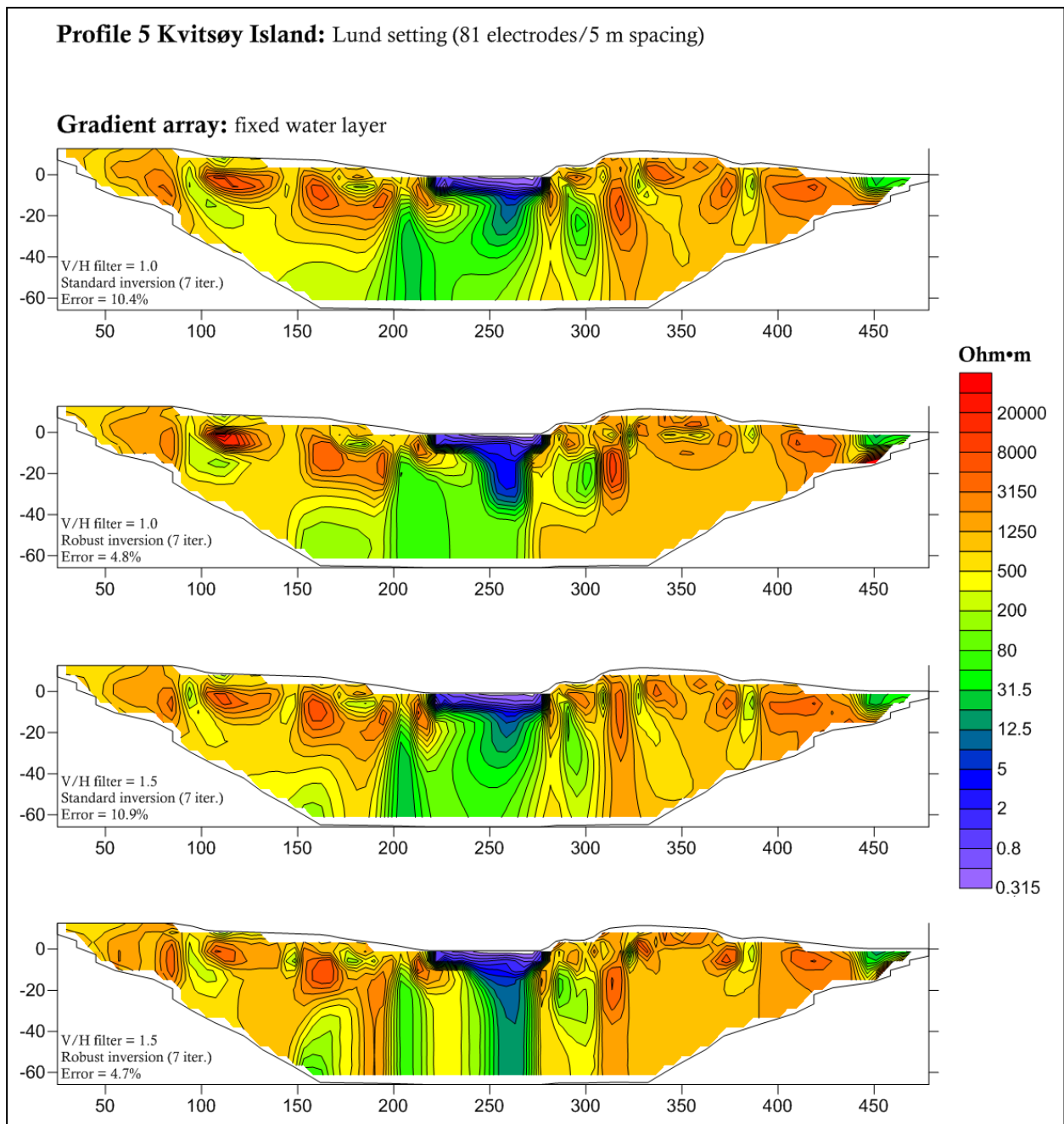


**Figure 6.4.2: Inverted multiple gradient resistivity from profile 5 Kvitsøy with correct fixing water layer. From top: standard inversion V/H filter 1.0, robust inversion V/H filter 1, standard inversion V/H filter 1.5 and robust inversion V/H filter 1.5.**

## 6.5 Validation of the Kvitsøy data inversion

In figure 6.5.1, the measured data along profile 5 at Kvitsøy are inverted using the DC2DPro code (Kim 2012).

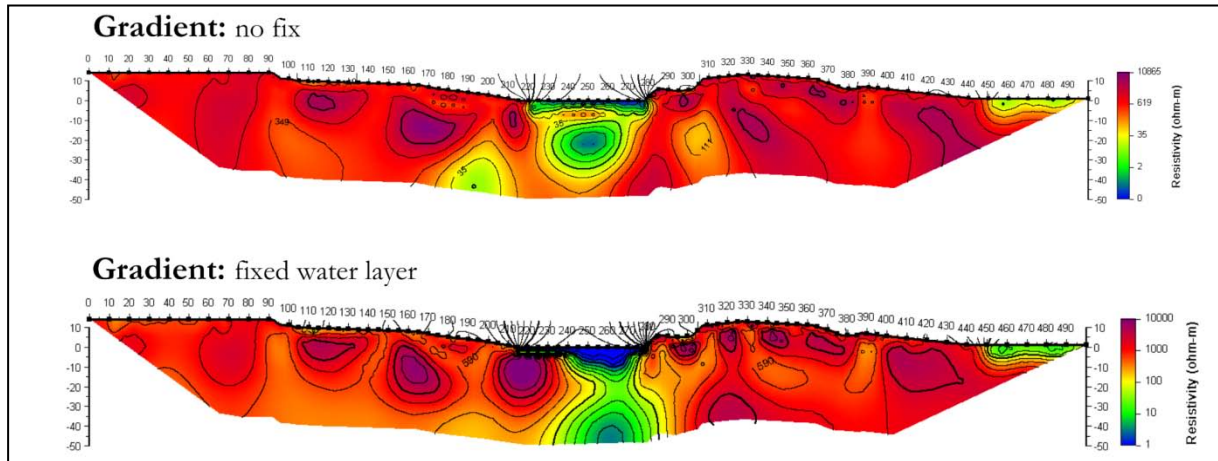


**Figure 6.5.1: Real data from Kvitsøy measured with a multiple gradient array, (fixed water body: 3.5 m depth with 0.25 Ohm·m, starting at 217 m and ending at 280 m).**

It is once again shown that by constraining the sea water layer to its real values, the inversion result becomes significantly clearer, and artificial effects in the vicinity of the water become less pronounced. This inversion confirms that there is a fracture zone underneath the sea-water in the strait (see figure 6.1.1).

## 6.6 Field results from Kvitsøy vs. modeled synthetic data.

The mixed model presented in section 4.10 includes essentially the same structures as those found along profile 5 at Kvitsøy. In figure 6.6.1 we present model data with and without a fracture zone underneath the strait, and measured data inverted with and without fixing the water body; all data are collected or modeled using a Multiple gradient array.

The model data without a fracture zone underneath the water body shows artificially high resistivity under the water body. If we introduce a 15 m wide fracture zone with resistivity 50 Ohm·m under the strait, the image changes dramatically and shows a low resistivity structure which is visible as far down as we are able to see with this electrode configuration. Artificial high and low resistivity values can be seen on both sides of the strait, and at depth the resistivity level is too high.

All the inversions of measured data presented here show a structure similar to that obtained from a modeled fracture zone, and we even see some artificial low resistivity values at the edges of the strait. From this we can conclude that there is an approximately 10 m wide fracture zone underneath the strait along profile 5 at Kvitsøy. There also seems to be a fracture zone at coordinate 100, but this is not as pronounced as the fracture zone in the modeled data (15 m wide and resistivity 50 Ohm·m).



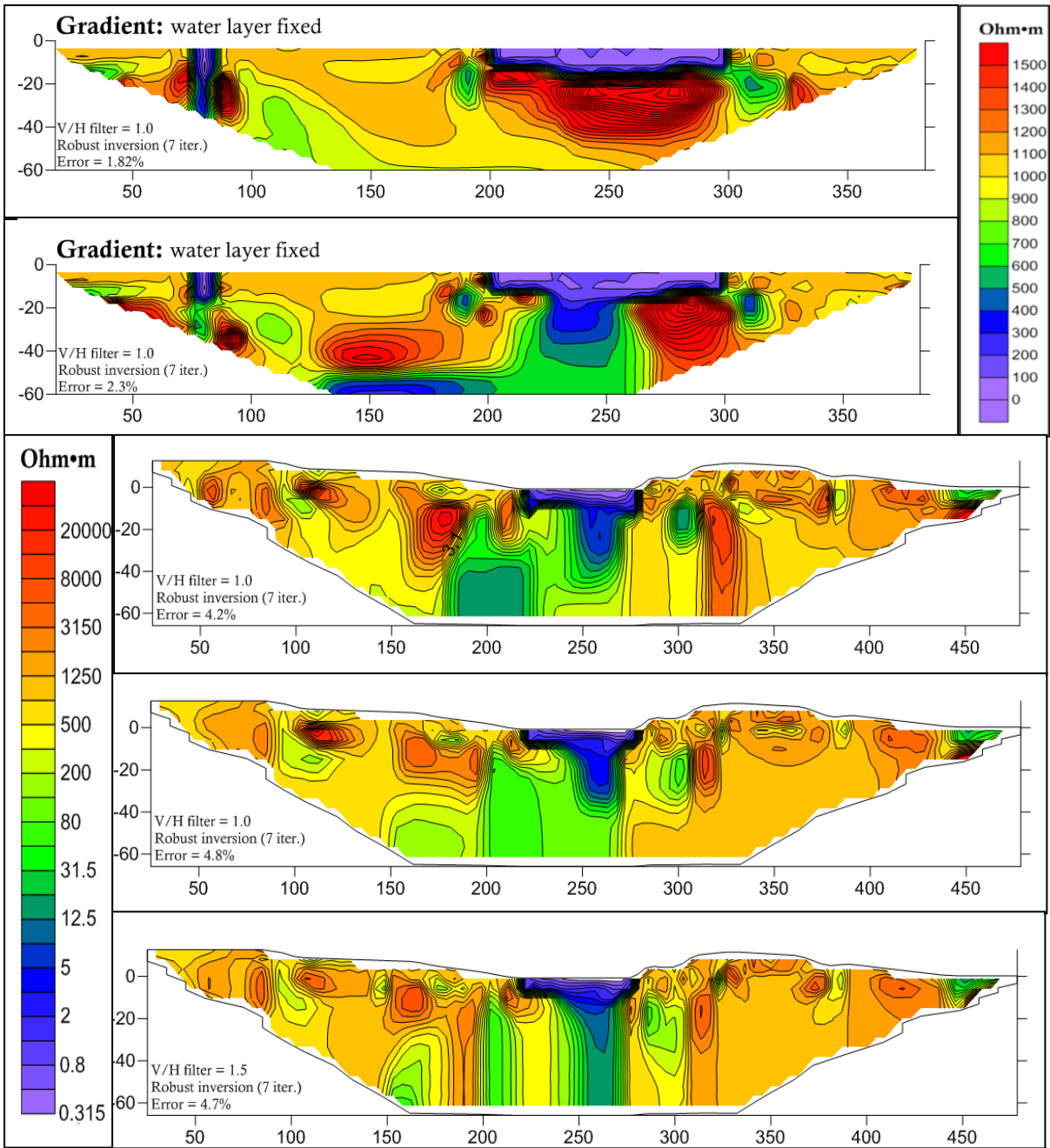


Figure 6.6.1: Profile 5 at Kvitsøy, robust inversion of different data multiple gradient array. From top: Modeled data without fracture zone, modeled data with fracture zone, measured data with no fix of water layer, measured data with fixed water layer and (bottom) measured data with fixed water layer and V/H filter 1.5.

## 7. DISCUSSION

### 7.1 Modeling performance

Our initial test (chapter 4.1) showed that the dipole/dipole array gave the best response to subsea fracture zones in bedrock. The modeling performed by Reiser et al. (2009) and the work presented in this report show that the multiple gradient array performs almost as well. These are similar results to those found by Dahlin & Zhou (2004). In field measurements, the dipole/dipole array may give signal-to-noise problems due to its electrode arrangement. For this reason NGU prefers to use a multiple gradient array in field investigations; however to ensure best possible results, we have chosen dipole/dipole arrays in our modeling work.

In our modeling work, we have used an electrode setup similar to the Lund system (Dahlin 1993) with 5 meter electrode spacing, giving a penetration depth of approximately 60 meters. The penetration depth could be increased to 120 meters by increasing the electrode spacing to 10 meters; however in doing so, the resolution would decrease, and thin fracture zones (of thickness less than 10 m) could be lost. Our modeling results show that the ideal situation is an electrode separation of half the expected fracture zone thickness. However, below 30 meters depth, anomalies tend to become unreasonably wide and resolution is reduced to unacceptable levels. In other words, we can successfully image fracture zones, but only for the first 30 meters of their depth.

Electrical resistivity traversing (ERT) in marine environments can be performed in three ways: with floating electrodes; with sea-bottom electrodes; and with electrodes positioned somewhere in between. We have tested here floating and sea-bottom electrode modes. The difference in response from these two methods, shown both by modeling studies and field measurements, is not great for shallow water. However, electrodes at sea-bottom give the best results, and should be used in field investigations. This means that the position of the cable should be fixed in one way or another. To obtain good results, it is essential to know the sea depth and the resistivity of the seawater, and to fix this during the inversion.

In our study we have used RES2DINV (Loke 2010) to invert our measured data; this software is standard in the industry today. To ensure that the software produces satisfactory results, we have performed a validation against the software DC2DPRO (Kim 2012). In general these two codes produced similar results, but with differences at a more detailed level. The inversion using RES2DINV was performed using robust inversion and a V/H smoothness filter factor equal to 1. Robust inversion is recommended when there are large variations in resistivity; such large variations are found in marine investigations where seawater resistivity can be as low as 0.25 Ohm•m, and resistivity in unfractured crystalline bedrock is typically 1000 Ohm•m. The imaging of vertical fracture zones could have been improved by using a V/H filter value of 2.

Throughout the processing stage of this work we have noticed an increased instability when performing inversion in several of our models. Loke's software has a standard 7 iteration inversion procedure, with the iterations representing intermediate steps towards a mathematical fit between the calculated values and the measured data. Normally these steps start off with a percentage error which is quite high and which decreases at each step. In our case, and especially in the mixed survey models, this inversion procedure became extremely unstable after 3 or 4 iterations; the instability manifested itself by dramatic changes in the structures and values of the calculated resistivities. Most of the figures in section 4.10 have



been plotted and presented with a clipped color scale, since values as high as 50.000 Ohm•m have been calculated by RES2DINV. In other cases, the inversion would stop after only several iterations with a result that did not resemble the initial model at all. We believe that the main reason for this instability lies with the extremely low resistivity of seawater. If one checks the release notes of RES2DINV, it will be found that the underwater resistivity surveys presented there are mostly performed with brackish water resistivity (at least 1 Ohm•m). As we have already concluded, higher water resistivities significantly increase our chances of success, and inversion procedures become much more stable and smooth; such stable behavior is not seen with values as low as 0.25 Ohm•m. This means that the inversion code used by commercial software like RES2DINV is not designed for such extreme conditions; this is another example of difficulties connected with marine ERT processing.

We have already concluded that fixing the water depth is essential to our success. Performing either sea-bottom or floating electrode ERT, the water depth should be known in detail, and should be no more than 10 meters. When using sea-bottom electrode configurations, RES2DINV does not offer the possibility of inversion without fixing the seawater layer above the electrodes. Floating electrode configurations on the other hand can be run both with and without water fixing; however results significantly improve with water fixing. In many cases, fixing the water layer leads to results almost identical to the ones obtained from a sea-bottom electrode configuration. However, in real conditions it is anticipated that sea-bottom mode will in general yield better results than floating electrodes, and for larger water depths sea-bottom mode is the only option.

In today's market one can easily find specially designed instruments for marine ERT measurements. Those instruments' main characteristic is that they are more powerful than more usual ERT equipment, which means that they can handle stronger electrical currents, and subsequently can provide more current to the ground. However, this does not mean that the percentage of current loss in the seawater is any less, since the ratio of the current that infiltrates the ground to the current lost in the sea will remain constant. Ohm's law dictates that resistance can be calculated by dividing potential with current. Therefore, a higher current will result in a proportionately higher measured potential and if we divide those quantities, their proportionate higher levels will be annulled resulting in the same calculated resistance (or resistivity) as in the case of less powerful currents. Nevertheless, a high-current feature like that can prove useful in cases where the measured resistance is close to the noise level and we need to boost our signal above it. Higher current output means, however, that standard type multi-electrode cables cannot be used, which can have significant implications for the field logistics and thereby the cost of the survey.

## **7.2 Model parameters**

Our modeling has shown that the resistivity method is very sensitive to the resistivity in the seawater, in the bedrock and in the fractured bedrock. To obtain reliable modeling data, it is essential to use correct values for these parameters.

The salinity of seawater can vary from 3.1 to 3.8% (Wikipedia, Salinity). Resistivity in seawater of different salinity and temperature is described in chapter 2 in this report. With a salinity of 3.5% and temperature 5 °C, the sea-water resistivity is 0.30 Ohm•m: a salinity of 4% and temperature of 10 °C reduces the sea-water resistivity to 0.23 Ohm•m. In our modeling we have used a sea-water resistivity of 0.25 Ohm•m which is a reasonable assumption for Norwegian conditions. However, if we have more brackish or even fresh water

conditions, the water resistivity will be much higher, and fracture zone detection and characterization will be more successful than that which we have observed in our saline water studies.

Bedrock in the coastal areas of Norway consists mostly of crystalline basement. Resistivity in subsea crystalline basement is not well known in Norway, but a few observations do exist. In cooperation with the Norwegian Public Roads Administration (Statens Vegvesen), NGU has carried out resistivity logging of boreholes close to the coast. At the small island of Alstein north of Stavanger, the subsea resistivity in gabbro varies from 700 to 1500 Ohm•m (Elvebakk & Saintot 2011). At Bjarkøy, north of Harstad northern Norway, the subsea resistivity in gneiss varies from 1500 to 2500 Ohm•m (Dalsegg & Elvebakk 2012). In an attempt to extrapolate resistivities in gneisses in the North-Western part of Norway to reservoir levels at the "Frøya High", Rønning & Elvebakk (2005) found an average subsea resistivity of 750 Ohm•m at a temperature of 90 °C. If we correct this to a temperature of 10 °C we will obtain a resistivity of approximately 2600 Ohm•m. Based on this, a resistivity for unfractured subsea crystalline bedrock of 1000 Ohm•m seems reasonable, and we have used this value in our modeling. In sedimentary rocks such as Cambro-Silurian limestones and shales in the Oslo area, we can expect to find even lower resistivity (Elvebakk 2011), which may give more favorable conditions for subsea fracture zone detection and characterization.

In our modeling, we have used a resistivity of the overburden (soil at sea-bottom) of between 5 and 50 Ohm•m. We know from measurements on land that the resistivity in unleached marine clay is less than 10 Ohm•m (Solberg et al. 2008). Porous sand with pore space filled with saline water will probably have the similar resistivity levels, dependent on porosity. In most of our models we have used 30 Ohm•m, which is expected to give more favorable conditions for detecting subsea fractured zones in bedrock.

Resistivity in the fractured bedrock is the most uncertain parameter in our marine resistivity modeling work. In our dry land studies we have found that resistivities above 3000 Ohm•m in crystalline bedrock represent stable bedrock with only minor construction problems; resistivities between 500 and 3000 Ohm•m may represent fractured bedrock with water leakage problems, while resistivities less than 500 Ohm•m may represent fractured bedrock with clay alteration giving stability problems (Rønning et al. 2009, Rønning et al. 2013). Exchanging fresh water (resistivity 50 Ohm•m) with seawater (0.25 Ohm•m) in all pore space will reduce the resistivity in fractured crystalline bedrock from 1000 Ohm•m to 5 Ohm•m. From this we can conclude that resistivity in subsea fracture zones of 50 Ohm•m may be too high. However, modeling with different resistivity contrasts between the fracture zone and the host rock (Figure 4.7.1) produce only slightly better results for a contrast of 100 (10 Ohm•m in fracture zone) compared with contrast of 20.

Our choice of seawater depth and subsea soil thickness is guided by the results of the modeling. When there is no response of a fracture zone in bedrock beneath 20 meters of seawater, there is no need to test deeper seawater values.

### **7.3 Possibilities and limitations in marine resistivity**

Our modeling has shown that it is possible to detect and characterize subsea fracture zones in bedrock using the resistivity method. However, there are some critical limitations related to the distribution of current between the seawater and the underlying bedrock. As a strategy to

overcome these limitations we have tried to use optimal conditions in our modeling. We have used:

- the most sensitive electrode configuration (dipole-dipole)
- electrodes at sea-bottom as well as floating
- reasonable or favorable resistivity values
- optimal inversion conditions with fixed water model parameters
- simple models with no geological noise
- no instrument noise

The first three of these are discussed above. The models we have used are as simple as possible. In nature, there will be lateral variations in seawater depth, seawater resistivity, soil thickness, soil resistivity, bedrock resistivity and fracture zone resistivity. All these parameters will influence the inverted resistivity sections, and give some geological noise that can preclude a clear image of a fractured zone. As shown in our modeling, the seawater depth and resistivity are the most critical parameters. During modeling it is usual to add 5 to 10 % noise to the synthetic data to simulate instrument noise. In our case, we use synthetic data generated from the models without the addition of on any noise in order to achieve optimal conditions for the detection and characterization of fractured zones.

Despite the use of reasonable or optimal conditions in our modeling work, it seems that seawater of depth exceeding 10 meters will preclude effective detection and characterization of subsea fractured zones. This result is corroborated by an alternative inversion code. Due to this discouraging result, modeling of the dip and depth extent of fracture zones is not performed here.

#### **7.4 Field data vs. modeled data.**

Our modeling has showed that electrical resistivity traversing is a challenge in marine environments. The seawater conducts away a large portion of the injected current, and a fracture zone in bedrock is not visible when seawater depth exceeds 10 meters. However, in the field study at Kvitsøy, we could locate a fracture zone in bedrock under ca. 4 metres of seawater. To do so it was necessary to have information about seawater resistivity and depth in order to fix those parameters during inversion.

In the field study at Kvitsøy, water depth and resistivity were estimated; it would have been preferable to have used carefully measured depth and resistivity values so as to better evaluate the resistivity method's possibilities and limitations.

In the presence of challenging conditions it could prove useful to follow the following procedure: careful inversion of our measured data; construction of a probable model similar to the inverted result; testing of this model by submitting it to new inversion; and evaluating the success of the model. Repeating this procedure after each failure could lead to improved results.

## 8. CONCLUSIONS

2D sea-bottom and floating electrode ERT modeling reveals important guidelines that anyone performing such measurements should follow.

Our results indicate that dipole-dipole and multiple gradient configurations produce the best results when mapping sea-bottom fracture zones. However, dipole-dipole appears to excel only when using ideal modeling parameters; in a real situation the multiple gradient configuration would give much better signal to noise ratio.

Accurate measurement of the water resistivity and topography of the sea-bottom is of utmost importance when conducting marine ERT. This information can significantly improve inversion results especially for floating electrode measurements. Here it must be noted that RES2DINV does not offer the possibility of inverting sea-bottom acquired data without water fixing.

In general colder and less saline conditions increase our chances of detecting sea-bottom fracture zones in their true dimensions. Therefore, winter ERT in marine environments is advisable.

Taking into account that real conditions will not be as favorable as in our models, our modeling indicates that sea-bottom topography that exceeds 10.0 m of water depth should disqualify sea-bottom ERT as a prospection method. The limit for floating electrode configuration on the other hand appears to be somewhere around 5.0 m.

A general rule derived from this modeling is that in order to get a clear image of a fracture zone, we should use an electrode spacing which is half the expected fracture zone width.

A sediment cover of 5.0 m overlying a fracture zone of 50 Ohm•m resistivity does not shield its response. How accurate compared to the actual formation causing the anomaly our inversion would be, depends on the resistivity of the sediments. Generally, a lower sediment layer resistivity will result in more accurate identification of the layer.

In the presence of a conductive overburden, a higher resistivity contrast between bedrock and fracture should exist in order to be able to detect the fracture with sea-bottom ERT. If the whole environment is resistive however, even a favorable resistivity contrast may not be sufficient.

The most important conclusion is that when working with marine environment ERT, we are pushing the method to its limits. This is reflected in our results in the sense that small changes in modeling resulted in large changes in the inversion process. It has proved challenging to create models which result in a stable inversion behavior. Grouping and illustrating the results coming from each modeling scenario has also proved difficult. It can be anticipated that when additional noise is incorporated into the modeling, results will vary even more, and the resolving power of the method will deteriorate. It could be beneficial to extend the work of this report in several areas: a study of the effectiveness of inversion methods (L1 versus L2 inversion mode); a study of the technique's resolving ability compared to commercial ERT instruments; and the carrying out of sea-bottom ERT in real conditions.

Based on the modeling results, we have been able to improve interpretations of ERT measurements made across the straits at Kvitsøy.

## **9. ACKNOWLEDGEMENTS**

The authors would like to thank Robin Watson for his extensive English language corrections on the original text and his well placed comments. The authors like thank "Statens vegvesen vegdirektoratet" (The Norwegian Public Road Administration) for financial support, good cooperation and for permission to publish the data.

## 10. REFERENCES

- ABEM 2012: ABEM Terrameter LS. Instruction Manual. ABEM 20120109, based on release 1.10. ABEM, Sweden.
- Chiang, C.W., Goto, T.N., Mikada, H., Chen, C.C. and Hsu, S.K. 2012: Sensitivity of Deep-Towed Marine Electrical Resistivity Imaging Using Two-Dimensional Inversion: A Case Study on Methane Hydrate. *Terr. Atmos. Ocean. Sci.*, Vol.23, No. 6, 725-732, December 2012. DOI:10.3319/TAO.2012.06.19.01(T).
- Dahlin, T. 1993: On the Automation of 2D Resistivity Surveying for Engineering and Environmental Applications. Dr. Thesis, Department of Engineering Geology, Lund Institute of Technology, Lund University. ISBN 91-628-1032-4.
- Dahlin T. & Zhou B 2004: A numerical comparison of 2D resistivity imaging with 10 electrode arrays. *Geophysical Prospecting* Vol. 52, Issue 5, p. 379 – 398. DOI: 10.1111/j.1365-2478.2004.00423.x .
- Dahlin, T., Loke, M.H., Siikanen, J. & Höök, M. 2014: Underwater ERT Survey for Site Investigation of a New Line for the Stockholm Metro. Presentation at the 31st Nordic Geological Winter Meeting, Lund, Sweden, January 8-10 2014. Abstract in conference proceedings.
- Dalsegg, E. 2012: Geofysiske målinger på Kvitsøy, Kvitsøy kommune, Rogaland. NGU Report 2012.033, pp. 1-17, [http://www.ngu.no/upload/Publikasjoner/Rapporter/2012/2012\\_033.pdf](http://www.ngu.no/upload/Publikasjoner/Rapporter/2012/2012_033.pdf)
- Dalsegg, E. & Elvebakk, H. 2012: Geofysiske målinger i forbindelse med undersjøisk tunnel til Bjarkøy, Troms. NGU Rapport 2012.027, 41 sider. [http://www.ngu.no/upload/Publikasjoner/Rapporter/2012/2012\\_027.pdf](http://www.ngu.no/upload/Publikasjoner/Rapporter/2012/2012_027.pdf)
- Elvebakk, H. 2011: Sammenstilling av resistivitet, seismiske hastigheter og naturlig gammastråling i norske bergarter. NGU Rapport 2011.042 (60 sider). [http://www.ngu.no/upload/Publikasjoner/Rapporter/2011/2011\\_042.pdf](http://www.ngu.no/upload/Publikasjoner/Rapporter/2011/2011_042.pdf)
- Elvebakk, H. and Saintot, A. 2011: Geofysisk logging av borehull på Alstein, Randaberg kommune, Rogaland. NGU Report 2011.032, pp. 1-43, [http://www.ngu.no/upload/Publikasjoner/Rapporter/2011/2011\\_032.pdf](http://www.ngu.no/upload/Publikasjoner/Rapporter/2011/2011_032.pdf)
- Ganerød, G. V., Rønning, J.S., Dalsegg, E., Elvebakk, H., Holmøy, K., Nilsen, B. & Braathen, A. 2006: Comparison of geophysical methods for sub-surface mapping of faults and fracture zones in a section of the Viggja road tunnel, Norway. *Bull. Eng. Geol. Env.* (2006) 65: 231 – 243). ISSN: 1435-9529 (Paper) 1435-9537 (Online).
- Kim, J.H. 2012: DC 2DPro v. 0.99. User's Guide. <http://kigam.en.ecplaza.net/>
- Lile, O.B., Backe, K.R., Elvebakk, H. and Buan, J.E. 1994: Resistivity measurements on the sea-bottom to map fracture zones in the bedrock underneath sediments. *Geophysical Prospecting*, 42, 813-824.

Loke, M.H. 2002: RES2DMOD ver 3.01 Geoelectrical Imaging 2D & 3D. Instruction manual. [www.geoelectrical.com](http://www.geoelectrical.com).

Loke, M.H. 2010: RES2DINV ver. 3.59. Geoelectrical Imaging 2D & 3D. Instruction manual. [www.geoelectrical.com](http://www.geoelectrical.com).

Reiser, F., Dalsegg, E., Dahlin, T., Ganerød, G. & Rønning, J.S. 2009: Resistivity Modelling of Fracture Zones and Horizontal Layers in Bedrock. NGU Report 2009.070, pp. 1-120, 2009 [http://www.ngu.no/upload/Publikasjoner/Rapporter/2009/2009\\_070.pdf](http://www.ngu.no/upload/Publikasjoner/Rapporter/2009/2009_070.pdf)

Rønning, J.S. 2003: Miljø- og samfunnstjenlige tunneler. Sluttrapport delprosjekt A, Forundersøkelser. Statens vegvesen, Publikasjon 102.

Rønning, J.S., Dalsegg, E., Elvebakk, H. & Storrø, G. 2003: Characterization of fracture zones in bedrock using 2D resistivity. 9th EGS European Meeting, Prague, August 31 – September 4 2003. Extended Abstract: Proceedings P005.

Rønning, J.S., Dalsegg, E., Elvebakk, H., Ganerød, G.V. & Heincke, B.H. 2009: Characterization of fracture zones in bedrock using 2D resistivity. Proceedings from 5th Seminar on Strait Crossings, Trondheim, June 21 – 24 2009, p. 439 - 444 (SINTEF/NTNU).

Rønning, J.S. & Elvebakk, H. 2005: Onshore – Offshore Resistivity studies. Basement resistivity at the Frøya High. NGU Report 2005.032 (20 pp.). [http://www.ngu.no/upload/Publikasjoner/Rapporter/2005/2005\\_032.pdf](http://www.ngu.no/upload/Publikasjoner/Rapporter/2005/2005_032.pdf)

Rønning, J.S., Ganerød, G.V., Dalsegg, E. & Reiser, F. 2013: Resistivity mapping as a tool for identification and characterization of weakness zones in bedrock - definition and testing of an interpretational model. Bull. Eng. Geol. Environment 10.1007/s10064-013-0555-7.

Rucker, D.F. & Nooman, G.E. 2013: Using marine resistivity to map geotechnical properties: a case study in support of dredging the Panama Canal. Near Surface Geophysics, 2013, 11, 625-637. doi:10.3997/1873-0604.2012017.

Saintot, A. & Solli, A. 2011: Geological investigations by drill core logging for the Rogfast tunnel project. NGU Report 2011.034 (64pp.). [http://www.ngu.no/upload/Publikasjoner/Rapporter/2011/2011\\_034.pdf](http://www.ngu.no/upload/Publikasjoner/Rapporter/2011/2011_034.pdf)

Satriani, A., Loperte, A. & Proto, M. 2011: Electrical Resistivity Tomography for coastal salt water intrusion characterization along the Ionian coast of Basilicata Region (Southern Italy). Fifteenth International Water Technology Conference , IWTC-15 2011, Alexandria, Egypt.

Solberg, I.L., Rønning, J.S., Dalsegg, E., Hansen, L., Rokoengen, K. & Sandven, R. 2008: Resistivity measurements as a tool for outlining quick-clay extent and valley-fill stratigraphy: a feasibility study from Buvika, central Norway. Canadian Geotechnical Journal, 45: 210-225, doi:10.1139/T07-089.

Tsourlos, P.I., Tsokas G.N. & Albanakis, K. 2001: Geoelectrical surveys in marine environments. Geowaters Project Report, 2001.





Norges geologiske undersøkelse  
Postboks 6315, Sluppen  
7491 Trondheim, Norge

Besøksadresse  
Leiv Eirikssons vei 39, 7040 Trondheim

Telefon 73 90 40 00  
Telefax 73 92 16 20  
E-post [ngu@ngu.no](mailto:ngu@ngu.no)  
Nettside [www.ngu.no](http://www.ngu.no)

*Geological Survey of Norway  
PO Box 6315, Sluppen  
7491 Trondheim, Norway*

*Visitor address  
Leiv Eirikssons vei 39, 7040 Trondheim*

*Tel (+ 47) 73 90 40 00  
Fax (+ 47) 73 92 16 20  
E-mail [ngu@ngu.no](mailto:ngu@ngu.no)  
Web [www.ngu.no/en-gb/](http://www.ngu.no/en-gb/)*